Theses and Dissertations

Theses and Dissertations

5-3-2019

Beta-Cyclodextrins as Agents for Improved Protection Methods of Wood and Strand-Based Wood Composites

Lili Cai

Follow this and additional works at: https://scholarsjunction.msstate.edu/td

Beta-cyclodextrins as agents for improved protection methods of

wood and strand-based wood composites

By

Lili Cai

A Dissertation
Submitted to the Faculty of
Mississippi State University
in Partial Fulfillment of the Requirements
for the Degree of Doctor of Philosophy
in Forest Resources
in the Department of Sustainable Bioproducts

Mississippi State, Mississippi

May 2019

Beta-cyclodextrins as agents for improved protection methods of

wood and strand-based wood composites

By

Lili Cai

Approved:

_____   _____
Dragica Jeremic   Hyungsuk "Thomas" Lim
(Director of Dissertation)   (Major Professor)

_____
Yun Sang Kim
(Co-Major Professor)

_____
Hui Wan
(Committee Member)

_____
Jeffery J. Morrell
(Committee Member)

_____
H. Michael Barnes
(Committee Member /Graduate Coordinator)

_____
George M. Hopper
Dean
College of Forest Resources

Name: Lili Cai

Date of Degree: May 3, 2019

Institution: Mississippi State University

Major Field: Forest Resources

Major Professor: Hyungsuk Thomas Lim

Title of Study: Beta-cyclodextrins as agents for improved protection methods of wood and strand-based wood composites

Pages in Study 121

Candidate for Degree of Doctor of Philosophy

This study examined the feasibility of using β-cyclodextrins (βCDs), which are derived from starch, as agents to stabilize volatile and leachable biocides for the protection of wood and wood composites. The encapsulation of volatile natural antimicrobial compounds, such as allyl isothiocyanate (AITC) and essential oils (EOs), in βCDs was qualitatively confirmed by Attenuated total reflection Fourier-transform infrared spectroscopy (ATR-FTIR) method and the maximum inclusion yield was quantitatively estimated by ultraviolet-visible spectrophotometry (UV/VIS) while the partial fixation of leachable borates with βCD was confirmed by ATR-FTIR and nuclear magnetic resonance (NMR) techniques. The efficacy of the βCD complexes as wood preservatives of southern yellow pine and randomly Oriented Strand Board (OSB) was examined in soil block tests (AWPA Standard E10-16 and E22-16). The results indicate that (A) βCDs suppress the premature leaching of otherwise volatile natural compounds and suggest a novel approach to the application of volatile or water-immiscible natural preservatives for wood and wood composites protection; (B) βCD can be used as an agent for partial fixation of boric acid to form boric acid esters. However, the borate esters are susceptible to leach out after AWPA

Standard E11-16 test and not suitable for protection against *Gloeophyllum trabeum* and *Postia placenta* in outdoor conditions.

DEDICATION

To my family, my husband and my son, for their tremendous love, endless support, constant encouragement, and sacrifices.

ACKNOWLEDGMENTS

Firstly, I would like to thank my major advisor, Dr. Hyungsuk Lim, without his mentorship, time, knowledge, and patience throughout this study, it would have been impossible to complete this task on time.

I would like to express my sincere appreciations to my co-advisor Dr. Yunsang Kim, for teaching me how to think critically and write scientifically, and providing tremendous help and guidance.

I also owe a debt of gratitude to my previous major advisor, Dr. Dragica Jeremic, offered me this great opportunity, always provided me with lots of great advice and support to complete this study.

I also extend my thanks for my committee members, Dr. Hui Wan, Dr. H. Michael Barnes, Dr. Jeffrey J. Morrell for the great suggestions, kind assistance, and continuous supports.

I am grateful for Dr. Darrel D. Nicholas for the generously of his time and wise thoughts and suggestions. To Dr. Elizabeth Stokes, Dr. El Barbary Hassan and Dr. Sean Stokes for providing me access to work in their labs. To Dr. Nicholas Fitzkee for the training and assisting in the Boron NMR analysis. To Dr. Daniel Seale for the training on using the hot press and mechanical testing instruments. To Dr. Brian K. Via, Dr. Charles Essien and Dr. Frank Owens for providing technical assistance in preparing wood sections

by the microtome. To Mr. Mike Freeman, Dr. David Schubert and Dr. Antonio Pizzi for discussion of boron hydrolysis.

I am thankful for my friends and colleagues, Dr. Laya Khademibami, Dr. Telmah Telmadarrehei, Dr. Lakshmi Narayanan, Mr. Bojan Cosovic, Dr. Xuefeng Zhang, at Mississippi State University for their support and help in the experiment. To my other friends and colleagues, Ms. Nasim Maafi, Ms. Guangmei Cao, Ms. Yawei Cao, Ms. Laurice Spinelli, Mr. Sachin Tripathi, Mr. Ismail Khan and Dr. Olanrewaju Adeyemi Raji, Mr. Islam Elsayed for all of your help and support whenever I needed.

I would like to thank my family for supporting me all through my years in school and my husband, and my son for being there every step of the way.

Finally, I am grateful to have had the privilege to study at the Department of Sustainable Bioproducts, Mississippi State University. This experience allows me to work with some of the best and brightest professors, colleagues and friends and provides me the opportunity to grow and thrive.

Thanks all!

TABLE OF CONTENTS

LIST OF TABLES

LIST OF FIGURES

x

CHAPTER I

INTRODUCTION

1.1 Literature review

1.1.1 Wood as a sustainable construction material

Southern pines are the primary sources of softwood products in the United States (Koch, 1972). There are 11 species of pines and all of them are from diploxylon members of the genus *Pinus*, family *Pinaceae*, and order *Coniferales*. The four principal southern pine species are loblolly (*Pinus taeda* L.), shortleaf (*Pinus echinate* Mill.), longleaf (*Pinus palustris* Mill.), and slash pine (*Pinus elliottii* Engelm.), which make up about 90% of the total inventory. The remaining seven minor pine species are often found to be mixed in with the major species. Southern pines have outstanding strength, are easily dried, and highly receptive to chemical treatments, which have made them popular for pulp and paper products, residential construction and other applications such as utility poles, piling, and railway ties when treated with preservatives as well as raw material for making wood composites, such as oriented strand board (OSB) (Koch, 1972).

Southern pines are mainly composed of longitudinal and horizontal elements, as shown in Figure 1.1. Longitudinal elements of pine include longitudinal tracheids, strand tracheids, epithelial cells, and longitudinal parenchyma while the rays contain all the horizontal elements including ray tracheids, ray parenchyma, and epithelial cells. Longitudinal tracheids and rays occupy about 90% and 9% of the wood volume of the

major southern pines, respectively. The longitudinal and horizontal cells are interconnected through pits in the cell walls. There are six types of pit pairs in southern pine wood, as shown in Table 1.1. Those pit pairs (Figure 1.2) create passageways for the movement of liquids and gases from cell to cell in the living tree, which allows modification and/or conversion of wood to other products through drying and preservatives treatments. Generally, southern pine sapwood has high permeability in the longitudinal, radial and tangential directions because of their simple wood structure and the various openings on the cell walls. High retentions of preservatives by pressure treatment is readily given and southern pine sapwood can be easily kiln-dried.
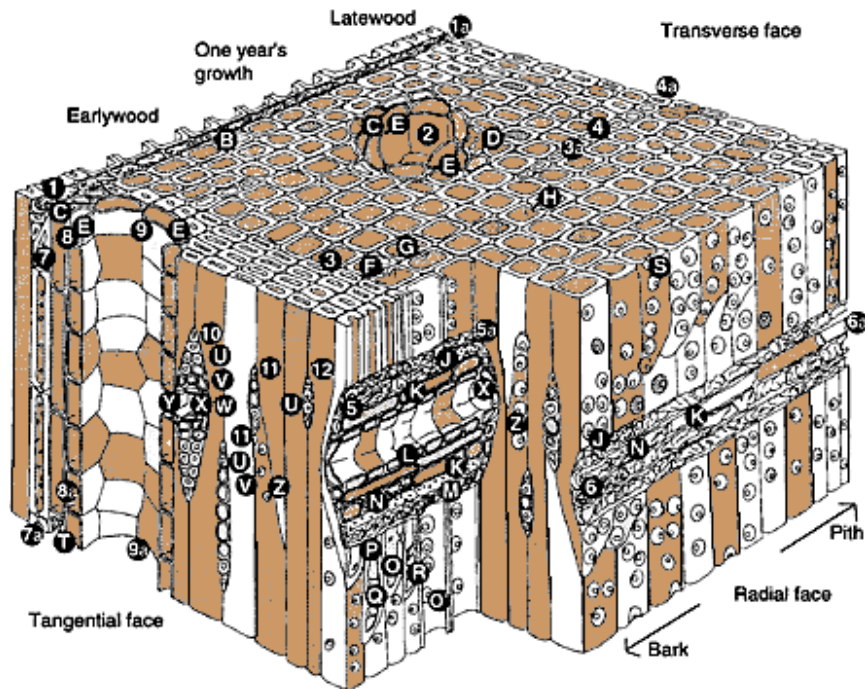
Figure 1.1   Schematic drawing of typical southern pine wood

Adapted from Koch, Peter. 1972. Utilization of the Southern Pines. USDA Forest Service Ag Handbook No 420. Based on Howard, E.T., and Manwiller, F.G. 1969. Wood Science 2: 77-86. **Transverse view**. 1-1a, ray; B, dentate ray tracheid; 2, resin canal; C, thin-walled longitudinal parenchyma; D, thick-walled longitudinal parenchyma; E, epithelial cells; 3-3a, early wood longitudinal tracheids; F, radial bordered pit pair cut through torus and pit apertures; G, pit pair cut below pit apertures; H, tangential pit pair; 4-4a, latewood longitudinal tracheids. **Radial view.** 5-5a, sectioned fusiform ray; J, dentate ray tracheid; K, thin-walled parenchyma; L, epithelial cells; M, unsectioned ray tracheid; N, thick-walled parenchyma; O, latewood radial pit; O1, earlywood radial pit; P, tangential bordered pit; Q, callitroid-like thickenings; R, spiral thickening; S, radial bordered pits; 6-6a, sectioned uniseriate heterogenous ray. **Tangential view.** 7-7a, strand tracheids; 8-8a, longitudinal parenchyma (thin-walled); T, thick-walled parenchyma; 9-9a, longitudinal resin canal; 10, fusiform ray; U, ray tracheids; V, ray parenchyma; W, horizontal epithelial cells; X, horizontal resin canal; Y, opening between horizontal and vertical resin canals; 11, uniseriate heterogenous rays; 12, uniseriate homogenous ray; Z, small tangential pits in latewood; Z1, large tangential pits in early wood.

Table 1.1   Pit pairs in southern pines

Pit pairs	Size (nm)	Sources
Tracheid to tracheid-bordered	200-500	Koch, 1972
Tracheid to ray tracheid-bordered	20-4000	Hansmann et al., 2002
Ray tracheid to ray tracheid bordered		
Tracheid to ray parenchyma-half-bordered pinoid		N/A
Ray tracheid to ray parenchyma-half-bordered		
Ray parenchyma to ray parenchyma-simple		
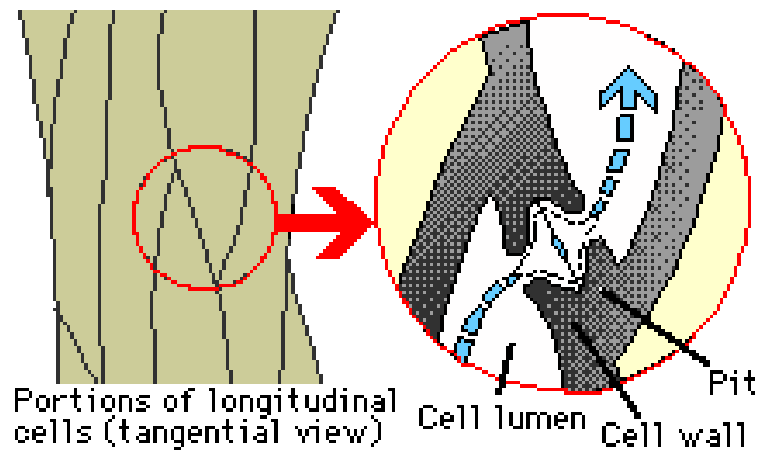
Figure 1.2   Pits provide tiny passageways for flow of water and liquids.

Adapted from Forest Products and Wood Science, 2nd Edition, by J.G. Haygreen and J.L. Bowyer. © 1982. Reproduced with permission.

The main composition of the wood cell includes cellulose (40-45%), hemicellulose (25-35%), and lignin (20-30%) as well as minor extraneous materials ($<$ 5%). The differences in these components contribute to fiber properties and ultimately impact product properties.

1.1.2 Biodeterioration of wood by fungi

Because of its hierarchical and mesoporous structure (Figure 1.1) and richness in carbohydrates, wood can be readily colonized by a variety of microorganisms including bacteria, molds, blue stain, fungi (i.e. soft, white and brown rots), insects and marine borers (Morrell, 2018). Wood decay fungi are deemed as primary hazards to wood products in service and are generally more difficult to control than other types of biodeterioration (Nicholas, 1982). To reduce the risk of their damage on wood and develop effective strategies for wood protection, it is necessary to understand the factors that affect fungal colonization of wood and microbial mechanisms that leading to wood degradation.

1.1.2.1 Factors affecting fungi growth on wood

Fungal attack of wood is affected by many factors: water, oxygen, temperature, pH of wood, nutrients and vitamins (Morrell, 2018) (Figure 1.3). Water is a key ingredient for the growth of fungi by serving as a solvent for their metabolic processes. A minimum wood moisture content at or above fiber saturation point is required for fungal growth and a minimum residual air volume of 20% in wood is needed to ensure a sufficient amount of oxygen (Arantes and Goodell, 2014). Temperature significantly affects the decay rate of wood and the optimum temperature for fungi growth is between $20^{\circ}C$ to $36^{\circ}C$. In addition, a pH range of 3 to 6 is preferable for general wood fungi growth. Moreover, the development and growth of fungi require a trace amount of nutrients and vitamins, such as nitrogen, phosphorus, iron and Thiamine. (Arantes and Goodell, 2014).
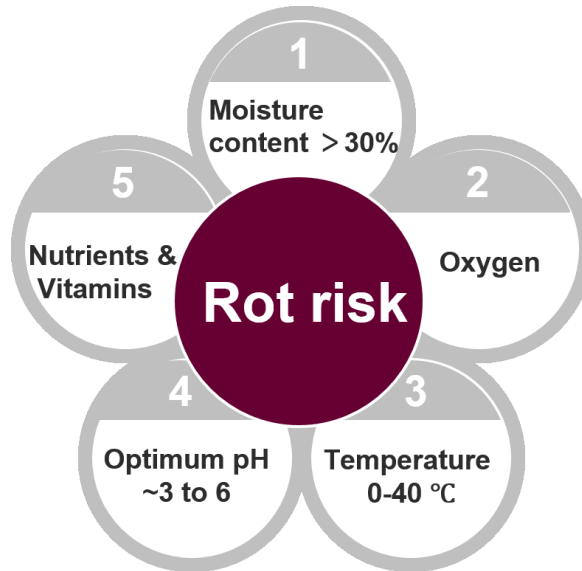
Figure 1.3   Various factors that contribute to the risk of rot

1.1.2.2   Fungal decay mechanism on wood

Once fungi colonize wood under favorable conditions, the degradation process usually will start at the rays, where access to the non-structural nutrients contained in parenchyma cells is relatively easy. Then the hyphae spread into wood fibers or tracheids and further via pits. Although the general path for fungal colonization is similar, the decay mechanisms vary between different types of fungi, especially for brown rot fungi and white rot fungi, as they attack different chemical components of the wood cell wall (Arantes and Goodell, 2014).

Brown rot fungi, such as *Gloeophyllum trabeum* and *Posia placenta*, are the most destructive decayers of conifers (Arantes and Goodell, 2014). These fungi actively metabolize the cellulose and hemicellulose of wood and chemically modify lignin. Brown rot decay fungi cause extensive wood strength loss due to the rapid depolymerization of

the cellulose and resulting in brown color of lignin (Green III and Highley, 1997). The severely decayed wood generally appears as a cubic residue and is crumbly and fragile. The degradation of brown rot on wood includes both enzymatic pathways of polysaccharides and non-enzymatic pathways of lignin. The brown rot decay mechanism of lignin degradation is not fully understood, but it has been generally considered that the Fenton reactions based on iron (*Fe*) are suggested for the decay process (Arantes and Goodell, 2014; Ringman et al., 2014) (Figure 1.4).

$$\text{Haber-Weiss reaction}$$

$$Fe^{3+} + O_2^{-\bullet} \longrightarrow Fe^{2+} + O_2$$

$$Fe^{2+} + H_2O_2 \longrightarrow Fe^{3+} + OH^- + OH^\bullet \text{ (Fenton reaction)}$$

$$\text{Net reaction: } O_2^{-\bullet} + H_2O_2 \longrightarrow OH^- + OH^\bullet + O_2$$
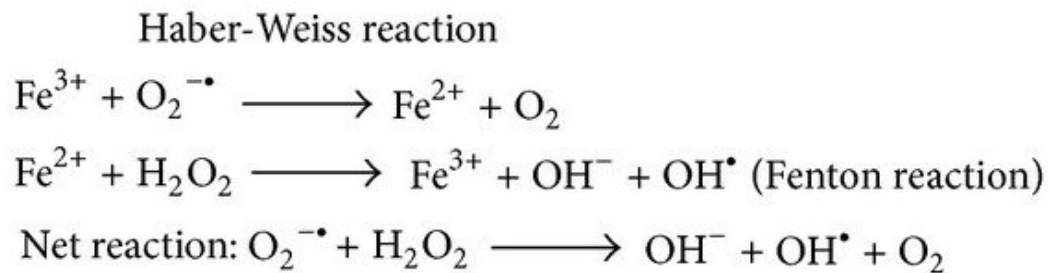
Figure 1.4   Generation of hydroxyl free radical by the Haber-Weiss Reaction and Fenton reaction.

Adapted from Liang et al. (2013)

White rot fungi typically include simultaneous white rot and selective white rot in terms of different amounts of components (lignin, cellulose and hemicellulose) being degraded (Messner, 2003). Simultaneous white rot fungi usually attack lignin, cellulose and hemicellulose almost at the same time. Selective white rot fungi prefer removing lignin and hemicellulose and leaving modified cellulose. Unlike brown rot fungi, many white rot fungi have a full array of enzymes to degrade cellulose, hemicellulose and lignin.

1.1.3   Preservation of wood from deterioration

1.1.3.1   Wood preservatives

1.1.3.1.1   Classical wood preservatives and the challenges

Preservative treatment on wood is one of the most effective and economical ways to prolong the service life of wood. The classical three wood preservatives include creosote, pentachlorophenol and chromated copper arsenate (CCA). Creosote is the oldest oil-borne preservatives patented in the 1830s and is also one of the widely used preservatives (~25% of the treated wood in North America) for railway sleepers, marine piling and utility poles. Creosote-treated wood has long-lasting efficacy against various microorganisms due to the main effective polycyclic aromatic hydrocarbons, which can dissolve the lipids in the membrane of microorganism and disrupt their growth (Engelman et al., 1986). Creosote treatment also helps to improve the dimensional stability of wood (Groenier, James Scott, 2006; Morrell, 2018).

Pentachlorophenol is one of the first synthetic organic preservatives since the 1930s and the main active compounds in this preservative are chlorinated phenols. These compounds are able to inhibit the oxidative phosphorylation of enzymes and suppress fungal growth (Weinbach, 1954). Generally, pentachlorophenol is more effective in heavy oil solvent than the light oils and is mainly used to treat wood utility poles and timber bridges (Morrell, 2018).

CCA was the most commonly used water-borne preservatives developed in the 1930s in India. The main components of CCA are chromium trioxide, copper oxide, and arsenic pentaoxide. CCA was initially used to treat utility poles and expanded rapidly for residential applications because of its proven biocidal effects in above-ground and ground-

contact applications. The popularity of CCA is also due to its being waterborne, clean and odorless after treatment. CCA treated wood is resistant to leaching by virtue of the fixation of chromium within wood via converting the hexavalent chromium into the less harmful trivalent state (Honeychurch, 2016).

However, these three preservatives, creosote, pentachlorophenol and CCA, are under restricted uses due to the environmental and human health concerns as well as the disposal problems of those treated wood at the ends of their service lives. The voluntarily phasing out of toxic chemicals, such as CCA in residential applications, has drawn increasing attentions on developing new protection methods that can provide significant advantages over existing ones. (Lebow, 2004).

1.1.3.1.2 Current copper-based wood preservatives

Copper-based preservatives, such as Alkaline Copper Quat (ACQ), Copper Azole (CA) and Micronized Copper Azole (MCA) are the major preservatives used now in the treated wood industry. These preservative systems are either based on soluble copper or particulate copper, coupling with carbon-based co-biocide, to provide desirable protection performance. In fact, particulate copper becomes more prevalent than the dissolved formulations as it may require lower concentration to provide similar or even better biocidal effects for wood protection (Kartal et al., 2009).

The fungicidal mechanisms of Cu-based wood preservatives are not yet fully understood. The main questions remained in whether their toxicity is brought by the nanoparticles themselves or by the release of Cu ions, or the synergistic effects in conjunction with secondary biocides (Pařil et al, 2017). Nevertheless, the principal action mode of Cu-based preservatives has been identified, which is due to the large specific

surface area of the nanoparticles that assists in the production of reactive oxygen species (mainly peroxides) (Chen et al., 2006; Oberdürster, 2000). These chemicals induce a series of chain reactions, which cause oxidative stress to the exposed organism and lead to DNA damages (Heinlaan et al., 2008; Saliba et al., 2006), and eventually inhibit the activity of enzymes (Shah et al., 2010).

The other action mode of Cu-based preservatives may induce damages of proteins and mitochondria (Chang et al., 2012) and cause strong interactions with the cell walls of the microorganisms (Heinlaan et al., 2008; Shah et al., 2010) or impair the homeostatic processes by Cu dissolution (Chang et al., 2012).

Cu-based preservatives are effective and inexpensive and have been widely used for wood protection (Freeman and McIntyre, 2008). The major problem of using these preservatives is the low efficiency against Cu-tolerant fungi. Several brown rot fungi, such as *Postia placenta*, *Antrodia xantha*, *Fibroporia radiculosa*, and *Wolfiporia cocos* show the ability to grow and survive at Cu concentrations up to 1.6 mM or 100 mg/kg (Clausen and Green, 2003; Kubicek and Druzhinina, 2007). Other concerns are the negative impacts on our environment due to the accumulation of copper (Sankhla et al., 2016) and questionable effects of ultimate disposal of Cu-based preservatives treated wood (Mohajerani et al., 2018).

1.1.3.1.3 Plant extracts/essential oils as potential wood preservatives

Plant extracts and essential oils are phytochemicals produced by a plant that can help growth and defense against competitors, pathogens, or predators. These chemicals can be obtained from various plants parts (flowers, buds, seeds, leaves, twigs, bark, wood, fruits and roots. etc.) Plant extracts and essential oils have shown promising antimicrobial

properties for wood protection (Murphy, 1999; Singh and Singh, 2012; Yang, 2009). Examples include non-aromatic compounds, such as allyl isothiocyanate (AITC), and aromatic compounds, such as essential oils (EOs).
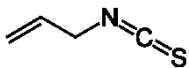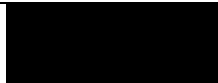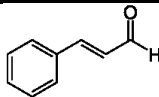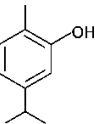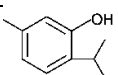
AITC, also known as mustard oil, can be obtained from cruciferous vegetables, such as wasabi, broccoli, and cabbage. These plants are rich in allyl glucosinolate (sinigrin), which can be hydrolyzed to AITC by the enzyme myrosinase released from the plant tissues when they are disrupted. The hydrolysis yield of AITC can reach as high as 90% by a proper cellulolytic pretreatment (Szakacs-Dobozi et al., 1988). The isothiocyanate functional group (N=C=S) is known to confer insecticidal, antibacterial and fungicidal properties (Lin et al., 2000). This functional group affects the metabolic functions of microorganisms by inhibiting the oxygen uptake in yeasts and fungi (Park et al., 2012). It was also reported that AITC could serve as an inhibitor for dehydrogenases and other sulfhydryl enzymes in fungi (Kalnins, 1982). In the wood preservation field, AITC was shown to form a polymer within wood in the presence of pyridine (Kalnins, 1982). Gaseous AITC treatment was proven to be effective in retarding the fungal growth and as a remedy treatment for wood already infested by fungi (Tsunoda, 2000). However, the further use of AITC in wood preservation has been limited by the toxicity of pyridine and the long-term volatility of AITC. Moreover, strong pungent odor and poor solubility of AITC in water have hampered its widespread use.

Essential oils have been reported to exhibit remarkable antimicrobial, antimycotic, antioxidant, and insecticidal activity because of the membrane lytic phenolic compounds (Chapman, 2003; Murphy, 1999). Cinnamon extract (i.e., *trans*-cinnamaldehyde (CN)), clove extract (i.e., eugenol (EG)), basil and oregano extracts (i.e., carvacrol (CV) and

thymol (TM)) have been found to be some of the most effective antimicrobials against wood decay fungi (Singh and Singh, 2012; Yang, 2009). However, many of these compounds are easily oxidized or decomposed in the presence of oxygen, light, or heat (Turek and Stintzing, 2013). Thus, their uses as wood preservatives are problematic due to loss of activity or leaching (Tascioglu et al., 2013).

The detailed chemical structures of the abovementioned natural products are summarized in Table 1.2.

Table 1.2   Physical properties and chemical structure of selected plant-derived antimicrobial compounds

Antimicrobial compound	Chemical formula	Chemical structure	Molar mass (g/mol)	Density (g/cm^3, 20°C)	Class*
Allyl isothiocyanate	C_4H_5NS		99.15	1.01	----
Eugenol	$C_{10}H_{12}O_2$		164.20	1.06	Essential oil
*trans-*Cinnamaldehyde	C_9H_8O		132.16	1.05	Terpenoid
Carvacrol	$C_{10}H_{14}O$		150.22	0.98	Terpenoid
Thymol	$C_{10}H_{14}O$		150.22	0.96	Terpenoid

Note: * According to the classification by Murphy, 1999

1.1.3.1.4   The fixation of borates preservatives systems

Borates are well-known non-metallic water-borne preservatives with excellent fungicidal, insecticidal and fire-retardant properties (Obanda et al., 2008). They also have a low level of toxicity to mammals and the environment. Borates treated wood are non-

corrosive to metal fasteners, colorless, and odorless after treatment. Their natural abundance and relatively low price are desirable as commercially available preservatives. Boron-based preservatives have been reported to account for about 1% of all treated wood in North America (Schultz et al., 2007).

The use of borates as preservatives dates back to ancient Egypt for the preservation of mummies. In 1913, the first record for boron-based wood preservation was proposed by Wolman as chromium-boron. The preservative properties of borates may be mainly attributed to tetrahydroxyborate ion $[B(OH)_4]^-$, which can be formed upon exposure of borates to water (Figure 1.5a). This ion complexes with polyols from the microorganism (Figure 1.5b and c) and thus attack the pathogens through extracellular and intracellular substrate sequestration, enzyme inhibition, and changes in membrane function of the organisms (Figure 1.6) (Lloyd et al., 1990).
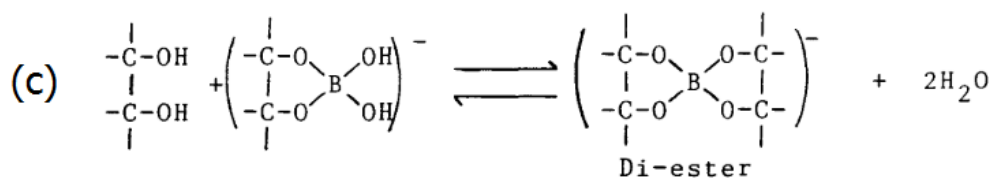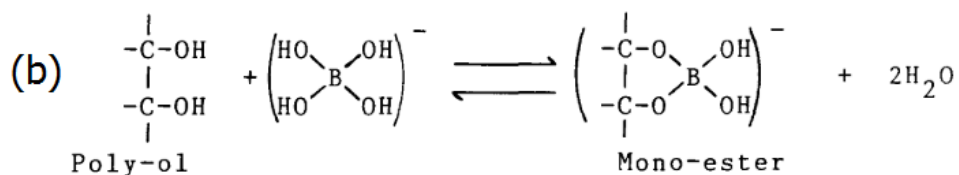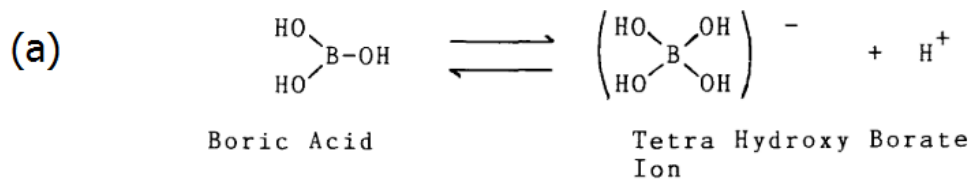
Figure 1.5   (a) Conversion of boric acid to tetrahydroborate ion; (b) formation of mono-ester and Di-ester with *cis*-adjacent hydroxyl groups and α-hydroxyl carboxylic acids in aqueous solution

Reproduced with permission (Lloyd et al., 1990).

The borate ion forms stable complexes with cis-adjacent hydroxyls and alpha-hydroxy carboxylic acids

$$-\overset{|}{\underset{HO}{C}}-\overset{|}{\underset{OH}{C}}=O \qquad -\overset{|}{\underset{HO}{C}}-\overset{|}{\underset{OH}{C}}-$$
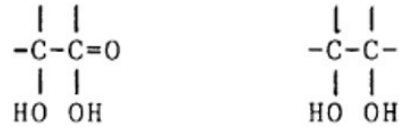
And could have an effect on the following:

Extracellular Substrates	Intracellular Substrates	Vitamins & Co-enzymes	Membranes

Intracellular compounds accumulate/deplete	Enzyme inhibition	Change in membrane function

Altered metabolism	Altered electron transport	Altered transport/uptake change in K^+ flux

Altered phosphorous metabolism

No protein synthesis	No carbohydrate synthesis	No ATP synthesis	No DNA/RNA synthesis

NO GROWTH.

Figure 1.6   Fungicidal mechanism of borates

Reproduced with permission (Lloyd et al., 1990)

Borates can penetrate deeper into wood at higher moisture contents and be used to treat refractory and low permeable wood species, such as Douglas fir (Cabrera and Morrell,

15

2009). However, due to the mobility of borates in aqueous solutions, borates are vulnerable to leaching, which reduces the life-span of borate-treated wood in outdoor applications considerably.

Borate anion cannot be fixed to wood directly because of the repulsive forces between active sites in wood (carboxylic acid and hydroxyl of the phenolic groups) and borates, thus resulting in unstable salts when formed (Cui and Kamdem, 1999). To reduce the leaching of borates from wood, various methods have been adopted, as summarized in several studies (Caldeira, 2010; Freeman et al., 2009; Obanda et al., 2008; Romero et al., 1995; Williams, 2016).

One of the most common approaches is to improve the water-repellence of boron-treated wood by combining borates with polymers, such as resins, paraffin and coatings (Peylo and Willeitner, 1995). Research has also been reported on using different agents, such as albumin and soja protein (Ratajczak and Mazela, 2007; Thevenon et al., 1997), biguanide derivatives (Anderson et al., 1997), carboxyphenylboronic acid (Jebrane and Heinmaa, 2016), furfuryl alcohol (Baysal and Ozaki, 2004; Ozaki et al., 2001), glyoxal/glycerol (Toussaint-Dauvergne et al., 2000), polyethylene glycol (Gezer et al., 2007), and tannins (Efhamisisi et al., 2017; Pizzi and Baecker, 1996; Tondi et al., 2012), to immobilize borates. For example, boric acid was partially fixed to flavonoid tannins by auto condensation and formation of a network inside the wood structure (Pizzi and Baecker, 1996). The leaching of boron from wood was greatly reduced by premixing proteins with boric acid or using premade protein borate salts (Thevenon et al., 1997). Treating wood with sodium borate, then with polyethylene glycol also decreased boron

leaching (Gezer et al., 2007). However, high leachability of boron has not yet been completely addressed.

1.1.3.2   Methods of applying wood preservatives

Injection of preservatives into wood can be done either by pressure or non-pressure treatment (Morrell, 2018). Non-pressure treatments typically include surface treatments methods (*e.g.* brushing, spraying, dipping, cold soaking, steeping, and hot and cold baths (thermal process)), diffusion, vacuum processes, and preservative pads/bandages.

In terms of wood composites, their protection can be achieved by the following methods (Kirkpatrick and Barnes, 2006). First, using natural durable wood species or treated wood as raw materials for composites manufacturing (pre-process treatment). Second, incorporating the biocides during the composites manufacturing process (in-process treatment). The third approach is to treat the finished board with biocides (post-process treatment). The in-process treatment is the most attractive because the biocides can be incorporated into the composites manufacturing process with minor modifications. This process is also considered to be less expensive than conventional pressure treatment. Moreover, there is a possibility that the preservatives can be distributed homogeneously by an efficient blending process (Kirkpatrick and Barnes, 2006).

1.2   β-cyclodextrins (βCDs) as host molecules for antimicrobial guests

1.2.1   Chemical and physical properties of cyclodextrins

Cyclodextrins (CDs) are cyclic oligosaccharides with donut shapes and were first discovered by A.Villiers, a French scientist in 1891, who isolated the crystalline substance from bacterial digests of potato starch (E. M.Martin Del Valle, 2004). Generally, CDs can

be divided into two categories: naturally-occurring CDs and chemically-modified CDs (Szejtli, 1988). There are three major naturally-occurring CDs, namely, α-, β- and γ-CD with 6, 7 and 8 D-glucopyranoside units linked by α-1,4 glycosidic bonds in a ring, respectively (Table 1.3). Among these, βCD is the most attractive because of its commercial availability, low cost and suitable cavity size for a wide range of guest molecules. Chemically-modified CDs can be obtained by substituting one or more hydrogen atom of the primary and/or secondary hydroxyl to form various cyclodextrin derivatives. The most commonly used βCD derivatives are hydroxy propylated-β-cyclodextrins (HPβCDs) and methylated β-cyclodextrins (MβCDs), which have significantly higher aqueous solubility than the native βCD.

Table 1.3   Basic properties of native cyclodextrins (CDs)

Property	α-CD	β-CD	γ-CD
Number of glucopyranose units	6	7	8
Molecular weight (g/mol)	972	1135	1297
Solubility in water at 25 ∘C (%, w/v)	14.5	1.85	23.2
Outer diameter (Å)	14.6	15.4	17.5
Cavity diameter (Å)	4.9-5.3	6.0-6.5	7.5-8.3
Height of torus (Å)	7.9	7.9	7.9
Cavity volume (Å3)	174	262	427

Adapted from E. M Martin Del Valle (2004)

The truncated cone shape of cyclodextrins is resulting from the linking of various chair forms of glucopyranose units in a ring. This unique conformation imparts CDs with hydrophilic exteriors and hydrophobic interiors. The inner and outer diameters of CDs are 0.47-0.83 nm and 1.46-1.75 nm, respectively (Turek and Stintzing, 2013). The detailed structures of βCD and its commonly used derivatives are shown in Figure 1.7.
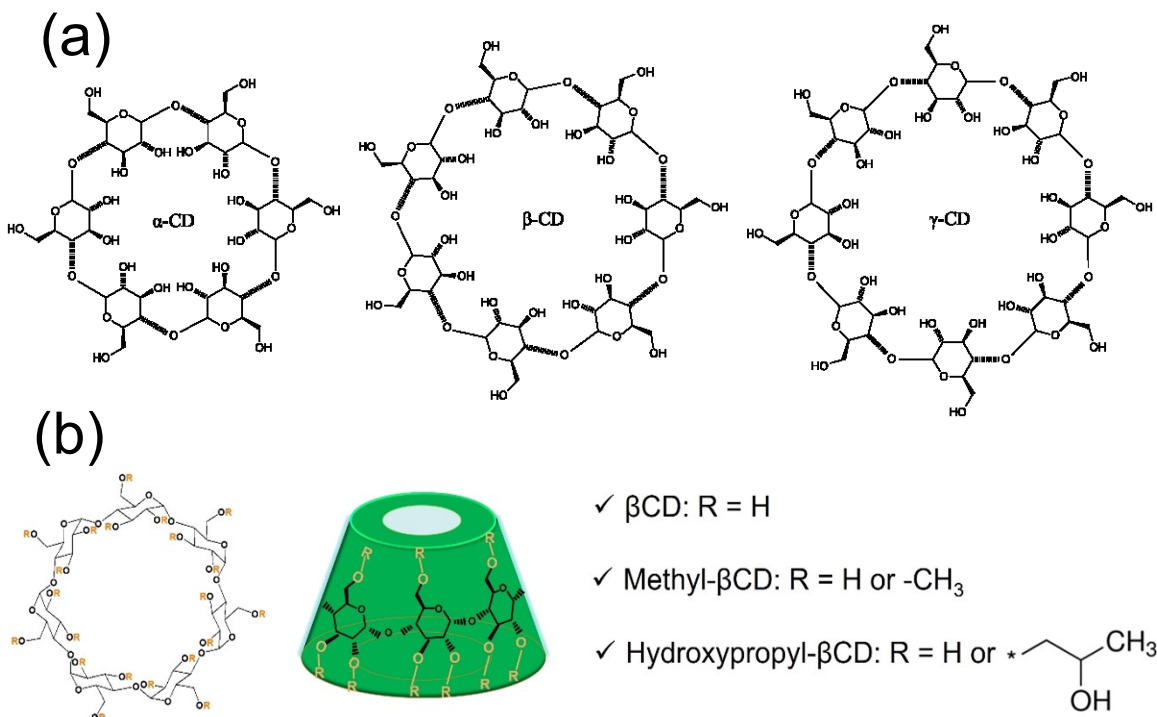
Figure 1.7   Chemical structure of (a) perspective drawing of native CDs and (b) methyl-βCD (MβCD) and hydroxypropyl-βCD (HPβCD)

1.2.2   Complexation of cyclodextrins with guest molecules and their applications

Cyclodextrins can be used as hosts to encapsulate a wide variety of guest molecules, such as plant extracts and essential oils, and the formation of the inclusion complex can be achieved either in a solution or crystalline state (Szejtli, 2013). During the encapsulation process, enthalpy-rich water in the cavity of cyclodextrins is replaced by guest molecules (Figure 1.8). The main driving forces for this process are *Van der Waals* force, hydrophobic effect and dipole-dipole interactions (Marques, 2010). The formation of the complex is affected by various factors including types of cyclodextrins, host-guest ratio, preparation

techniques (co-precipitation and kneading method), and drying methods (spray, vacuum and freeze drying) (Wadhwa et al., 2017).

Hydrophobic compound   **Cyclodextrins**   **Complexes**
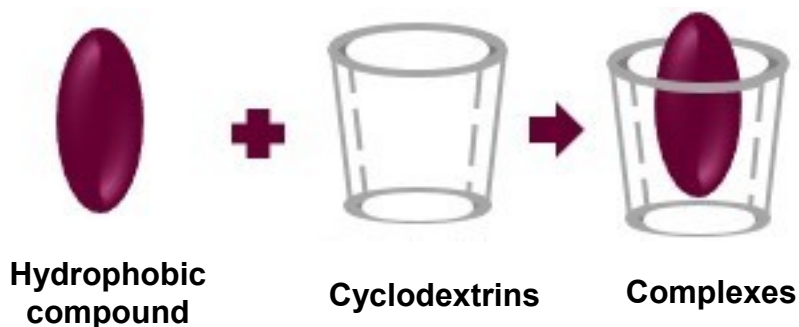
Figure 1.8   Schematic representation of cyclodextrin inclusion complex formation

The capability of cyclodextrins to encapsulate guest molecules offers several advantages: 1) improving the solubility of guest molecules, 2) enhancing the stability of liable compounds against degradation due to light, heat, volatilization, and oxidation, 3) masking the unpleasant odors, and 4) providing controlled release of guest molecules. These advantages allow the applications of cyclodextrin complexes in various products, such as pharmaceuticals (Jansook et al., 2018), foods (Ozkan et al., 2019), cosmetics, toiletry (Muthumani et al., 2015; Trinh et al., 1997), and pesticides (Mattos et al., 2017).

For example, different types of cyclodextrins and their derivatives have been used to encapsulate AITC to suppress its volatility and mask the unpleasant odor. The studies examined the inclusion of AITC into αCD, βCD, MβCDs and HPβCDs (Zhang et al., 2007; Neoh et al., 2012). The retention of AITC in MβCD-AITC was reported to be as high as 80% when exposed at 120 °C for 30 min (Neoh et al., 2012). The controlled release of

AITC from βCD-AITC can effectively suppress fungal and bacterial growth on food packaging materials (Aytac et al., 2014; Piercey et al., 2012).

The encapsulation of essential oils in cyclodextrins has been described in details elsewhere (Kfoury et al., 2018). The complexation of essential oils, such as eugenol, linalool, thymol, carvacrol and *trans*-cinnamaldehyde, with cyclodextrins showed improved solubility and stability as well as taste masking, which have been demonstrated potential for food pathogen control (Hill et al., 2013; Kayaci et al., 2013; Chun et al., 2015; Santos et al., 2015; Celebioglu et al., 2018). In addition, incorporating textile material with cyclodextrin-cedar oil showed prolonged antimicrobial properties compared to that containing free cedar oil (Voncina and Vivod, 2013).

Boric acid can be fixed to βCDs through the formation of a covalent bond (Bhat and Chandrasekaran, 1996). The resultant βCDs-boric acid complex (βCD-B) has high thermal stability and decomposes at temperatures above 200°C (Baur and Macholdt, 2000), making it attractive for treatment of wood composites prior to hot pressing. βCD-B has potential applications for the production of toners, powder coatings, binders for electret materials and as chemical catalysis (Baur and Macholdt, 2000). βCD-B has not been evaluated for wood composite preservation.

1.3   Overview and organization of the dissertation

1.3.1   Objectives

The overall objectives of this study were (1) to address the feasibility of using cyclodextrins as agents to improve the inherent instability problems of two wood preservatives systems: (A) volatile natural antimicrobial compounds (i.e., allyl isothiocyanate and essential oils) and (B) water-borne preservatives (i.e., borates), and (2)

to assess the efficacy of the proposed preservatives systems against fungi for southern yellow pine wood and strand-based wood composites.

The specific objectives were:

1) To investigate the feasibility of β-cyclodextrins as sustained-release carriers for non-aromatic natural antimicrobial compound (i.e., allyl isothiocyanate) and assess the antifungal properties of the cyclodextrin complexes in solid wood

2) To study the fungi-resistance of aromatic natural antimicrobial compounds (i.e., eugenol, *trans*-Cinnamaldehyde, thymol, and carvacrol) encapsulated in cyclodextrins for solid wood protection

3) To explore the applicability of β-cyclodextrins- allyl isothiocyanate as a natural preservative for strand-based wood composites

4) To study the feasibility of cyclodextrins as "fixing agent" for boric acid and assess their antifungal properties for strand-based wood composites

1.3.2   Organization of the dissertation

Chapter 1 lays the backgrounds of how wood deteriorated by various fungi and the commonly used wood preservation methods. This chapter also proposes the issues exist in current wood preservative systems and introduces the basic concepts and approaches to examining the feasibility of βCDs for the stabilization of volatile natural antimicrobial compounds and leachable borates.

The detailed experimental methods were described in Chapter 2, which includes the preparation and confirmation of cyclodextrins complexes, treatment of wood with cyclodextrin complexes, and the soil block test procedures.

Chapter 3 and 4 present the findings of the effect of βCD complexes on the fungal resistance of wood. The feasibility of using βCD-AITC complex for randomly Oriented Strand Board (OSB) protection and the results were presented in Chapter 5.

In Chapter 6, βCD-B complex was added in OSB construction. The interaction between the preservative and resin was studied. The density profiles and internal bonding strength of the constructed panels, as well as the fungal resistance of the treated panels, were presented.

Chapter 7 includes the summary of this dissertation and recommendations for future studies.

CHAPTER II

EXPERIMENTAL DETAILS

2.1   Materials

Southern pine (*Pinus Spp.*) sapwood samples were cut to 14 mm × 14 mm ×14 mm ($L \times T \times R$, end matched) and 5 mm × 19 mm ×19 mm ($L \times T \times R$, end matched) according to American Wood Protection Association Standard E10-16 (AWPA, 2016a) and E22-16 (AWPA, 2016b), respectively. The soil used for soil block test was collected from Dorman site at Starkville, Mississippi and was screened through a sieve of approximately 6 to 8 mesh for further use.

β-cyclodextrins (βCD, 98%), methyl-β-cyclodextrin (MβCD, ≥ 98%, M_w 1,303.3 g/mol), hydroxypropyl-β-cyclodextrin (HPβCD, 97%, M_w 1,180.05 g/mol), ethanol (99.5%), eugenol (EG, 99%), *trans*-cinnamaldehyde (CN, 99%) and thymol (TM, 99%) were purchased from Acros Organics. Allyl isothiocyanate (AITC, ≥ 94.5 %) and toluene (99.8%) were supplied by Sigma-Aldrich. Carvacrol (CV, ≥98.0% (GC)) was obtained from TCI America while acetonitrile (HPLC Grade) was bought from Fisher Chemical. Polymeric methylene diphenyl diisocyanate (pMDI, 100% solid content), and commercial southern pine wood strands were generously furnished by Huntsmen (Conroe, TX) and Norbord Inc (Guntown, MS), respectively. The degree of substitution (DS, the average number of substituents on a cyclodextrin molecule) of MβCD is between 1.7 and 1.9, which corresponds to 0.24 to 0.27 substituents per glucose unit. DS of HPβCD is between 2 and

24

6, which corresponds to 0.28 to 0.86 substituents per glucose unit. These substituents in HPβCD are located mainly at O (2) of the anhydroglucopyranose units. All the chemicals were used as received without further purification.

2.2   Preparation of βCD complexes

2.2.1   Preparation of βCD-allyl isothiocyanate (AITC) complexes

MβCD-AITC complex was prepared using a co-precipitation method with minor modifications (Li et al., 2007). Briefly, aqueous solutions of different concentrations of MβCD (1, 3, 10, 20, 50, 60 and 65 w/v (%)) were prepared by using distilled water at room temperature. AITC in ethanol (1:1, v/v) was slowly added to the solution with continuous stirring (Figure 2.1). The molar ratio of AITC to MβCD was kept constant at 3:1. A vessel containing the mixture was sealed and kept under stirring for 6 h. The resulting slurry was equilibrated at 4 °C for 24 h and the free AITC on the surface was pipetted out. The slurry was subjected to liquid nitrogen before freeze-drying for 36 h. The dry complex in a powder-form was stored in an airtight glass desiccator at room temperature before further analysis.

HPβCD-AITC complex was prepared by the same procedure except that the concentration of HPβCD solution used was varied between 10 to 70 w/v (%) at an interval of 20 w/v (%). For βCD-AITC complex, the βCD solutions of 1, 3 and 5 w/v (%) were used to encapsulate AITC.

MβCD-EOs complexes were also prepared in the same manner except that different MβCD water solutions (10, 30 and 50 w/v (%)) and molar ratios of MβCD to EOs (1:0.5, 1:1, 1:1.5 and 1:2) were used.
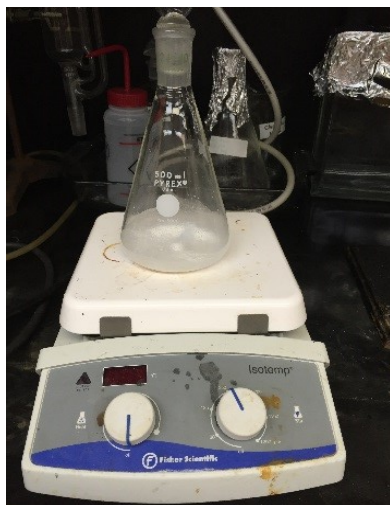
Figure 2.1   Preparation of β-cyclodextrin complexes in the hood

2.2.2   Preparation of βCD-borates complex

The βCD-B complex was prepared by mixing βCD with boric acid at a molar ratio of 1:7 and refluxing the mixture in toluene in a Dean-Stark apparatus for 18 h (Bhat and Chandrasekaran, 1996) (Figure 2.2). The residual toluene was removed in a rotary evaporator and the resultant mixture was kept in a desiccator prior to analysis.
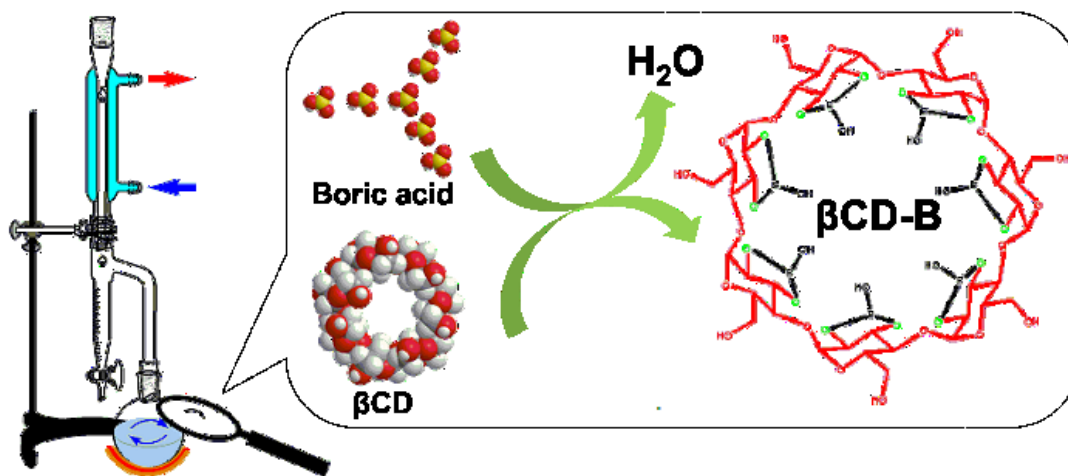
Figure 2.2   Schematic of the process for preparing β-cyclodextrin-boric acid complex

2.3   Characterization of βCD complexes

2.3.1   Attenuated total reflection - Fourier-transform infrared spectroscopy (ATR-FTIR)

To confirm the formation of βCD complexes, spectra of obtained powders were analyzed by Attenuated total reflection - Fourier-transform infrared spectroscopy (ATR-FTIR, PerkinElmer Spectrum Two equipped with a universal ATR element, Perkin Elmer Ltd, Bucks, UK). Three replicates of ATR-FTIR spectra in the spectral range of 4000 to 400 cm^{-1} at a resolution of 4 cm^{-1} were obtained for every sample. The spectra were baseline-corrected and normalized over the total spectral area using Spectrum® Quant software (PerkinElmer, Waltham, MA, USA).

2.3.2   Ultraviolet-visible spectrophotometry (UV/VIS)

The inclusion yield of AITC or EOs in βCDs was estimated using an Ultraviolet-visible spectrophotometry (UV/VIS) method (Zhang et al., 2007), which consisted of 1) estimating the amount of encapsulated AITC or EOs in βCDs and 2) taking the ratio

27

between an encapsulated and theoretical maximum of encapsulated AITC or EOs in βCDs. In a typical example, 10 mg of βCD-AITC complex dissolved in 200 μl DI water was mixed with 10 mL hexane in a test tube, which was subjected to 2 cycles of 10 min of ultrasonication to free encapsulated AITC. The mixture was centrifuged at 3000 rpm for 10 min and the supernatant was analyzed using a UV-Vis spectroscopy (Cary 100 Bio UV-Vis double-beam spectrophotometer). Each sample was extracted in triplicate and all measurements were carried out at room temperature. The amount of encapsulated AITC in βCDs was determined by using the calibration curve in Figure 2.3(b), which displayed a linear relationship between the concentration of AITC (C_{AITC}) and an absorbance intensity at 249 nm in the range of 0.1 to 2 mM ($r^2 = 0.999$). Thus, the mass ratio of encapsulated AITC in the βCD-AITC complex was calculated as follows:

$$\text{AITC}_{encapsulated} \ (g/g) = \frac{C_{AITC} \times M_{AITC} \times V}{m} \tag{2.1}$$

where,

C_{AITC} − Concentration of AITC from βCD-AITC complexes extracted by hexane (mol/L)

M_{AITC} − molecular weight of AITC (g/mol)

V − total volume of the supernatant (L)

m − amount of βCD-AITC used for inclusion yield estimation (g)

The theoretical maximum of AITC encapsulation in βCD is known to be 1 mole of AITC in 1 mole of βCD (Zhang et al., 2007). Thus, the inclusion yield of AITC in βCD can be determined using the equation below:

$$Inclusion \ yield \ (\%) = \frac{\text{AITC}_{encapsulated} \ (g/g)}{\text{AITC}_{theoretical} \ (g/g)} \times 100 \tag{2.2}$$

where $AITC_{theoretical}$ is the maximum mass ratio of encapsulated AITC in the βCD-AITC

complex based on the mole ratio of AITC to MβCD-AITC, HPβCD-AITC or βCD-AITC.
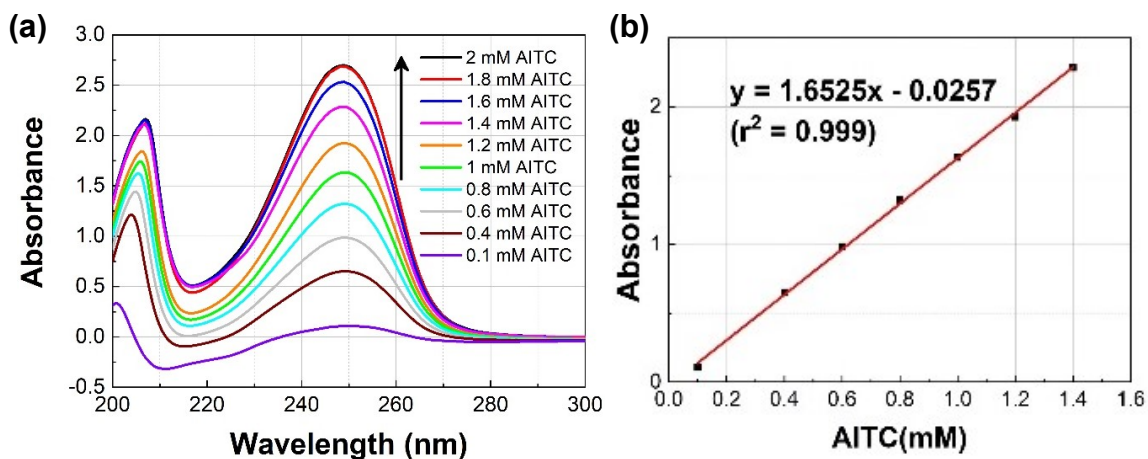
Figure 2.3   (a) UV-Vis absorption spectra of AITC in hexane at various concentrations and (b) the calibration curve.

For determination of the estimated amount of EOs in MβCD-EOs complexes, all

the experiment steps were the same except that 5 mg of the complex was mixed with 0.5

mL deionized water and 4.5 mL acetonitrile by a vortex mixer for 5 minutes at room

temperature. The calibration curve of different essential oil compounds in acetonitrile is

shown in Figure 2.4 to 2.7.
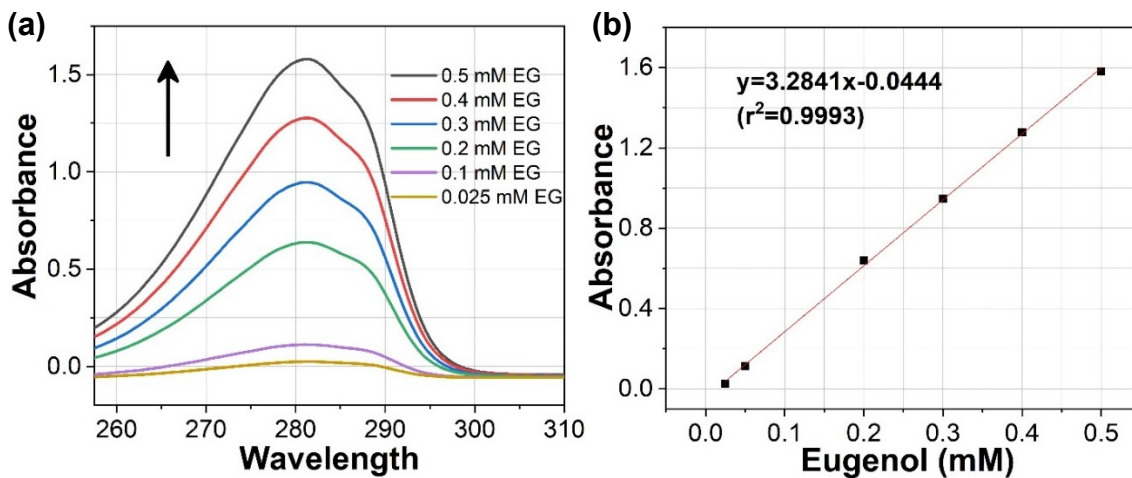
Figure 2.4   (a) UV-Vis absorption spectra of Eugenol (EG) in acetonitrile at various concentrations and (b) the calibration curve.
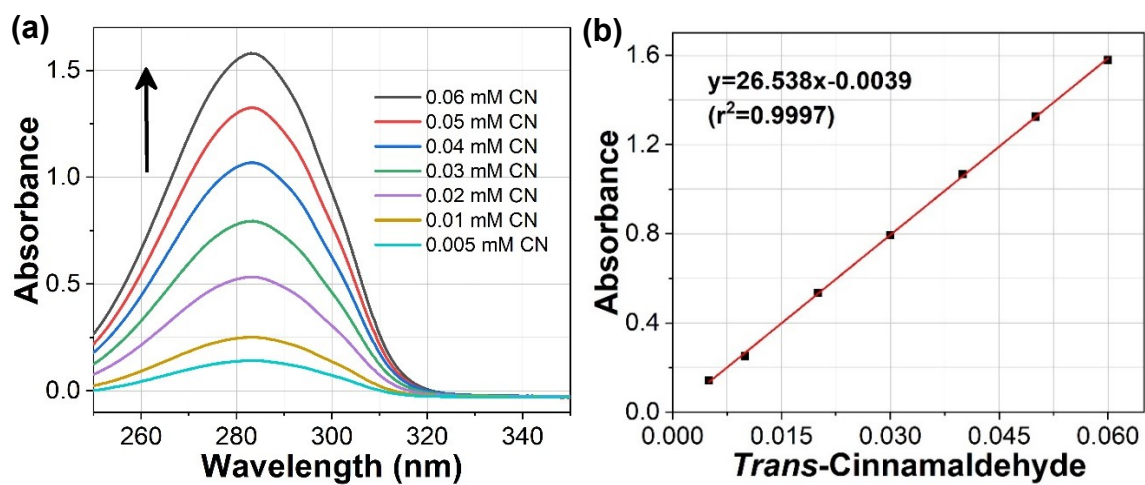
Figure 2.5   (a) UV-Vis absorption spectra of *tran*s-Cinnamaldehyde (CN) in acetonitrile at various concentrations and (b) the calibration curve.
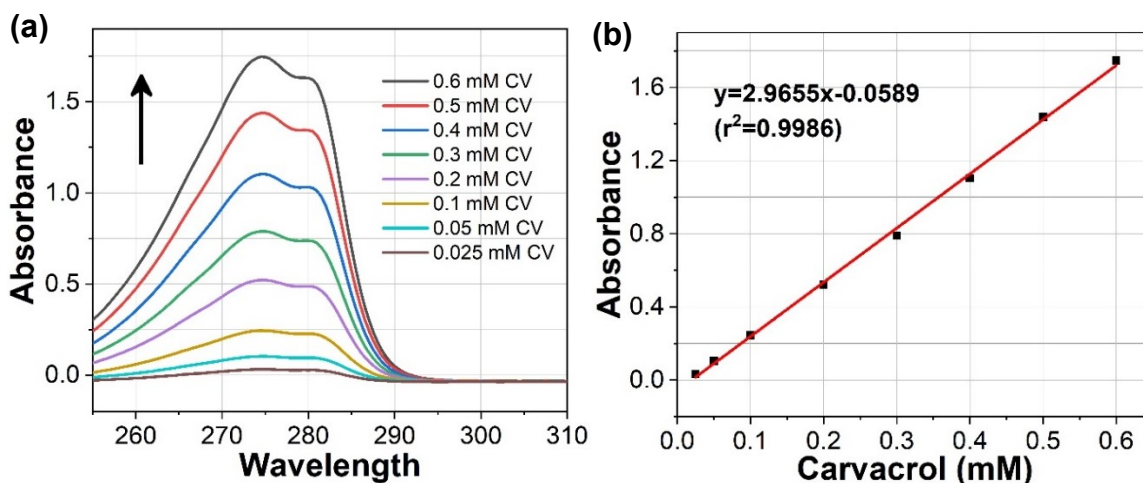
Figure 2.6   (a) UV-Vis absorption spectra of Carvacrol (CV) in acetonitrile at various concentrations and (b) the calibration curve.
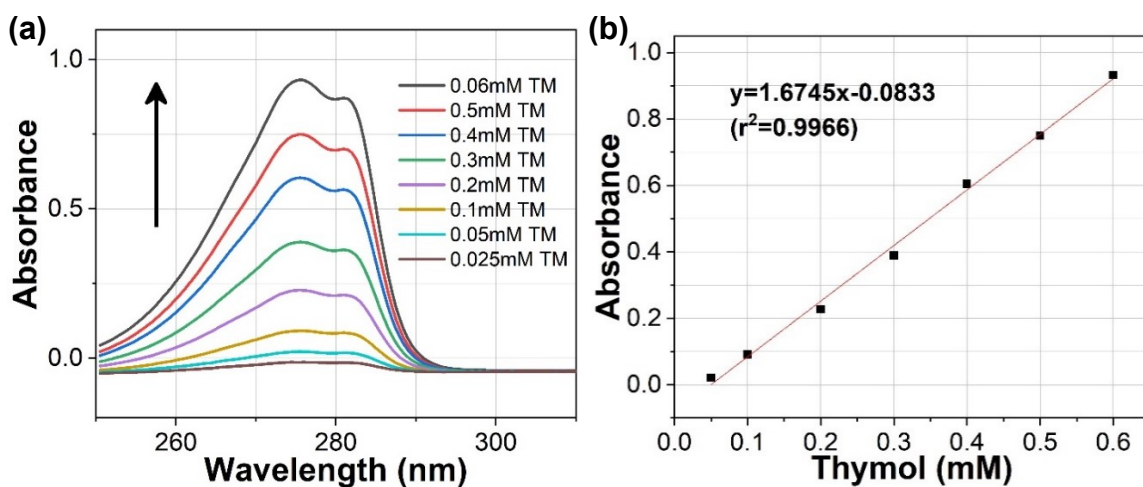
Figure 2.7   (a) UV-Vis absorption spectra of thymol (TM) in acetonitrile at various concentrations and (b) the calibration curve.

2.3.3   Nuclear magnetic resonance spectroscopy (NMR)

The βCD complex was further confirmed by ^{11}B and ^{1}H NMR using a Bruker AVANCE III spectrometer operated at 500 MHz. Deuterated dimethyl sulfoxide-d6

(DMSO-d6) was used as the solvent and tetramethylsilane (TMS) was used as an internal reference. The solutions were transferred into a 5 mm NMR tube to total sample height of 4 cm. The probe temperature was maintained at 25°C. Chemical shifts were expressed in parts per million downfield from the signal (0 ppm) of TMS.

2.3.4   Thermogravimetric Analyzer (TGA)

The effect of AITC encapsulation with βCD on heat stability was evaluated using a Thermogravimetric Analyzer (SDT Q600, TA Instruments Inc). The alumina pans loaded with 5 ± 0.5 mg samples were heated from room temperature to 600 ºC at a heating rate of 10 ºC /min with a nitrogen flow of 100 mL/min. βCD and βCD-AITC complex were freeze-dried to constant weight before the analysis, and each sample was analyzed in duplicate.

2.3.5   Scanning electron microscopy (SEM)

SEM (JSM-6500F, JEOL USA, Inc) was used to observe the morphologic changes of βCD complexes. The samples were fixed on an SEM stub using double-sided conductive carbon tape. Prior to examination, samples were sputter-coated with platinum (20 nm thick). The samples were photographed at a voltage of 5.0 kV.

2.4   Impregnation of wood in βCD complexes solutions in water

All wood cubes were submerged in a given treating solution and subjected to vacuum (3.33 kPa) for 3 h (Figure 2.8). The vacuum was released and the samples were then left in the solution for 6 h. For AITC complexes treatment, aqueous solutions of 50 w/v (%) MβCD- and HPβCD-AITC were used based on the maximum encapsulation yield of AITC in βCD-AITC. Negative control samples were treated in the same manner with distilled water, while positive controls were treated with 2% AITC in 10% ethanol.

In terms of EOs complexes treatment, three levels of MβCD-EOs aqueous solutions (10, 30 and 50 w/v (%)) were tested. The control groups were treated in a similar way with distilled water (negative control) or with 5% of a given EOs in 10% ethanol/water solution (positive controls).
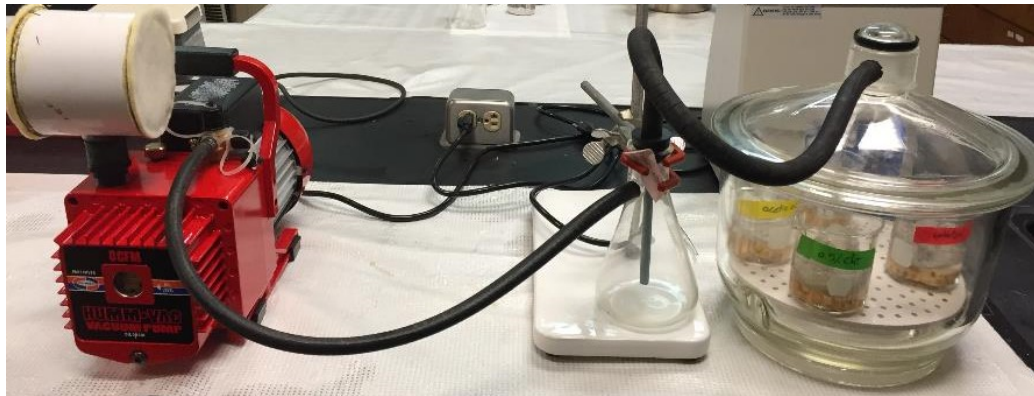
Figure 2.8   Impregnation of wood in βCD complexes solutions in water

2.5   Mass gain and bulking

Chemical uptake was measured in terms of mass and volume. The oven-dry mass of the samples before and after the treatment was measured to calculate the mass gain. The treated wood cubes were first air-dried at room temperature for 24 h, and subsequently oven-dried at 40 °C for another 24 h. Volumetric changes or bulking due to the incorporation of the chemicals into the cell walls were measured by buoyancy force in mercury (Jeremic and Cooper, 2009) (Figure 2.9). The mass gain and bulking were calculated as follows:

$$\text{Mass Gain (\%)} = \frac{(m_{trt.} - m_{untrt.})}{m_{untrt.}} \times 100 \qquad (2.3)$$

$$\text{Bulking (\%)} = \frac{(V_{trt.} - V_{untrt.})}{V_{untrt.}} \times 100 \qquad (2.4)$$

where $m_{untrt.}$ and $m_{trt.}$ were the oven-dried mass of samples before and after the treatment, respectively. $V_{untrt.}$ and $V_{trt.}$ were the oven-dried volume of samples before and after the treatment, respectively.
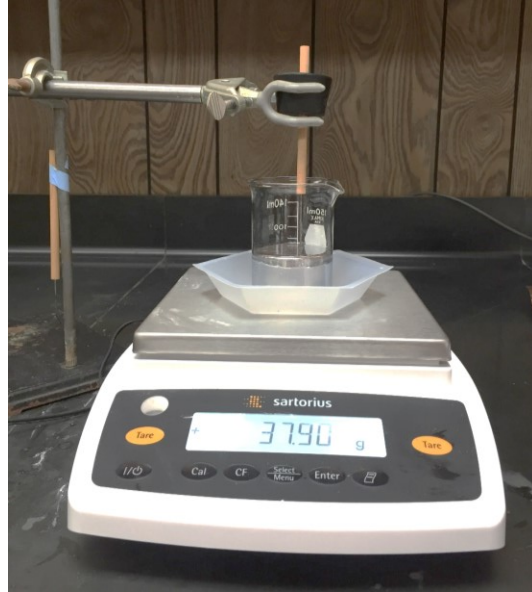
Figure 2.9   Measuring the volume of wood by buoyancy force in mercury

2.6   Estimation of preservatives amount in wood

The amount of active ingredients (AITC and EOs) in wood (*mass gain by active ingredients)* was calculated according to the inclusion yield (section 2.3.2) and mass gain data using the following equation:

$$Mass\ gain\ by\ active\ ingredients\ (\%) = \text{mass gain} \times \text{inclusion yield} \times$$
$$\text{theoretical maximum of encapsulated AITC or EOs} \qquad (2.5)$$

2.7   **Decay resistance test (soil block test)**

2.7.1   **Determination of soil water-holding capacity**

The sieved soil was transferred into the Buchner funnel (approximately 50 in diameter and 25 mm in depth) fitted with rapid-filtering paper. The soil was compacted by dropping the funnel through a height of 10 mm on a wooden table top three times. The excess soil on the top of the funnel was leveled by spatula and moved away. The filled funnel was transferred into a 400 mL beaker and retained in an upright position by wedges at the sides of the funnel. Water was added to the beaker to a depth slightly above the filter paper, which moistens the soil by capillarity, as shown in Figure 2.10. When the upper soil surface showed signs of wetting, more water was added again to the beaker to a depth slightly above the filter paper. The beaker was covered to allow the soil to soak for at least 12 hours.

Figure 2.10   Soil substrate filled in a Buchner funnel in a beaker

Then the soil-filled funnel was transferred to a suction flask, which is connected to a water aspirator (Figure 2.11). A full suction of 15 minutes was applied. Several spoons

of the obtained soil were weighed (denoted as W_1) and were oven dried (105 °C ±2°C) to a constant weight (denoted as W_2).
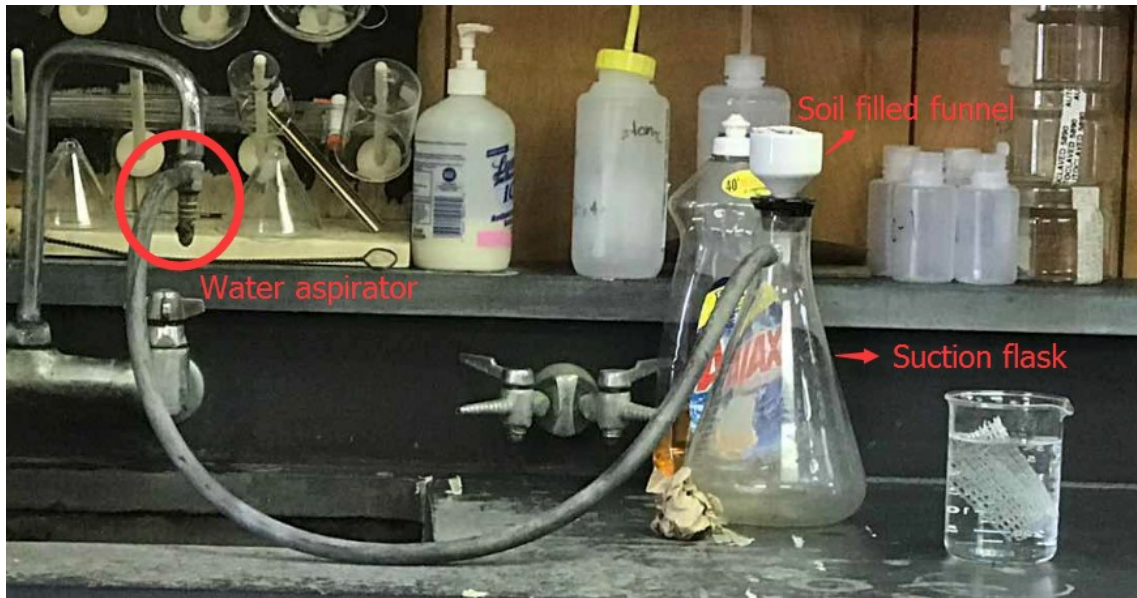
Figure 2.11   The suction of water from the soil

The water-holding capacity (WHC) of the soil was determined based on the following equation:

$$\text{WHC (\%)} = \frac{W_1 - W_2}{W_2} \times 100 \tag{2.6}$$

where W_1 and W_2 represent the mass of soil before and after oven drying, respectively.

2.7.2   Calculation of the soil for culture bottles

The air-dried soil (3/4 cup, weighed as W_3) was oven dried to a constant weight (W_4). The weight of the container was emptied. The amount of water needed to add to each culture bottles was calculated according to equation 2.7:

$$\text{Water added} = (0.13 \times \text{WHC} \times W_4) + (W_4 - W_3) \tag{2.7}$$

2.7.3 Preparation of Soil substrate

Based on the calculation (equation 2.7) of water needed for the soil in culture bottles, 3/4 cup of the air-dried soil was added slowly in a circular motion to a container that filled with 80 mL distilled water. Two feeder strips were placed on the top of the soil. Pine for brown rot and aspen for white rot. The containers were covered by lids with cotton plugs on the top and then wrapped with the foil. The culture bottles were autoclaved for 45 minutes and cooled under the hood for further use.

2.7.4 Inoculation with fungi

The plug plates (shown in Figure 2.12) were placed under the hood and the fungi inside the plates were cut by flame spatula. In each culture bottle, six plugs of fungi cut from the outer edge of the plate were placed upside down on the soil next to the feeder strips. The containers were closed with the lids and placed in the incubator for about 2 weeks.
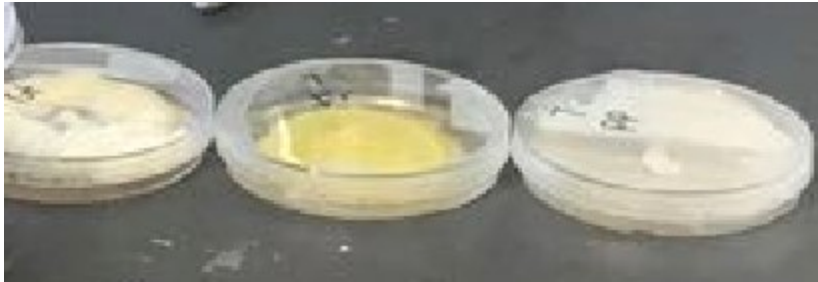
Figure 2.12   Fungi plates for soil block tests Suction of water from the soil

2.7.5 Sterilization and incubation of test blocks

The accelerated weathering of the samples was conducted before soil block test. Different accelerated weathering procedures were performed based on the intrinsic

properties of natural antimicrobial compounds and boric acid. The volatility test of βCD-AITC or βCD-EOs treated samples and the water leaching procedure for βCD-B treated OSB cubes were investigated according to AWPA Standard E10-16 (AWPA, 2016a) and AWPA Standard E11-16 (AWPA, 2016c), respectively.

Specifically, half of the samples were weathered per the procedure described for oil-type preservatives in order to compare the long-term performance of βCD complexes (βCD-AITC and βCD-EOs) preservatives with AITC-treated controls or EOs-treated controls. Each treatment was immersed in 400 ml of distilled water for 2 h at room temperature and then weathered in a forced-air oven for 334 h at 50°C. Six replicates were used for βCD-AITC treatments while eight replicates were used for MβCD-EOs treatments. The weathered test blocks were evaluated in the soil block test.

In terms of βCD-B-treated OSB, the specimens were subjected to a leaching period following procedures described in AWPA Standard E11-16 prior to decay testing. Briefly, 12 blocks from each treatment were placed into leaching vessels and weighed down to prevent floating. 240 mL of deionized water was added to each vessel, and the vessels were placed at room temperature on an orbital shaker rotating at a speed of 100 rpm. After 6, 24, 48 h and thereafter at 48 h intervals, 100 ml of leachate was removed from the vessels, and replaced with an equal amount of fresh deionized water. The leaching was performed for a total of 14 days.

The effect of βCD complexes on the fungal resistance of southern pine was evaluated according to the AWPA Standard E10-16 with minor modifications (AWPA, 2016a). The modifications included the number of replicates and sterilization of the samples. Samples were surface sterilized by dipping them into a 70% aqueous ethanol

solution for 10 s, followed by drying in a laminar flow cabinet. For βCD-AITC treatment, six replicates from each treatment were exposed to either a brown rot fungus (*Gloeophyllum trabeum*) for 8 weeks or a white rot fungus (*Trametes versicolor*) for 16 weeks at $26 \pm 2^{\circ}C$ and $78 \pm 2\%$ relative humidity in an incubator (Figure 2.13). For MβCD-EOs treatment, eight replicates were exposed to two brown rot fungi *Gloeophyllum trabeum* and *Postia placenta* for 4 weeks. Both weathered and un-weathered samples were used for a soil block test. For Decay resistance was evaluated in terms of mass loss, which was calculated as follows:

$$\text{Mass loss (\%)} = \frac{(m_{trt.} - m_{trt.\&expo.})}{m_{trt.}} \times 100 \tag{2.8}$$

where $m_{trt.}$ and $m_{trt.\&expo.}$ were an oven-dried mass of samples before and after exposure to fungi.

The decay resistance of βCD-AITC or βCD-B treated OSB was evaluated in the same way as described above except that twelve replicates were used.
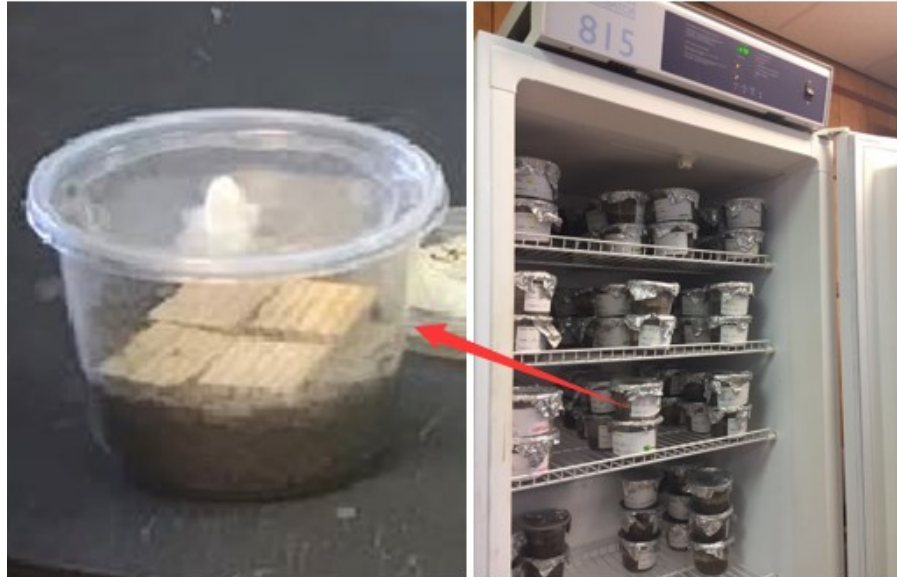
Figure 2.13   Samples in an incubator (at $26 \pm 2^\circ$C and $78 \pm 2\%$ relative humidity)

2.8   Scanning electron microscopy coupled with energy dispersive X-ray (SEM-EDX) analysis of wood and strand-based composites before and after exposure to fungi

Wood samples from different treatments used for SEM imaging were microtomed to 200 µm thick cross sections and were sputter-coated with platinum (30 nm thick). SEM images and elemental mapping of wood before exposure to fungi were taken at 15 kV (EVO50, Zeiss coupled with EDX, Bruker 133eV). Elemental mapping was collected at a working distance of 10 mm and the acquisition time of 300 s. SEM images of decayed wood were recorded by SEM (JSM-6500F, JEOL USA. Inc) at 5 kV. The tested samples include untreated samples before exposing to fungi, untreated and treated samples after exposing to fungi. Two replicates from each treatment were used for SEM imaging and the representative images were presented in this work.

40

2.9   Statistical analysis

All the statistical analyses were performed using commercial software, SAS (9.4, SAS Institute Inc., Cary, NC). Prior to analysis, the data were tested for normality with the Shapiro-Wilk test and Q-Q plots using the PROC UNIVARIATE function. One-way analysis of variance (ANOVA) along with the homogeneity of variance analysis was implemented using PROC ANOVA function. If the assumption of homogeneity of variance was satisfied ($p > 0.05$), then PROC GLM function was used for multiple comparisons. Otherwise, Games-Howell test was used. Also, the LSMEANS statement was used to examine the differences between the means of the treatment groups. The results were interpreted at a significance level of 0.05.

CHAPTER III

β-CYCLODEXTRINS AS SUSTAINED-RELEASE CARRIERS FOR NON-

AROMATIC NATURAL WOOD PRESERVATIVE: USING ALLYL

ISOTHIOCYANATE AS A MODEL MOLECULE

Authors: Lili Cai, Dragica Jeremic, Hyungsuk Lim and Yunsang Kim

The objective of this study is to investigate the utility of βCD as a sustained-release carrier of AITC as a natural wood preservative. In this proof-of-principle study, AITC was encapsulated within the cavity of βCDs and the βCD-AITC complexes were tested as natural wood preservatives. Two βCD derivatives, MβCD and HPβCD, were selected because of their enhanced water solubility compared to pristine βCD. The formation of βCD-AITC complexes was confirmed by Attenuated total reflection - Fourier transform infrared (ATR-FTIR) spectroscopy and the maximum inclusion yield of AITC in MβCD and HPβCD was estimated by ultraviolet-visible (UV-Vis) spectroscopy. The βCD-AITC complexes were applied to southern yellow pine wood cubes via impregnation in the aqueous complex solution. Fungal resistance of the treated wood was evaluated by soil block decay test.

For Materials and methods, please refer to Chapter 2.

3.1 Results and discussion

3.1.1 Formation of βCD-AITC complexes

The inclusion of AITC in MβCD and HPβCDs was qualitatively investigated by ATR-FTIR (Figure 3.1). The neat AITC was characterized by the appearance of N=C=S out-of-phase stretching bands at 2082 cm^{-1} and at 2165 cm^{-1}, as shown in Figure 3.1a and 3.1b at different spectra ranges. In MβCD- and HPβCD-AITC complexes, peaks in the vicinity of the neat AITC peaks indicated the presence of AITC in these compounds, with peak maxima shifting from 2165 and 2082 cm^{-1} to 2161 and 2105 cm^{-1}, respectively, due to the different bond environment. Overall, the relative intensity of the peaks from isothiocyanate in the HPβCD-AITC complex was lower than that in the MβCD-AITC complex in the spectra normalized to 1050 cm^{-1} (C-O-H) peak. This suggests the lower level of AITC inclusion in HPβCD and can be ascribed to the varying structure of βCD derivatives (Buchanan et al., 2007).
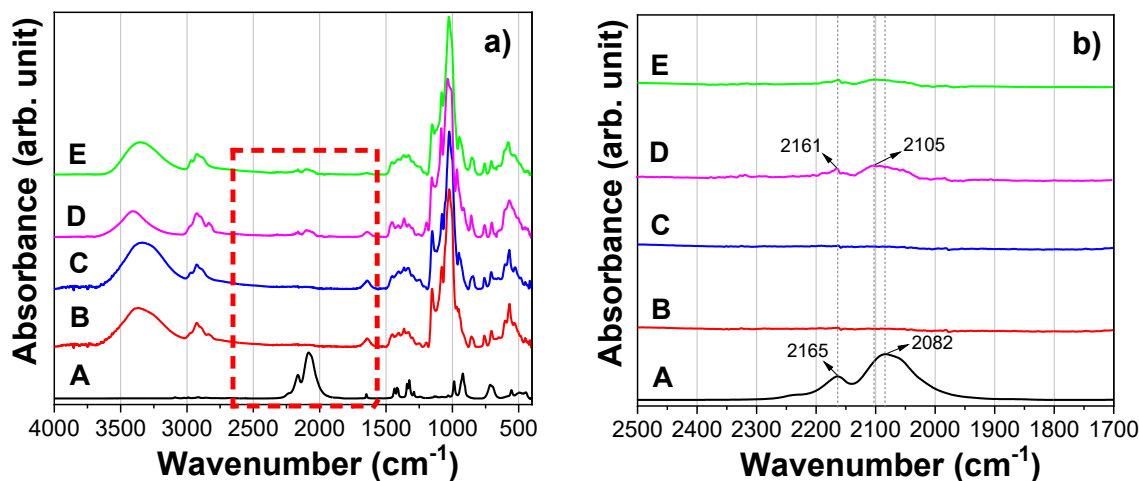
Figure 3.1   a) Infrared spectra of (A) neat AITC, (B) MβCD, (C) HPβCD, (D) MβCD-AITC complex, and (E) HPβCD-AITC complex. Spectra shown in (B) to (D) are normalized to 1050 cm^{-1} (C-O-H) peak. b) The same spectra in the range of 2500-1700 cm^{-1}.

The inclusion yield of AITC was quantitatively determined by UV-Vis absorbance. The inclusion yield of AITC reached a maximum of 39 % at aqueous MβCD concentration of 50 w/v (%) (Figure 3.2b). This is in accordance with a previous study showing AITC inclusion yield plateaued at an MβCD concentration around 50% (Landy et al., 2000). Thus, 50 % (w/v) MβCD was chosen for further wood treatment. However, the inclusion yield of AITC in HPβCD was not significantly affected by HPβCD concentration, as confirmed by ANOVA statistical analysis ($p < 0.05$), and was estimated to be around 14% (Figure 3.3). The lower inclusion yield of AITC in HPβCD as compared to MβCD estimated by UV-Vis is in accordance with the ATR-FTIR results (Figure 3.1b).
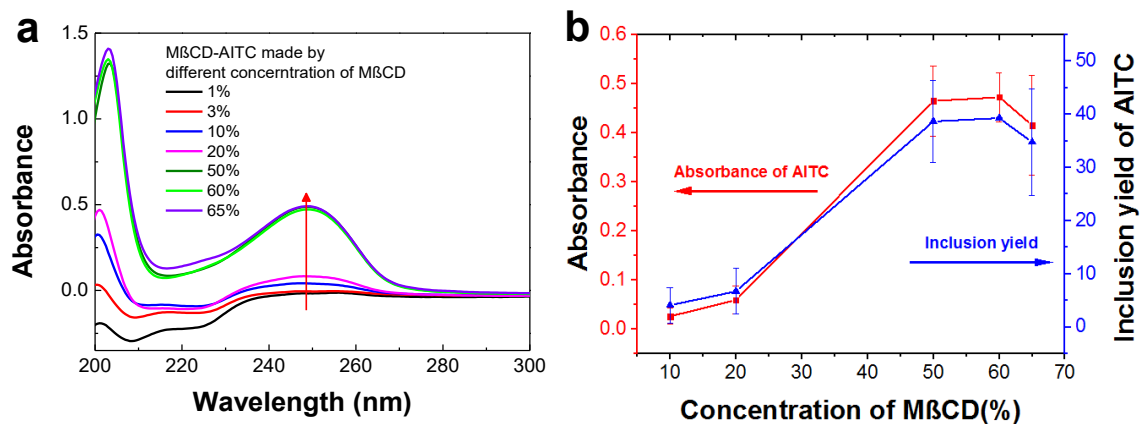
Figure 3.2 (a) Effect of MβCD-AITC concentration on UV-Vis absorption spectra, (b) the corresponding inclusion yield of AITC in the MβCD-AITC complexes.
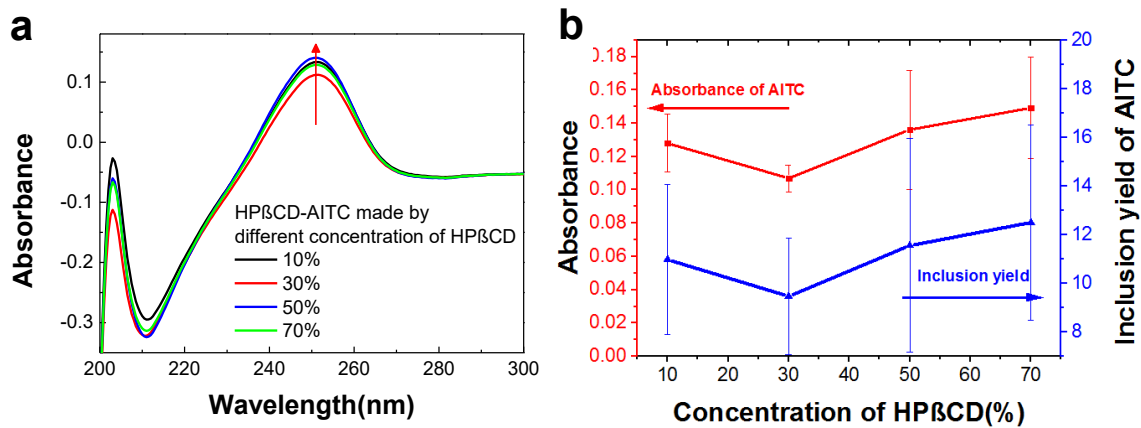
Figure 3.3 (a) Effect of UV-Vis absorption spectra of HPβCD-AITC based on different concentrations of HPβCD-AITC. (b) the corresponding inclusion yield of AITC in the HPβCD-AITC complexes.

3.1.2   The morphology of βCD-AITC complexes by SEM

SEM were used to observe the morphological changes of βCD-AITC complexes after the encapsulation process, as shown in Figure 3.4. The agglomeration and fusion of the complexes were observed. Instead, SEM micrographs of MβCD and HPβCD shows that the particle was spherical with small size scattered over the conductive tapes, which demonstrates they are not agglomerated.
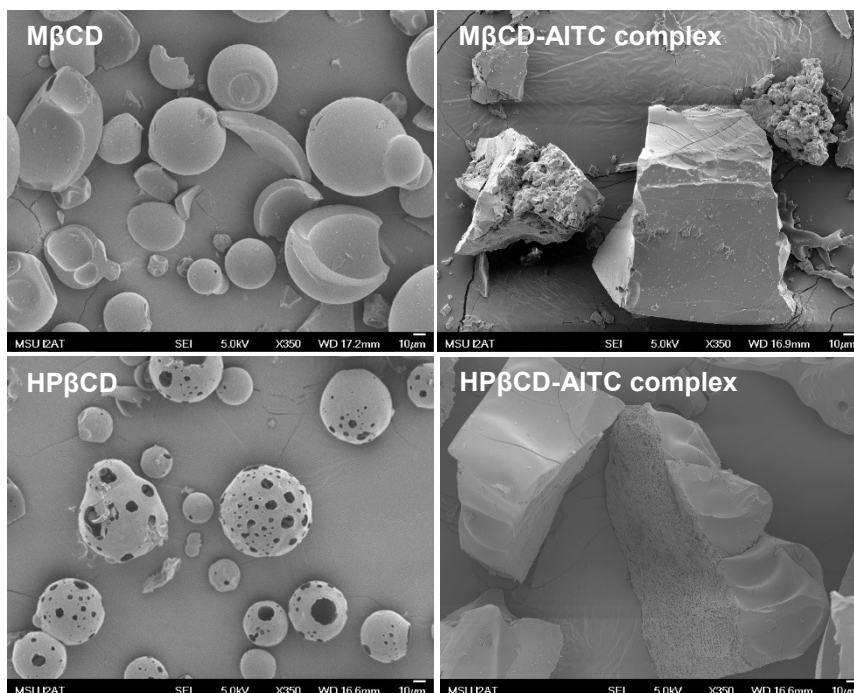
Figure 3.4   SEM images of HPβCD, MβCD and their complexes with AITC

3.1.3   βCD-AITC complexes in wood

The quality of a wood preservative treatment can be evaluated by the amount of preservatives retained (retention/mass gain), preservative location (penetration not only into cell lumens, but also into cell walls), and the preservative distribution across the sample width (Koch, 1972). The bulking and mass gain of wood specimens after each treatment and drying is shown in Table 3.1. There was no volume change or mass gain after neat AITC treatment, indicating that this molecule evaporated after 24 h of drying at 40°C. The low bulking and high mass gain of βCD-AITC modified wood may be attributed to the loading of the preservative primarily on the surfaces of wood lumens with only marginal cell wall penetrations.

46

Table 3.1   Bulking and mass gain of treated southern pine following vacuum impregnation with water, AITC in ethanol or AITC derivatives.

Treatment	Bulking (%, $\bar{x}$ ±SD)*	Mass Gain (%, $\bar{x}$ ±SD)	The Estimated Amount of AITC in Wood (%, $\bar{x}$ ±SD)
Control	0 (A)**	0 (A)	0 (A)
AITC	0 (A)	0 (A)	0 (A)
MβCD-AITC	0.5±0.1 (B)	52.1±4.1 (B)	1.42±0.11 (B)
HPβCD-AITC	0.7±0.1 (B)	61.2±9.4 (C)	0.60±0.08 (C)

* $\bar{x}$ ±SD: Mean and standard deviation
** Values followed by the same letters are not significantly different by LSD test (α=0.05)

In order to confirm that the bulking and mass gain results were not simply the result of the presence of the βCDs, SME-EDXA examination was used and it was found that AITC, in fact, remained in the wood after treatment. No sulfur was detected in the water-treated wood (Figure 3.5a). Sulfur potentially associated with MβCD-AITC was distributed evenly across the sample (Figure 3.5c). Preservative distribution across the cell walls is difficult to examine at the magnification level of the analysis because of the limited instrument capabilities, potentially introduced artifacts and redistribution of the preservatives during sample preparation. Although sulfur was visible in the sample treated with HPβCD-AITC (Figure 3.5e), the overall intensity was lower (Figure 3.6), as in agreement with UV-Vis results, and the distribution was less uniform when compared to MβCD-AITC-treated samples.
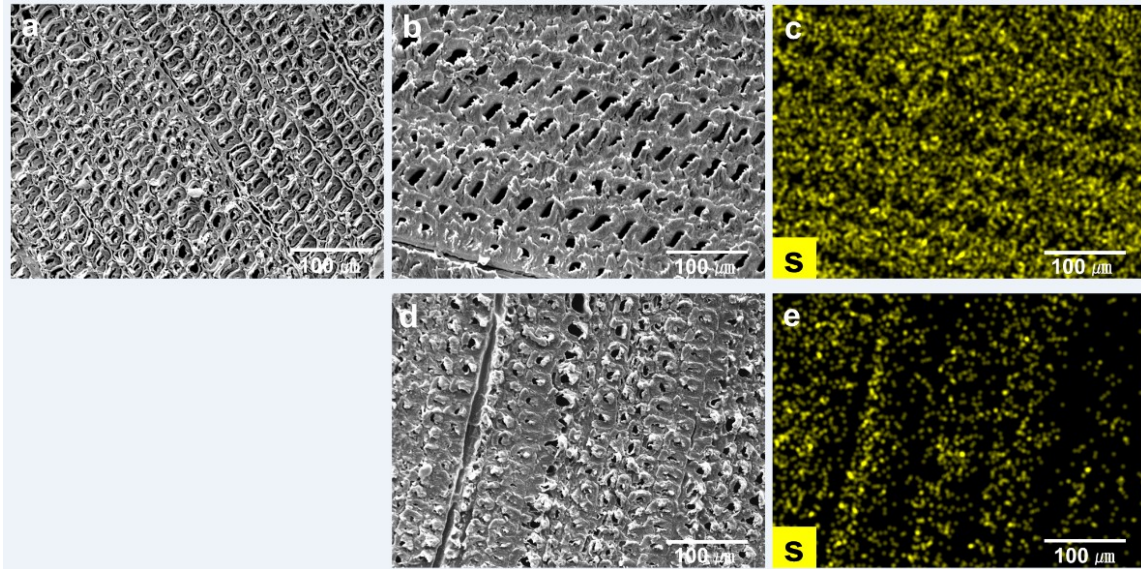
Figure 3.5   SEM images of (a) water-treated wood, (b) MβCD-AITC treated wood, (c) the corresponding EDX mapping of sulfur (S), (d) HPβCD-AITC treated wood, and (e) the corresponding EDX mapping of sulfur.
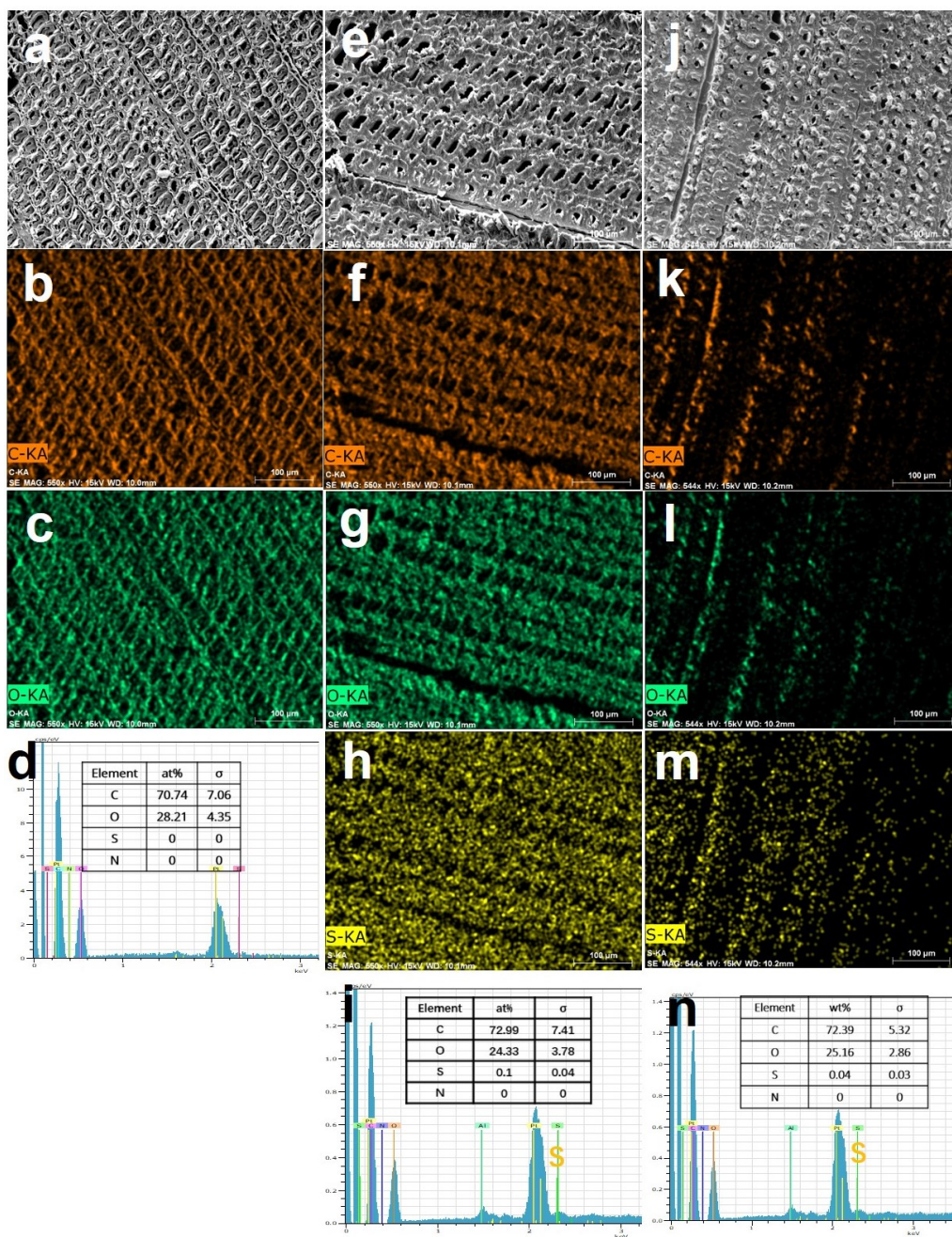
Figure 3.6   SEM images of (a) water-treated wood and the corresponding EDX mapping of (b) carbon, (c) oxygen, and (d) EDX spectra with atomic mass percentages. SEM images of (e) MβCD-AITC-treated wood and the corresponding EDX mapping of (f) carbon, (g) oxygen, (h) sulfur, and (i) EDX spectrum with atomic mass percentages. SEM images of (j) HPβCD-AITC treated wood and the corresponding EDX mapping of (k) carbon, (l) oxygen, and (m) sulfur, and (n) EDX spectrum with an atomic mass percentage. All scale bars are 100 μm.

49

3.1.4 Decay resistance of βCD-AITC complexes

Efficacy of the βCD-AITC complexes against brown-rot and white-rot fungi was evaluated using soil block tests. These tests provide a preliminary measure of decay resistance and are normally followed by more aggressive field trials. Mycelia of *G. trabeum* changed color in the presence of the βCD-AITC treated wood blocks (Figure 3.7) while *T. versicolor* mycelium remained white although its growth was also suppressed in the presence of βCD-AITC treated wood blocks. Water-treated and neat AITC-treated wood blocks were heavily decayed (Figure 3.8). The extensive decay of AITC-treated wood was probably due to the high volatility of AITC (vapor pressure: 0.493 kPa at 20 °C (Lim and Tung, 1997)) and the marginal mass gain achieved with the treatment. In contrast, the complex-treated specimens were visually unchanged, even after samples were subjected to accelerated weathering and fungal exposure.
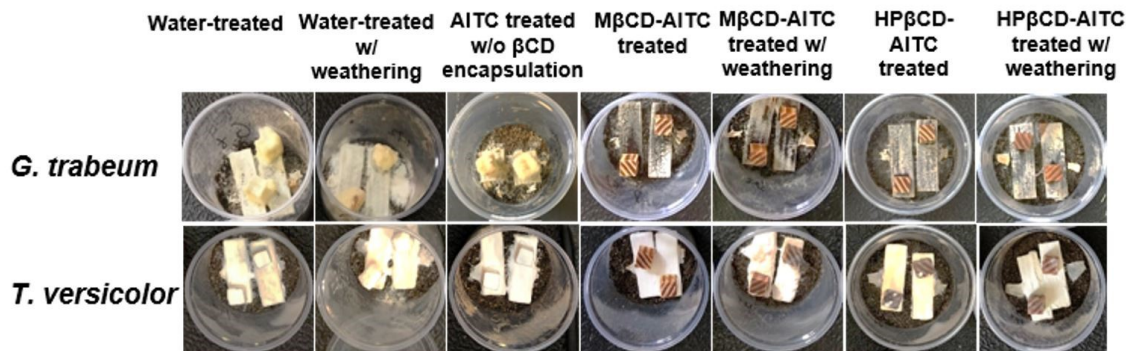
Figure 3.7   Fungal growth of *G. trabeum* or *T. versicolor* on wood exposed in an AWPA E10-16 soil block test
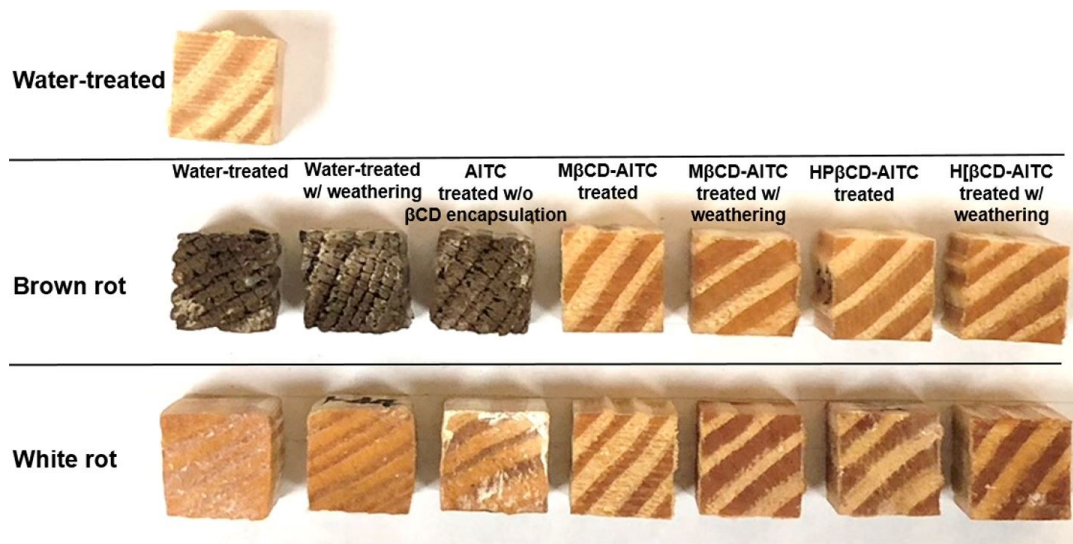
Figure 3.8   Examples of southern pine wood blocks with different treatments after exposure to *G. trabeum* or *T. versicolor*.

Mass losses in βCD-AITC-treated wood exposed to *G. trabeum* were significantly lower than those for water-treated and neat AITC-treated wood (Figure 3.9). Mass losses of the water-treated samples by *G.trabeum* (45%) were reduced to 25% and 28% after MβCD- and HPβCD-AITC treatments, respectively. As expected from the higher inclusion yield of AITC in MβCD than HPβCD (39% vs 14%), MβCD-AITC exhibited overall lower mass losses, but the differences were not significant. Mass losses of AITC-treated wood were not significantly different from the water-treated treated controls, and were significantly higher than those for βCD-AITC-treated samples, indicating that βCD helped retain activity of AITC by reducing volatility even after weathering. The stability of the complexes was also evident by the absence of significant mass losses after weathering.

βCD-AITC treatment had little effect on decay by *T. versicolor*. This could be a result of the longer exposure period (Rowell, 1995).
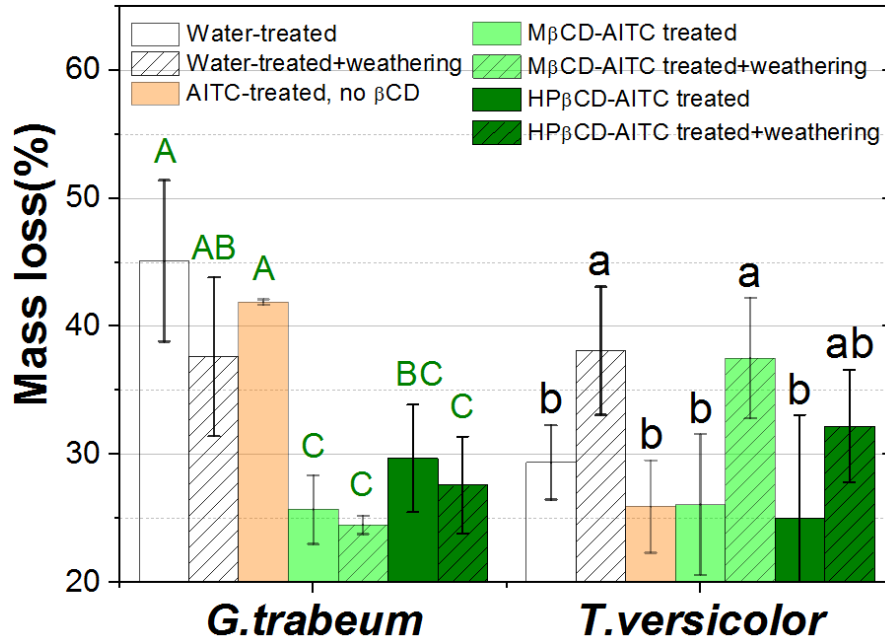
Figure 3.9   Mass losses of water-treated and preservative-treated pines with and without weathering pretreatment after exposure to *G. trabeum* (8-week) or *T. versicolor* (16-week).

Microscopic examination of the water-treated wood following fungal exposure showed that fungal hyphae readily grew and penetrated through pits (Figure 3.10c and i), which resulted in severely collapsed cell wall structure. Conversely, very few fungal hyphae presence was observed in the cell wall of βCD-AITC treated wood (Figure 3.10e, g, k and m), and those cell wall structures retained their overall shape, although it was slightly decayed by fungi (Figure 3.10f and i). These results indicate that fungal degradation was suppressed by the presence of βCD-AITC complexes.
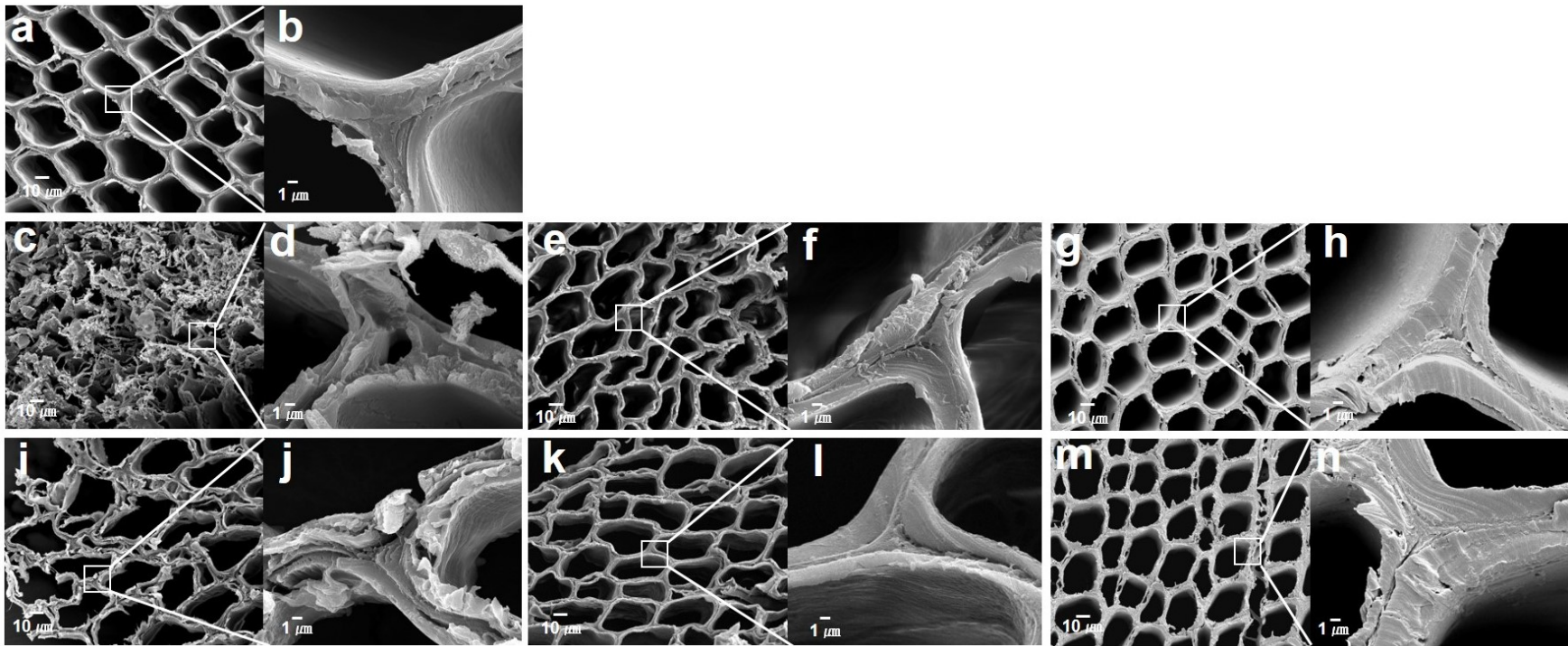
Figure 3.10   SEM images of cross sections of: (a and b) water-treated wood before decay, (c and d) water-treated wood after 8-week *G.trabeum* exposure, (e and f) MβCD-AITC treated wood after 8-week of *G.trabeum* exposure, (g and h) HPβCD-AITC treated wood after 8-week of *G. trabeum.* exposure, (i and j) water-treated wood after 16-week *T.versicolor* exposure (k and l) MβCD-AITC treated wood after 16-week *T.versicolor* exposure and (m and n) HPβCD-AITC treated wood after 16-week *T.versicolor* exposure.

3.2   Summary

We show that the complexation of AITC with βCDs not only enhanced the solubility of AITC (mustard oil), but also decreased the volatility of AITC. These compounds could potentially be used as carriers of other antimicrobial compounds that otherwise would not be considered for wood protection. The βCD-AITC complexes applied to wood in aqueous solutions were uniformly distributed across wood samples, although their penetration into wood cell walls seemed to be limited to the cell lumens. Combined results from mass loss, SEM-EDX before and after decay test show that the βCD-AITC complexes suppressed the attack of brown rot fungi on wood, and helped maintain the original appearance of wood. Although the mass losses of wood were still significantly higher than the mass losses of commercially available preservatives, the use of the βCD-AITC complexes still improves the applications of AITC for remedial treatments.

CHAPTER IV

β-CYCLODEXTRINS AS SUSTAINED-RELEASE CARRIERS FOR AROMATIC

NATURAL WOOD PRESERVATIVES: ESSENTIAL OILS

The objective of this study was to use MβCD as sustained-release carriers for four representative essential oils (EOs) with proven antimicrobial activity. Eugenol (EG), *trans*-cinnamaldehyde (CN), thymol (TM) and carvacrol (CV) (Panek et al., 2014) were encapsulated in MβCD and the complexes were labeled as MβCD-EG, MβCD-CN, MβCD-CV, and MβCD-TM complexes, respectively. Effect of mole ratio of guest molecules to MβCD and concentration of MβCD in water used for encapsulation process on maximum inclusion yield of EOs in MβCD-EOs were investigated. Accordingly, the maximum inclusion yields of respective EOs in MβCD were optimized. The efficacy of the four MβCD-EOs complexes with varying concentrations as natural water-borne preservatives were evaluated for their ability to protect wood from two brown rot fungi, *Gloeophyllum trabeum* and *Postia placenta.*

4.1   Methods

For Materials and methods, please refer to Chapter 2, except that the fungi resistance test was evaluated by following AWPA Standard E22-16 with compression strength test (AWPA, 2016b).

4.1.1 Compression strength test

After vacuum impregnation, the wood samples saturated with treating solutions were used for a compression test according to AWPA Standard E22-16 (AWPA, 2016b). The detailed testing procedures were summarized by Green et al (2010). Briefly, the compression strengths (σ_{cpr}) were obtained at 5% of the sample depth in the radial direction (Figure 4.1) at a loading speed of 0.5 mm/min by a universal testing instrument at Mississippi State University and calculated according to equation 4.1:
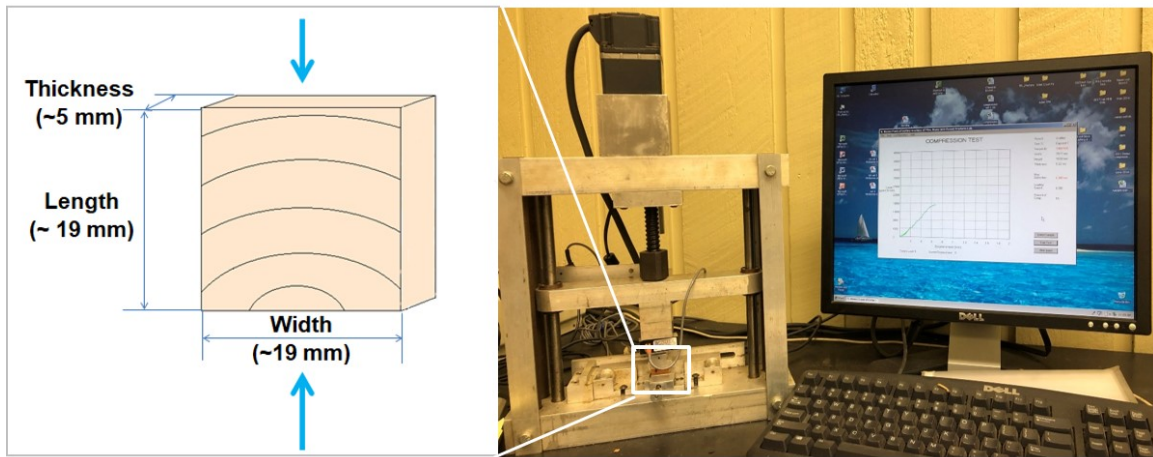
Figure 4.1   Compression strength test setup at Mississippi State University used to evaluate radial compression strength of test samples

$$\sigma_{cpr} \ (MPa) = \frac{maxmum\ load}{thickness \times width} \tag{4.1}$$

4.2   Results and discussion

4.2.1   Formation of MβCD-EO complexes

IR spectra of neat MβCD, neat EOs and MβCD-EOs inclusion complexes at 50% MβCD with a 1:1 loading mole ratio are shown in Figure 4.2. The stretching vibrations of C-O in the IR spectrum of MβCD were observed at around 1025 and 1076 cm^{-1} while the asymmetric stretching vibration of the pyranose ring was observed at 1149 cm^{-1}. Additionally, absorbance at 3383 and 2925 cm^{-1} can be assigned to CH and OH groups, respectively. Eugenol showed its characteristic peaks in a range from 720 to 1250 cm^{-1}, which are attributed to the C=C region of the molecule. In addition, the peaks at 1638, 1610, and 1510 cm^{-1} were related to the C=C stretching of the aromatic ring in EG. All three peaks, with some shifts (1638, 1604 and 1512 cm^{-1}) can be found in the inclusion complex of MβCD-EG, indicating the C=C stretching of the aromatic moiety. The lower intensity of the EG peaks in the complex may be explained by the relatively small amount of EG in the complexes, implying the trapping of EG molecules in the cavity of MβCD. Similar results were observed with the MβCD-CN, MβCD-CV and MβCD-TM complexes. For example, upon complexation, the signature picks of CN at 1677, 1628 and 1117 cm^{-1}, CV at 1456, 1368 and 808 cm^{-1}, and TM at the similar region were all found in the inclusion complexes for MβCD-CN, MβCD-CV, and MβCD-TM, respectively. The OH region in the complex also became more pronounced in comparison to the neat MβCD, possibly due to the substitution of high-enthalpy water molecules in the cavity with EOs (E. M.Martin Del Valle, 2004). These IR results indicate the formation of MβCD-EOs complexes.
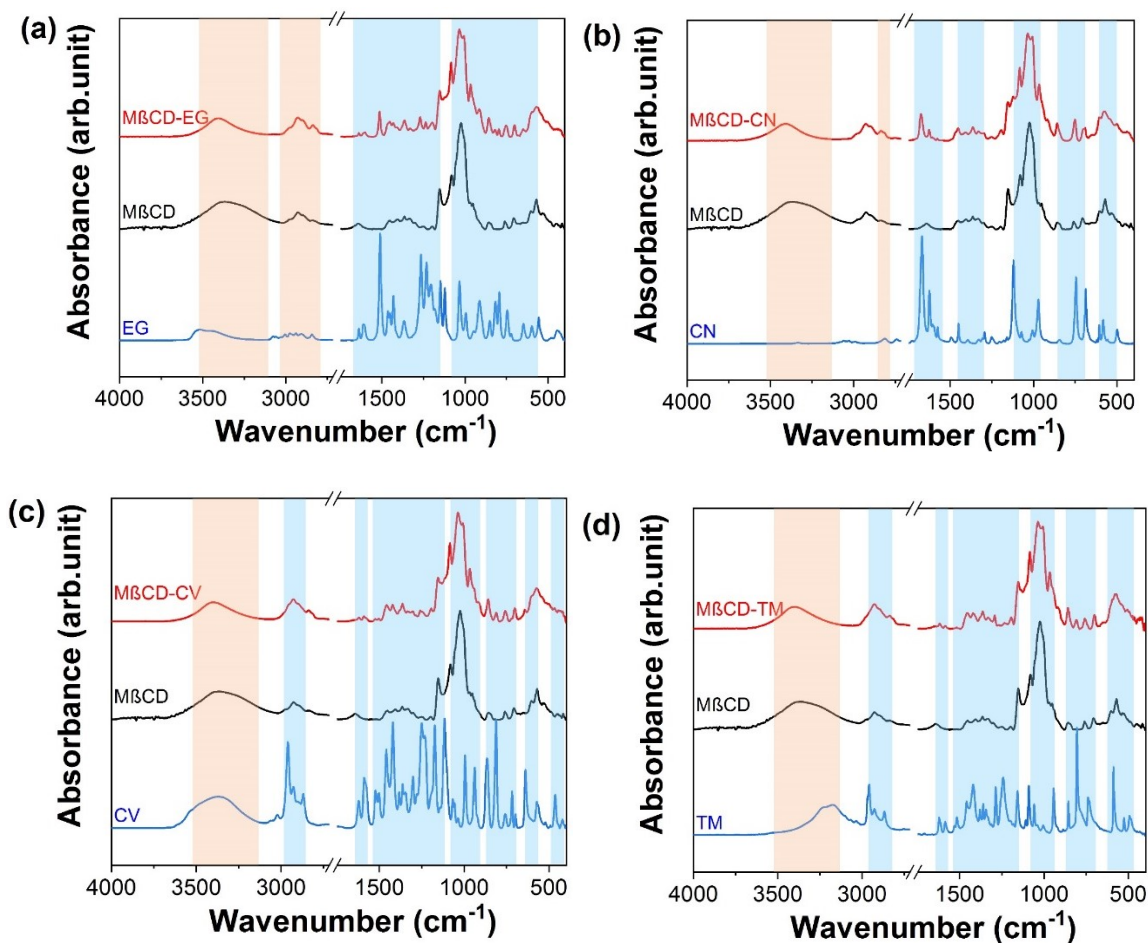
Figure 4.2   Infrared spectra of (a) neat EG, MβCD and MβCD-EG complex, (b) neat
CN, MβCD and MβCD-CN complex, (c) neat CV, MβCD and MβCD-CV
complex, and (d) neat TM, MβCD and MβCD-TM complex.

EOs are the main active biocides against microorganisms in the MβCD-EOs
complexes. The mole ratio of MβCD to EOs and the concentration of MβCD in water are
two main factors that affect the inclusion yield of guest molecules in cyclodextrin (Al-
Nasiri et al., 2018). In this study, their effect on the inclusion yield of EOs in MβCD was
studied and the corresponding inclusion yield was quantitatively measured using a UV/VIS
method. Figure 4.3a shows the effect of the mole ratio of MβCD to EOs on the inclusion

yield of MβCD-EOs. The inclusion yield of EG, CN, and TM in MβCD reached a maximum of ~100% at 1:1 mole ratio of MβCD to EOs. Further addition of the guest molecules did not significantly increase the inclusion yield ($p < 0.05$). These results were consistent with previous reports that EG, CN and TM form 1:1 guest and host molecule (Divakar and Maheswaran, 1997; Locci et al., 2004)). A similar pattern was observed in MβCD-CV complexes. However, the maximum inclusion yield of CV in MβCD was around 70%, which is significantly lower ($p < 0.05$) than the complexes with EG, CN, and TM as guest molecules. Similar phenomena were reported that the structure and properties of the guest molecules significantly affect the inclusion yields of the complex. (Locci et al., 2004).

The effect of MβCD concentration in water on the inclusion yield of MβCD-EOs was also investigated (Figure 4.3b) by using the UV/VIS method. The effect of MβCD concentration on the inclusion yield varied with the type of MβCD-EOs. MβCD did not significantly affect the inclusion yield of MβCD-EOs using EG or CV. The inclusion yield of MβCD-TM increased when the concentration of MβCD changed from 10% to 30 %, but further increase in MβCD did not significantly improve inclusion yield ($p < 0.05$). The inclusion yield of MβCD-CN increased as a function of MβCD concentration ($p < 0.05$). These results illustrate that the encapsulation process is highly dependent on the guest molecule type and cyclodextrin concentration (E. M.Martin Del Valle, 2004).
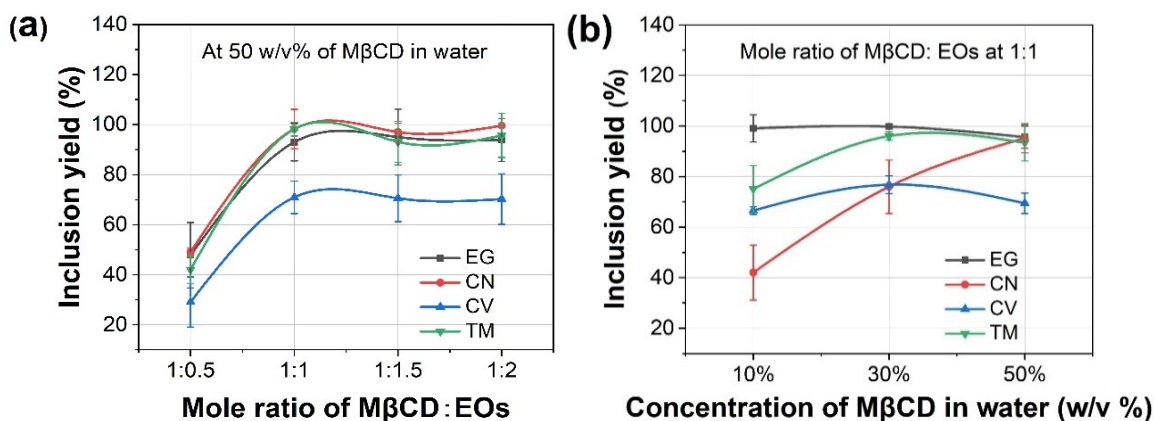
Figure 4.3   Effect of (a) mole ratio of MβCD to EOs on the inclusion yield of MβCD-EOs at a constant concentration MβCD at 50 w/v% MβCD, and (b) concentration of MβCD on the inclusion yield of MβCD-EOs at a constant mole ratio of MβCD to EOs at 1:1.

Even though the inclusion yield of EOs in MβCD was affected significantly by MβCD concentration for some EOs, it is still higher than the inclusion yield for mustard oil in the cyclodextrin complex, which was around 39%. In this study, we also demonstrated the potential of those complexes for wood protection (Cai et al., 2019). Thus, in current study, three levels of MβCD-EOs solution were selected as preservatives treatments.

4.2.2   MβCD-EOs complexes in wood

The treated wood samples did not change in color (Figure 4.4a). Mass gain of EOs in wood increased proportionally to the MβCD-EOs concentrations and reached a maximum loading of ~6.5% (Figure 4.4b). There were no significant differences between 5% EOs and 10% MβCD-EOs treatments except for TM ($p < 0.05$). Figure 4.4c shows the penetration of preservatives in the cell wall by bulking. There were some variations

among each treatment but the maximum bulking was less than 5%. Maximum bulking of wood is dependent on the wood species and the initial moisture content (Nicholas, 1982). In this case, all the samples used for measuring mass gain and bulking were derived from one stick and were oven dried at the time of treatment. These processes should have reduced the variability in physical properties between the wood samples.
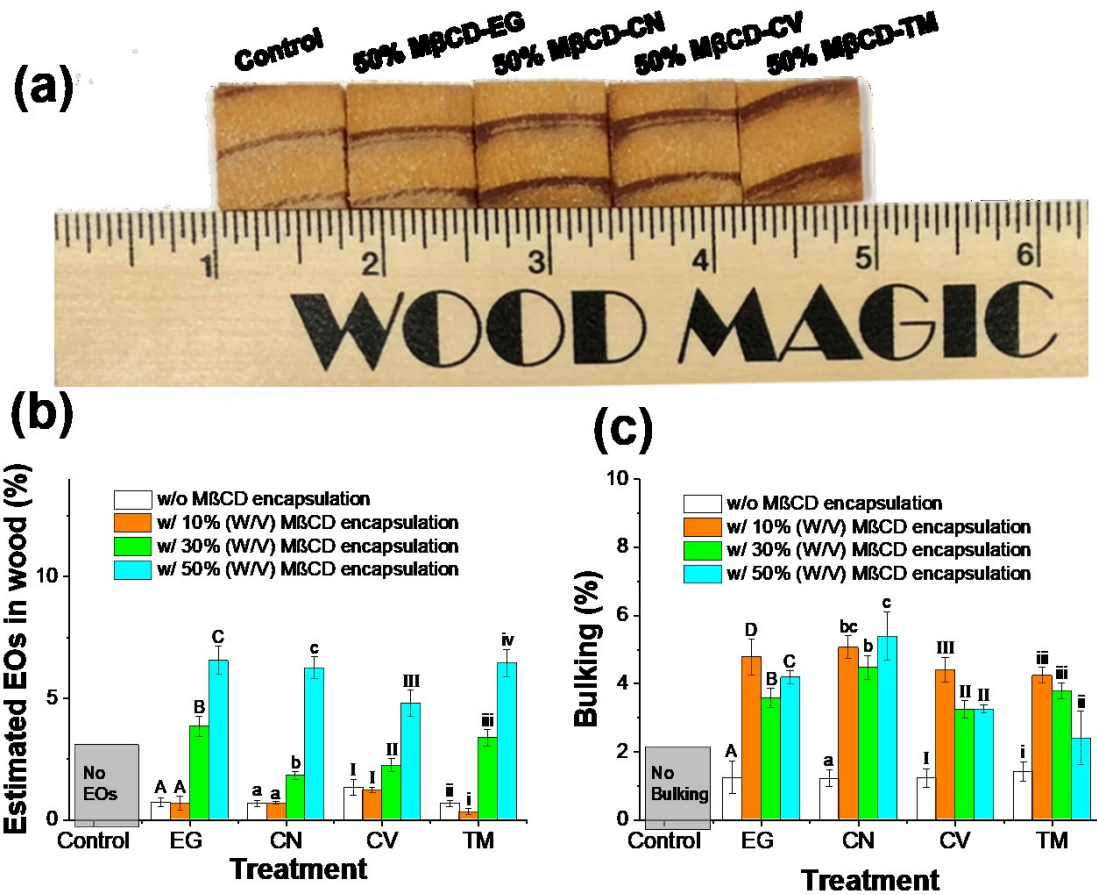
Figure 4.4   a) Southern pine samples after preservatives treatment, b) the estimated amount of EOs uptake and c) the effect of treatment on bulking in wood.

The effect of preservatives treatments on the compression strength was shown in Figure 4.5. Compression strength varied among the samples, despite the use of end-

61

matched samples from one stick. No statistical differences (Table 4.1-4.4) were observed among the treatments, indicating that treatment did not adversely affect this property.
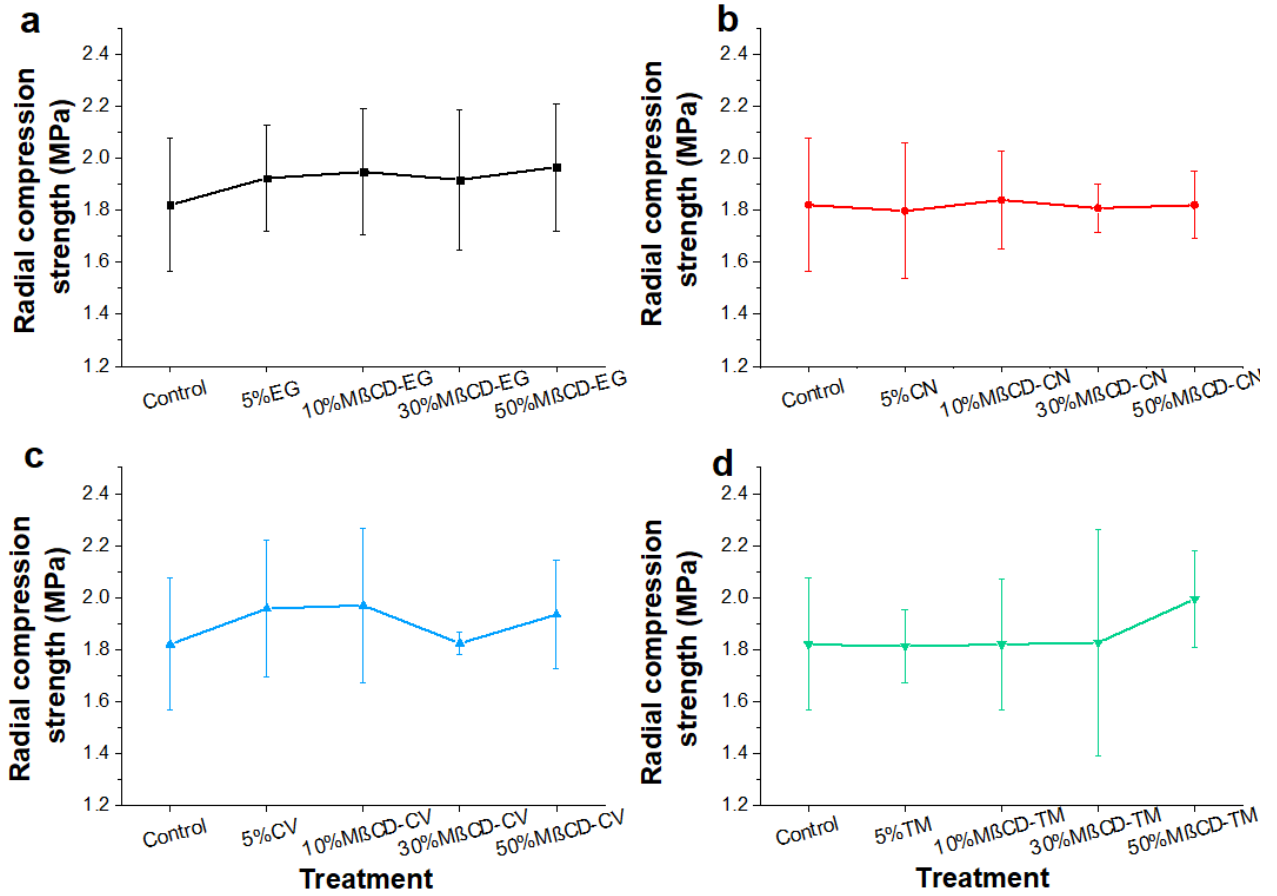
Figure 4.5   Effect of (a) MβCD-EG, (b) MβCD-CN, (c) MβCD-CV and (d) MβCD-TM treatment on the radial compression strength of southern pine

Table 4.1   Mean compression strength $\pm$ Standard Error after various eugenol (EG) solution treatment

Treatment	Compression strength (Mpa)
Control	1.82±0.25(A)
5%EG	1.81±0.14(A)
10%MßCD-EG	1.82±0.25(A)
30%MßCD-EG	1.83±0.44(A)
50%MßCD-EG	2.00±0.18(A)

Values represent means of 5 replicates per treatment. Values followed by the same letters do not differ statistically by Tukey test at α=0.05

Table 4.2   Mean compression strength $\pm$ Standard Error after various *trans*-Cinnamaldehyde (CN) solution treatment

Treatment	Compression strength (Mpa)
Control	1.82±0.25(A)
5%CN	1.80±0.26(A)
10%MßCD-CN	1.84±0.19(A)
30%MßCD-CN	1.81±0.09(A)
50%MßCD-CN	1.82±0.13(A)

Values represent means of 5 replicates per treatment. Values followed by the same letters do not differ statistically by Tukey test at α=0.05

Table 4.3   Mean compression strength $\pm$ Standard Error after various Carvacrol (CV) solution treatment

Treatment	Compression strength (Mpa)
Control	1.82±0.25(A)
5%CV	1.96±0.26(A)
10%MßCD-CV	1.97±0.3(A)
30%MßCD-CV	1.82±0.04(A)
50%MßCD-CV	1.93±0.21(A)

Values represent means of 5 replicates per treatment. Values followed by the same letters do not differ statistically by Tukey test at α=0.05

Table 4.4   Mean compression strength $\pm$ Standard Error after various thymol (TM)
            solution treatment

Treatment	Compression strength (Mpa)
Control	1.82±0.25(A)
5%TM	1.92±0.21(A)
10%MßCD-TM	1.95±0.24(A)
30%MßCD-TM	1.92±0.27(A)
50%MßCD-TM	1.97±0.24(A)

Values represent means of 5 replicates per treatment. Values
followed by the same letters do not differ statistically by Tukey test
at α=0.05

4.2.3   Decay resistance of MβCD-EOs complexes against brown rot fungi

Preservative and weathering treatments, as well as the interaction between those
two factors, significantly affected the mass loss of southern pine samples (Table 4.5 and
4.6). Since compression strength tests permanently deform the specimens, it is not possible
to test a sample, followed by exposing it to a fungus and then retest it to assess changes
occurring with fungal exposure. Instead, average compression strength was compared
between treatments based upon the initial tests performed on control samples.

Table 4.5   ANOVA results for mass loss of pine samples decayed by *G. trabeum* over
            4 weeks

Source	DF	Mean Square	F Value	Pr > F
Preservative treatment	16	589.968	17.94	<.0001
Weathering test	1	967.403	29.41	<.0001
Preservative treatment*Weathering test	16	108.989	3.31	<.0001

Table 4.6   ANOVA results for mass loss of pine samples decayed by *P. placenta.* over 4 weeks

Source	DF	Mean Square	F Value	Pr > F
Preservative treatment	16	469.3712	21.68	<.0001
Weathering test	1	658.188	30.4	<.0001
Preservative treatment*Weathering test	16	40.24063	1.86	0.0251

Differences in mass and compression strength loss caused by *G. trabeum* on blocks with different preservatives and weathering treatments were given in Figure 4.6 and Table 4.7. Unweathered and weathered water-treated blocks experienced mean mass losses of 20-40% and strength losses of 80-90%. The high mass and compression strength losses indicate that the test fungus was capable of causing aggressive wood decay. An inverse correlation was found between the concentration of encapsulated EOs. As the EOs concentration increase, the losses in mass and compression strength decrease, regardless of the weathering test. All the 50% MβCD-EOs treated samples showed mass (5-10%) along with compression strength losses (40-60%), much less than the control samples, indicating that the essential oils treatments retard the fungal growth. Weathering resulted in significantly higher mass and strength losses for un-encapsulated EOs treated groups, but not the MβCD encapsulated treatment groups, indicating that MβCD significantly improved leaching resistance. There were no significant performance differences between encapsulated-EG, CN, CV or TM.
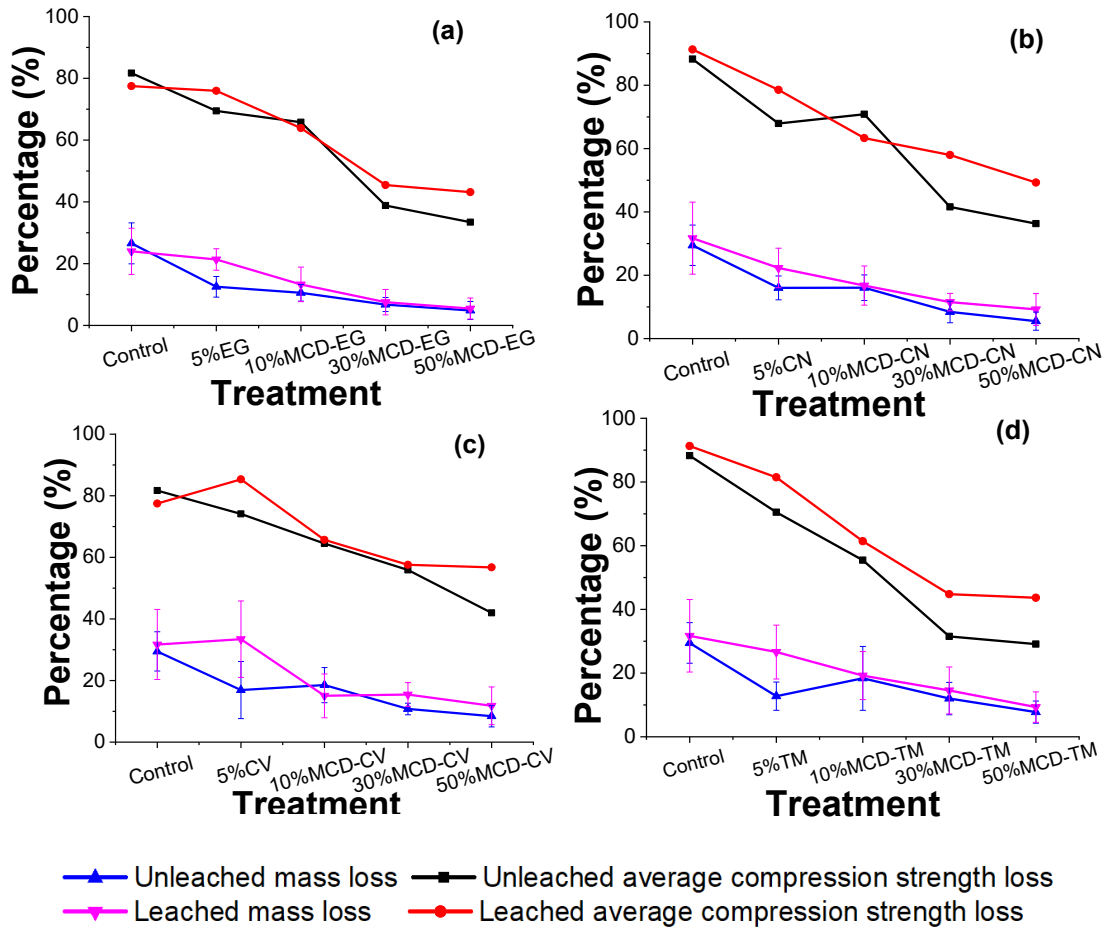
Figure 4.6   Mass and average compression strength loss for *G. trbeum* on pine samples at various treatment conditions.

Table 4.7   Effect of treatment with various oils coupled and exposed to *G. trabeum* in an AWPA Standard E22-16 decay test for 4 weeks

Preservatives treatment		Mass loss (%)														CS loss (%)	
EOs species	Level	Unweathered (UW)							Weathered (W)							UW	W
Control	0	26.58 (6.65)				B			23.97 (7.47)	C		B				81.68	77.47
EG	5%EG	12.51 (3.35)	M	I	K	L			21.35 (3.48)	C	E	B	D			69.46	75.94
	10% MβCD-EG	10.56 (2.71)	M	O	K	L		N	13.27 (5.59)	G	I	K	L		H	65.78	63.89
	30% MβCD-EG	6.76 (2.27)		O				N	7.53 (4.1)	M	O				N	38.80	45.45
	50% MβCD-EG	4.84 (2.93)							5.47 (3.41)		O					33.42	43.17
CN	5%CN	16.03 (3.77)	G	I	E			H	22.32 (6.24)	C		B	D			67.94	78.54
	10% MβCD-CN	16.06 (4.05)	G	I	E			H	16.76 (6.17)	G	I	E		D	H	70.82	63.33
	30% MβCD-CN	8.42 (3.4)	M	O		L		N	11.51 (2.75)	M	I	K	L		N	41.55	57.99
	50% MβCD-CN	5.50 (2.85)		O					9.19 (5.04)	M	O	K	L		N	36.28	49.29
CV	5%CV	16.91 (9.25)	G	I	E		D	H	33.44 (12.43)				A			74.09	85.32
	10% MβCD-CV	18.51 (5.7)	G	C	E		D		15.04 (7.09)	G	I				H	64.52	65.70
	30% MβCD-CV	10.76 (1.86)	M	O	K	L		N	15.45 (3.9)	G	I				H	55.88	57.60
	50% MβCD-CV	8.40 (3.43)	M	O		L		N	11.81 (6.12)	M	I	K	L		N	41.96	56.72
TM	5%TM	12.74 (4.43)	M	I	K	L		H	26.62 (8.45)				B			70.50	81.46
	10% MβCD-TM	18.36 (10.02)	G	C	E		D	H	19.23 (7.55)	C	E		D			55.43	61.43
	30% MβCD-TM	12.01 (5.09)	M	I	K	L		N	14.55 (7.35)	G	I	K			H	31.51	44.78
	50% MβCD-TM	7.75 (3.5)	M	O		L		N	9.32 (4.76)	M	O	K	L		N	29.09	43.64

Values represent means of 8 replicates per fungus while figures in parentheses represent one standard deviation. Values followed by the same letters do not differ statistically by Games Howell test at α=0.05

The trends in mass and compression strength losses caused by *P. placenta* were similar to those found with to the *G. trabeum* (Figure 4.7, Table 4.8). The control groups showed mass and compressive strength losses of 22-37% and 80-90%, respectively. These results again confirm that the conditions were suitable for the aggressive wood decay test. Increasing preservative concentration to a level of 50% resulted in significant reductions in mass losses (5-15%, $p < 0.05$) and compressive strength losses (40-60%) for all of encapsulated EO treated groups. However, the blocks treated with 5% EGs without MβCD encapsulation and weathered had significantly higher mass (20-25%, $p < 0.05$) and compression strength losses (70-80%), illustrating premature leaching of the non-complexed oils. These results are in full agreement with previous reports (Chittenden and Singh, 2011; Tascioglu et al., 2013) that essential oils are prone to leaching. Complexing EOs with MβCD suppressed leaching and helped retaining biological activity.
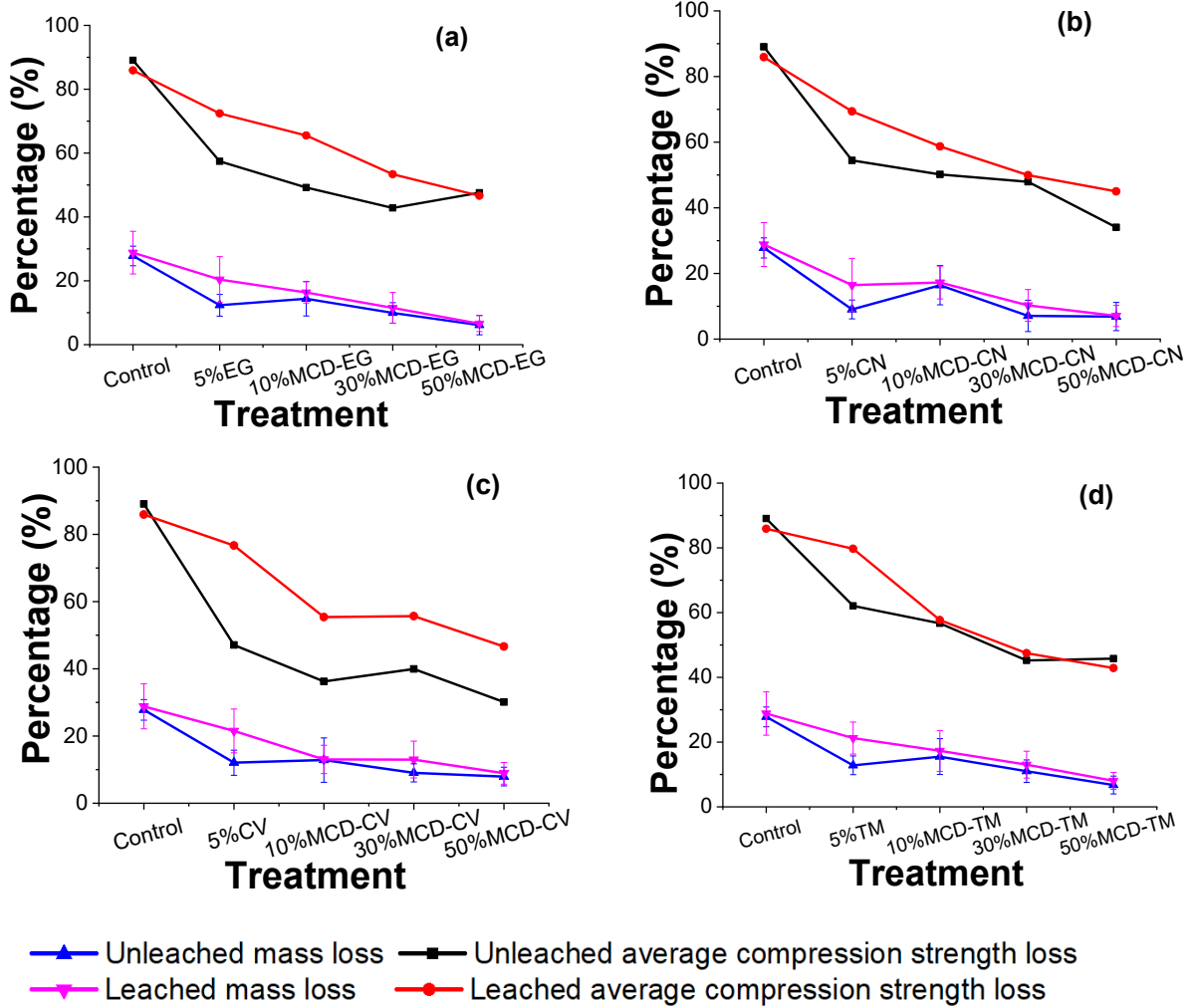
Figure 4.7   Mass and average compression strength loss for *P.placenta* on pine
            samples at various treatment conditions

Table 4.8   Effect of treatment with various oils coupled and exposed to P. placenta in an AWPA Standard E22-16 decay test for 4 weeks

Preservatives treatment		Mass loss (%)																Compression strength loss (%)	
EOs species	Level	Unweathered (UW)								Weathered (W)									UW	W
Control	0	27.78(3.04)	A							28.83(6.69)	A								89.02	85.88
EG	5%EG	12.34(3.39)			I	E	F	G	H	20.42(7.19)		B	C						57.41	72.41
	10% MβCD-EG	14.37(5.39)			D	E	F	G		16.38(3.34)			C	D	E				49.21	65.52
	30% MβCD-EG	9.94(3.18)		K	I	J	L	G	H	11.5(4.83)				I	J	F	G	H	42.82	53.39
	50% MβCD-EG	6.12(3.05)					L			6.6(2.49)			K			L			47.6	46.63
CN	5%CN	9.03(2.88)		K	I	J	L		H	16.48(8.12)			C	D	E				54.43	69.38
	10% MβCD-CN	16.42(5.98)		C	D	E				17.24(5.01)		B	C	D					50.19	58.7
	30% MβCD-CN	7.09(4.77)		K		J	L		H	10.29(4.84)			K	I	J	L	G	H	47.94	49.95
	50% MβCD-CN	6.86(4.3)		K			L			7.06(3.22)			K		J	L			34.02	45.02
CV	5%CV	12.06(3.74)			I	E	F	G	H	21.53(6.52)		B		D	E	F	G	H	47.07	76.69
	10% MβCD-CV	12.86(6.6)			D	E	F	G	H	13.05(4.22)				D	E	F	G	H	36.22	55.42
	30% MβCD-CV	9.05(2.69)		K	I	J	L		H	13(5.46)				D	E	F	G	H	39.92	55.67
	50% MβCD-CV	7.94(2.78)		K	I	J	L			8.92(3.23)			K	I	J	L		H	30.13	46.64
TM	5%TM	12.82(2.88)			D	E	F	G	H	21.25(4.94)		B							62.08	79.72
	10% MβCD-TM	15.52(5.53)			D	E	F			17.28(6.3)		B	C	D					56.69	57.69
	30% MβCD-TM	11.01(3.46)			I	J	F	G	H	13.03(4.15)				D	E	F	G	H	45.21	47.45
	50% MβCD-TM	6.75(2.76)		K			L			8.01(2.63)			K	I	J	L			45.78	42.86

Values represent means of 8 replicates per fungus while figures in parentheses represent one standard deviation. Values followed by the same letters do not differ statistically by Games Howell test at α=0.05

Radial compression strength loss and mass loss were highly correlated (Figure 4.6 and 4.7). Radial compression strength loss is generally considered to be a more sensitive indicator of incipient decay than mass loss (Janzen and Nicholas, 2016). It has been reported that a strength loss of 50-70% with a mass loss of 5-10% was observed in wood decayed by some brown rot fungi (Wilcox, 1978). In the current study, the changes in strength loss was 1.5-4 times greater than mass loss: the preservative treatments significantly reduce the strength losses from 80-90% to 40-60% with mass losses from 20-40% to 5-10%.

4.3   Summary

This report demonstrated the feasibility of using methyl-β-cyclodextrins-essential oils (MβCD-EOs) complexes as potential bio-based preservatives for wood protection. MβCD produced higher encapsulation efficacy with essential oils containing phenolic compounds, such as eugenol, *trans*-cinnamaldehyde, carvacrol and thymol, as compared to non-aromatic compounds, and significantly suppressed the instability. Pine sapwood blocks treated with MβCD-EOs complexes exhibited significantly improved decay resistance measured as either mass or radial compression strength loss.

CHAPTER V

β-CYCLODEXTRIN-ALLYL ISOTHIOCYANATE COMPLEX AS A NATURAL

PRESERVATIVE FOR RANDOMLY ORIENTED STRAND BOARD WOOD

COMPOSITES

In this study, βCD-AITC complex was applied as powders during the manufacturing process of a randomly oriented strand board (OSB). The maximum inclusion yield of AITC in βCD-AITC was optimized, and the effect of the preservatives on the setting behavior of pMDI resin was studied. The internal bonding and biological performance of the OSB panels were also evaluated. The natural compound based on βCD-AITC provides a potential option for producing eco-friendly wood preservatives.

For Materials and Methods, please refer to Chapter 2, except that βCD-AITC complex powder was applied during the manufacturing of OSB and additional steps (5.1.1. and 5.1.2.) were also performed.

5.1   Methods

5.1.1   Preparation of OSB

OSB panels (254 mm (length) × 254 mm (width) × 11.7 mm (thickness)) (10 in × 10 in × 0.46 in) were constructed using southern pine strands supplied by Norbord Inc. (Guntown, Mississippi). Three panels for each were manufactured without a preservative or with 5 or 10 % βCD-AITC (wt/wt % basis using strand dry weight). The panels were composed of the same amount of the strands and resin (Table 5.1).

72

Table 5.1   Experimental design of βCD-AITC complex treated OSB

Treatment	Target density (kg/m³)	Strands (kg)	4% Resin (kg)	Preservatives (kg)
Control	640.74	0.47		0
5% βCD-AITC	672.78	0.47	0.018	0.022
10% βCD-AITC	704.81	0.47		0.044

Prior to the OSB construction, the strands were dried to a moisture content of approximately 6% (Figure 5.1). The prepared βCD-AITC complex powders were screened through a U.S. No.400 sieve ($\leq$ 37 μm) and oven-dried before further application. The strands were blended with βCD-AITC powders in a rotary drum at a rotating speed of 20 rpm for 2 minutes. pMDI resin (4%, based on the oven-dry weight of the strands) was sprayed into the rotating drum, and the strands were blended for another 3 minutes before being formed into mats by hand using a 254 mm × 254 mm frame at random orientations. A hot press (Dieffenbacher North America.Inc) with a 34" x 34" pressing area was used to consolidate the mats into finished boards. A thickness-controlled pressing cycle was used, which consisted of closing, pressing, and degassing time of 60, 200, and 20 seconds, respectively. The temperature of the platens was 176 ± 3 °C. The finished boards were conditioned to a constant weight and moisture content at 21 °C and 64% relative humidity (RH). The conditioned boards were trimmed 30 mm from all sides, then cut into internal bonding (IB) and fungal resistance test specimens as shown in Figure 5.2.
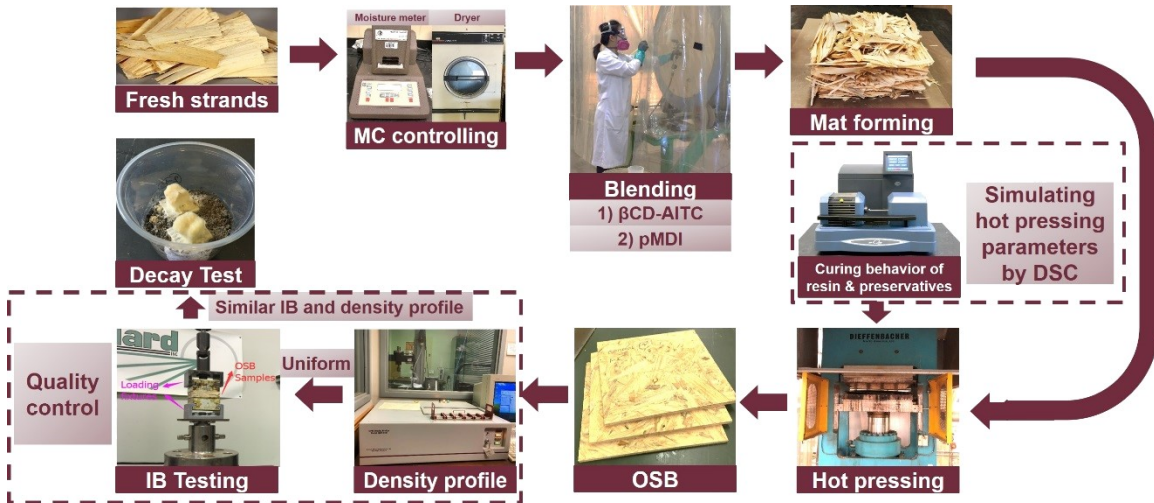
Figure 5.1   OSB manufacturing at Mississippi State University
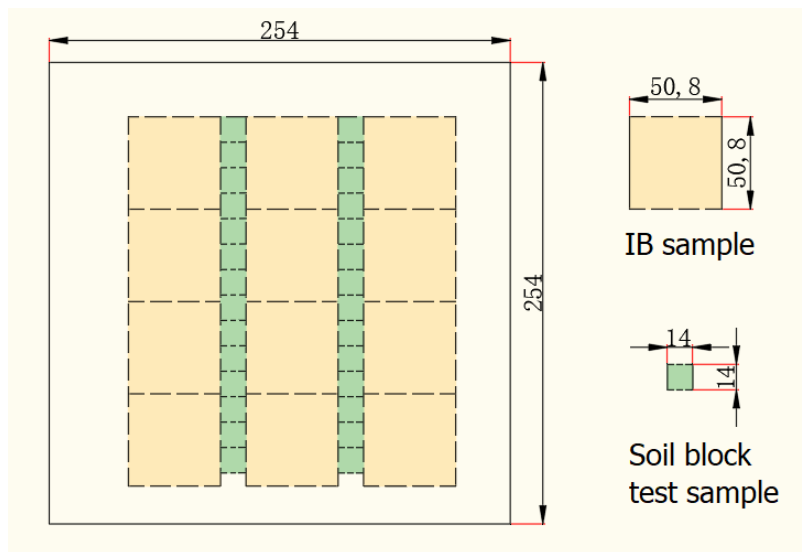
Figure 5.2   Cutting pattern of OSB for IB test and soil block test

5.1.2   Internal bonding and vertical density profile of OSB

The thickness-wise cohesion (i.e. internal bonding (IB) strength) of the OSB panels

was examined according to ASTM D1037-12 (ASTM International, 2012). Twenty-four

IB test specimens (51 mm x 51 mm by panel thickness) were prepared for each treatment. To ensure that the IB test specimens had the similar amounts of strands, resin, and additives, density variations throughout the thickness, vertical density profile (VDP) was measured using a QMS Density profiler model QDP-01 X (Quintek Measurement Systems, Inc. Oak Ridge, Tennessee). The measured VDPs were normalized by using linear interpolation according to the specimen thicknesses and averaged for each treatment. The specimens with VDPs having r^2 greater than 0.4 against the averaged VDP were selected for IB tests. The wide faces of the samples were glued to 51 mm × 51 mm aluminum alloy loading blocks using a hot melt adhesive (34614C, Applied Adhesives, MN, USA). The IB strength was measured by applying tensile loads perpendicular to the surface of the specimen at a rate of 0.93472 mm/min using a universal testing machine (Instron Corporation, Massachusetts, USA) (Figure 5.3). The average IB of each treatment was calculated according to the equation below:

$$\text{Internal bond (IB)} = \frac{\text{Maximum load (N)}}{\text{Length } (mm) \times \text{width (mm)}} \tag{5.1}$$
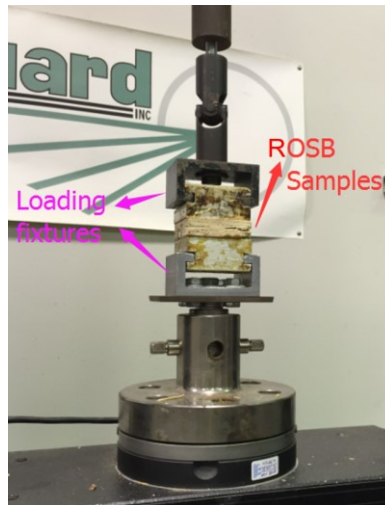
Figure 5.3   Internal bonding strength testing of OSB

5.2 Results and Discussion

5.2.1 Formation of βCD-AITC complex

A plot superimposing the ATR-FTIR spectra of βCD, AITC and βCD-AITC is shown in Figure 5.4a. The peaks for -N=C=S at 2097 cm^{-1} and 2164 cm^{-1} in AITC were present in the spectra of βCD-AITC, indicating the inclusion of AITC in βCD. UV/Vis absorbance analysis indicated that the inclusion yield of AITC in βCD-AITC increased and reached 17% when the concentration of βCD was 5% (Figure 5.4b). This level of AITC inclusion yield in βCD was similar to levels reported in the previous work (Cai et al., 2019).
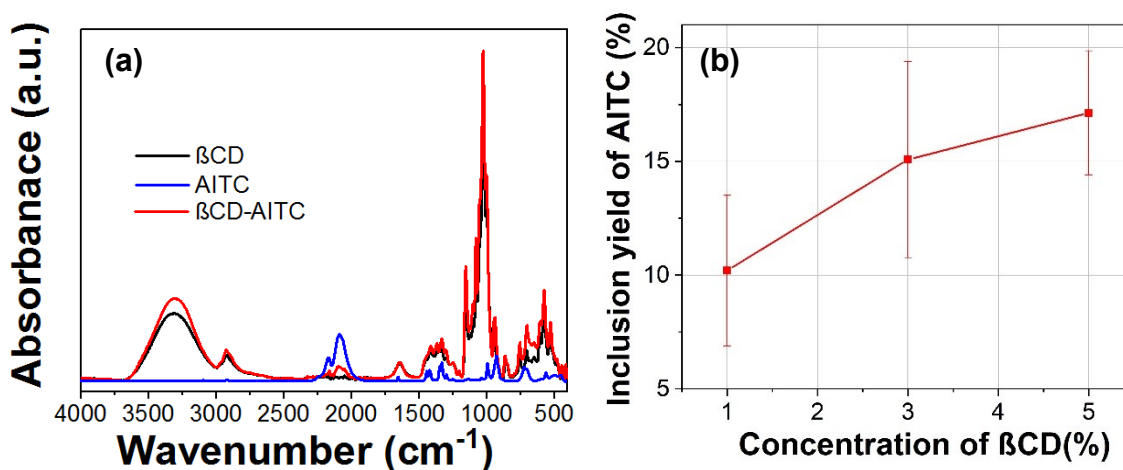
Figure 5.4   a) Baseline-corrected and normalized ATR-FTIR spectra of βCD, AITC and βCD-AITC complex, b) Inclusion yield of AITC in βCD from the UV/Vis method

5.2.2 Thermal stability of the βCD-AITC complex

Thermal behavior of AITC, βCD and the βCD-AITC complex is shown in Figure 5.5. A rapid weight loss was observed in the TGA curve of AITC due to its high volatility. The TGA-DTG curve of βCD showed three main steps of weight loss at 25°C to 100°C, 100°C to 300°C, and 300 to 400°C. Weight losses in the first and second steps were 3%

and 2%, respectively. The first weight loss is believed to be caused by the evaporation of water molecules (interstitial and intra-cavity) in βCD (Crupi et al., 2007). The second weight loss is ascribed to the partial decomposition of βCD (Plackett et al., 2007). The third weight loss from 300 to 400 °C is attributed to the decomposition of βCD. However, the βCD-AITC complex experienced 6% weight loss before 100°C, which is much greater than neat βCD. This greater mass loss is probably associated with the loss of water and loosely bound AITC in βCD. Between 100 °C and 300°C, 12% of weight loss occurred, which is mainly attributed to delayed evaporation of AITC. The remaining weight loss of around 70% between 300 °C to 400°C was related to the decomposition of βCD. Our TGA results suggested that the amount of AITC in the βCD-AITC complex was between 12% and 18%, which is in good agreement with the UV/Vis analysis. The greatly improved thermal stability of the βCD-AITC suggests that encapsulated AITC would be more stable during the OSB manufacturing process.
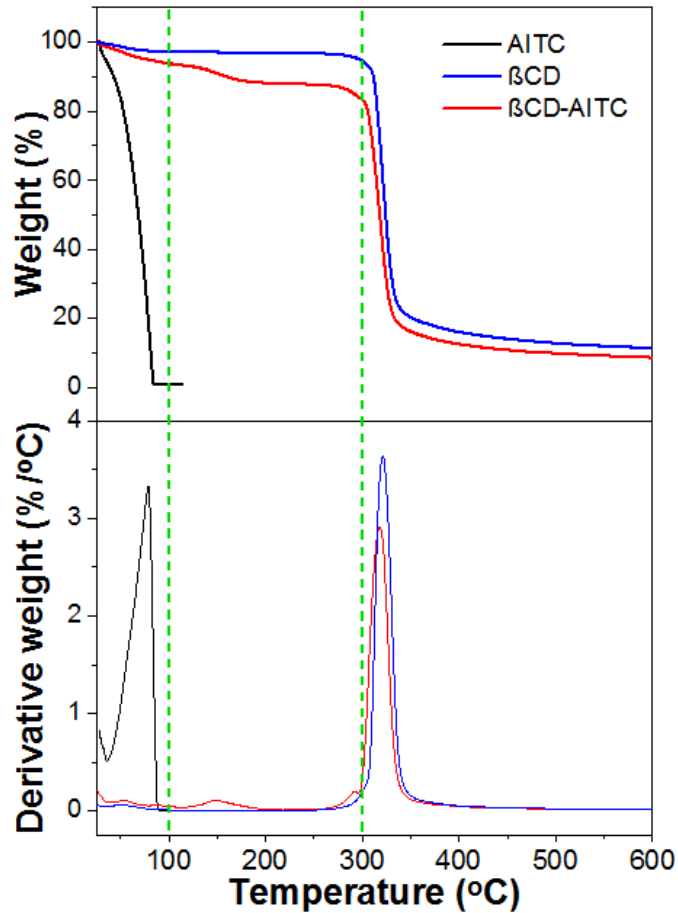
Figure 5.5   TGA (top) and TGA-DTA (bottom) curves of AITC, βCD and the βCD-
AITC complex

5.2.3   Curing behavior of polymeric methylene diphenol diisocyanate, βCD-AITC complex and wood mixture

DSC curves of pMDI, βCD-AITC, and wood, as well as their physical mixture are

shown in Figure 5.6. All the samples exhibited an endothermic peak around 60 °C due to

dehydration. The DSC curve of pMDI showed a broad transition point ranging from 90 to

200 °C due to the curing of various pMDI macromonomers in the pMDI resin (Harper et

al., 2001). βCD-AITC exhibited two broad endothermic peaks between 80 and 130 °C as

well as 155 and 200 ºC, and a narrow peak centered at 145 ºC, which may reflect AITC evaporation. A very broad endothermic peak between 75-200 ºC was also observed in wood. The peaks for neat βCD-AITC, pMDI and wood were compared with those for their mixtures to examine possible interactions between them. The endothermic peak in the mixture of pMDI and βCD-AITC complex was centered at 166 ºC, whilst the mixture of pMDI and wood was at 174 ºC. The overall DSC profile remained unchanged when βCD-AITC was added to pMDI and wood with a marginal broadening in the temperature range of 150-200 ºC, indicating that the addition of βCD-AITC did not obviously affect the curing temperature of the pMDI and wood mixture. These results led us to use a hot pressing temperature of 174 ºC for panel manufacturing.
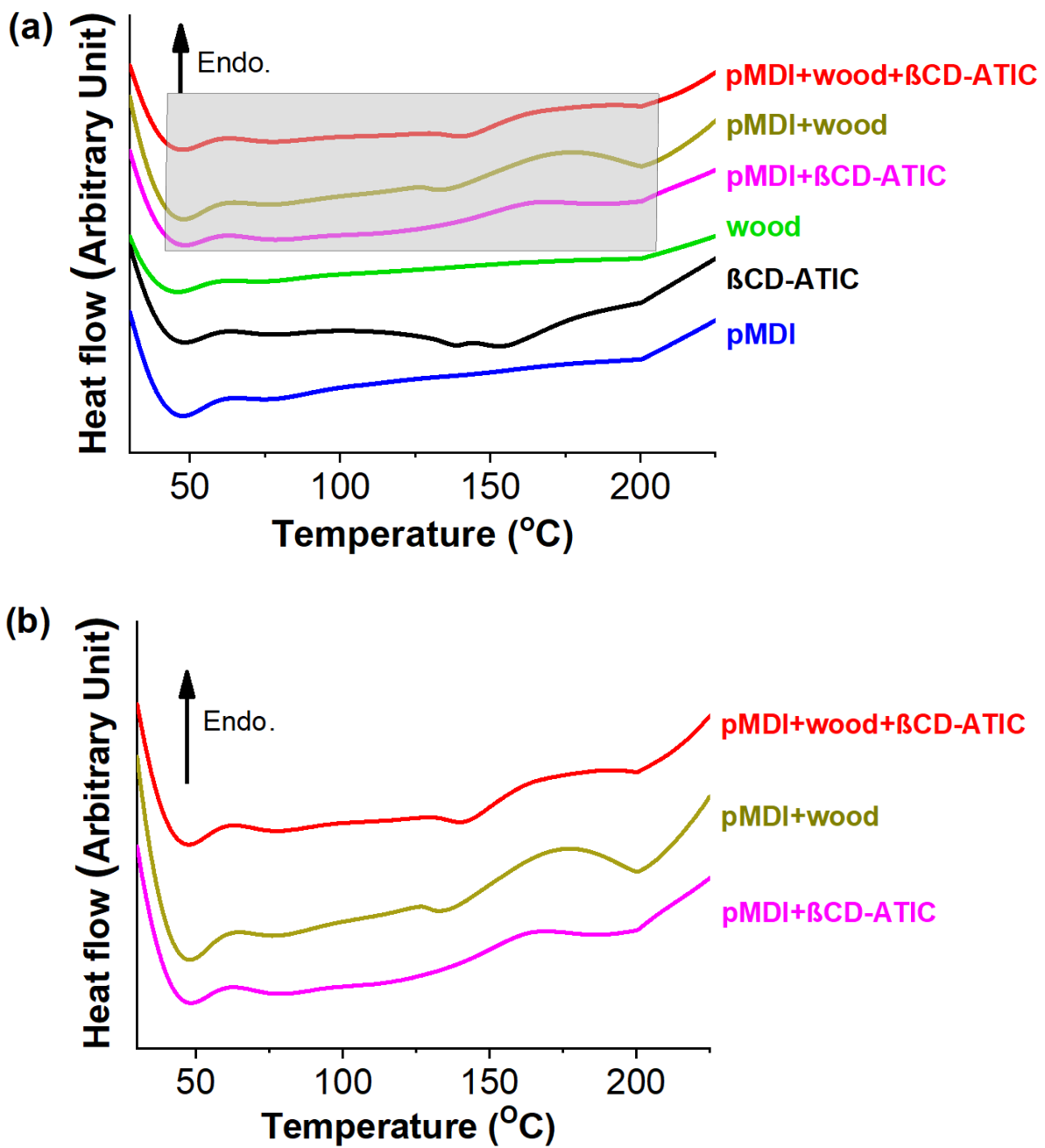
Figure 5.6   (a) DSC curves of pMDI, βCD-AITC, wood, and mixtures of the three
                 materials; and (b) enlarged DSC curves of the physical mixtures

It should be noted that interactions among preservatives, wood, and resin during

pressing could be far more complicated than the model DSC experiment in terms of the

sample shape and size, moisture in wood strands, and a heat transfer rate. Another major difference between the OSB manufacturing process and the DSC procedure is that moisture in the wood strands plays an important role in heat transfer from the surface to the core layer of the mats during the hot pressing cycle (Wong et al., 1999). Moisture also influences pMDI curing as the electrophilic isocyanate groups in the pMDI resin are active toward a variety of nucleophiles (Das, 2005), i.e. moieties containing free hydroxyl groups. Hence, pMDI would interact both with the hydroxyl groups of βCD-AITC complex and moisture of the strands during its curing process (Weaver and Owen, 1995; He and Yan, 2005). This would not be relevant in the DSC procedure because residual moisture was removed to erase the thermal history of the polymers and reduce the variations in data interpretation. In panel manufacturing, the mat was pressed between two hot plates at a constant temperature for approximately 3 minutes, while the DSC samples were sealed in the aluminum pan and heated on the top of the holder with linearly increased temperature as a function of time for about 30 minutes. The varying methods might affect the curing behavior of the polymers and lead to differences in bonding ability of the final products.

5.2.4   Presence of βCD-AITC in OSB

The presence of βCD-AITC in OSB was confirmed by SEM. Figures 5.7a and b show the tangential surface of the strands with clear resin canals. In comparison, the surface of wood strands treated with 5% and 10% βCD-AITC (Figures 5.7e-f) showed a deposition and associated coating of particulates, which presumably are the βCD-AITC complex.
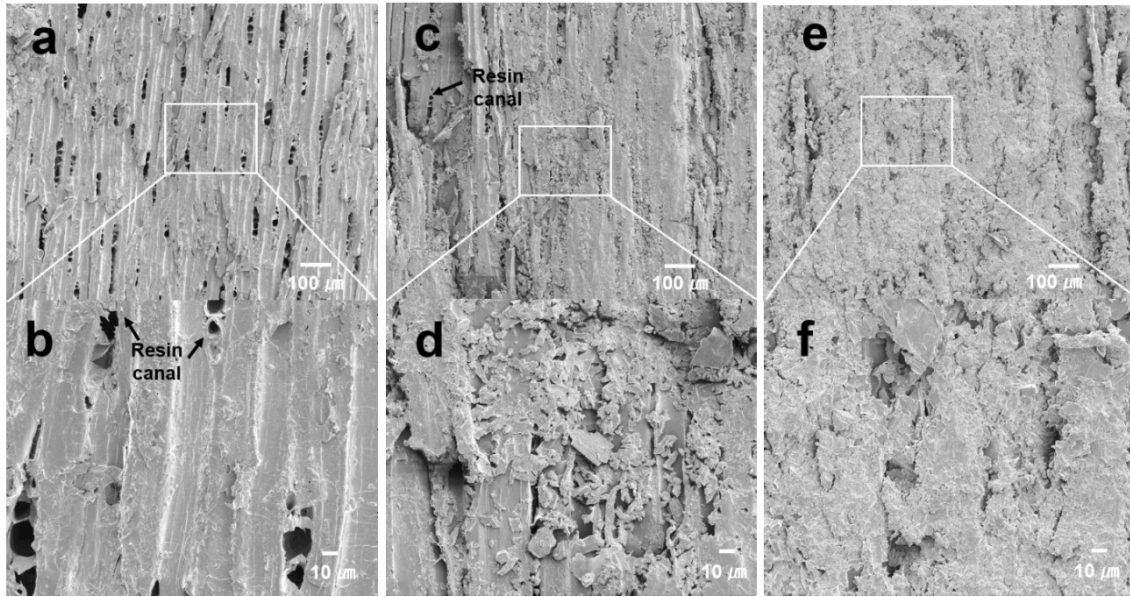
Figure 5.7   SEM images of wood strands at tangential surface resinated (a and b)
            without βCD-AITC, (c and d) 5% βCD-AITC, (e and f) 10% βCD-AITC.
            The fracture surface after internal bonding test was used for SEM imaging

5.2.5   Vertical Density profile of the panel

The distribution of resin and preservatives on the strands as well as the density of

the panels were confirmed by their thickness-wise density variations. Vertical density

profile of wood composites is mainly affected by the moisture contents of the furnish and

the hot pressing parameters, such as press closing speed, pressing time, pressing

temperature, etc. (Wong, 1998; Wang and Winistorferl, 1999). Figure 5.8 shows the

average VDPs of the 2 in x 2 in blocks cut from the OSB panels produced using three βCD-

AITC complex levels. All measured VDPs showed nearly symmetric "M" shapes

characterized with higher density regions near the surfaces (i.e. 10-20% and 80-90% of the

normalized thickness) and low-density regions (i.e. 45-55% of the normalized thickness)

in the cores of the blocks.

The average VDPs were statistically compared at these three regions as expressed in Table 5.2, which were significantly affected by the preservative loading as expected. As compared to the control group, 5% preservative addition caused the density of surface region #1 and #2 to increase by ~2.9% and ~5.4%, respectively, whereas 10% preservative addition caused the density of surface region #1 and #2 to increase by ~10.8% and ~14.7%, respectively. Meanwhile, the core region density was significantly increased by approximately ~5.8% in the 10% treatment panels, but decrease by ~3.1% in case of 5% preservative addition, although not significantly different from the control ($p < 0.05$). These results show that the compactness of the strands near the surface of the treated groups was significantly higher than the cores given the assumption that the preservatives were evenly distributed in the mat. On the other hand, the reduced compactness in core zone might affect the interfacial adhesion and the internal bond strength of the panels.
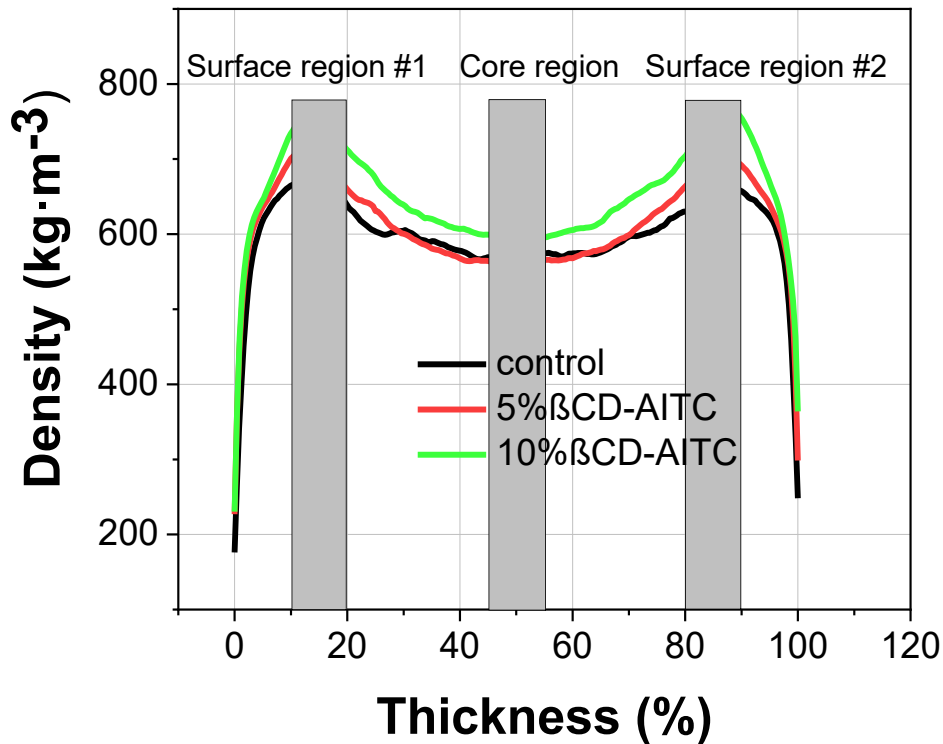
Figure 5.8   Average vertical density profiles of OSB panels containing: 0, 5 or 10% βCD-AITC complex. The data were normalized based on the thickness of each panel.

Table 5.2   Average density (±Standard error) at different regions in OSB panels prepared using different preservatives levels

Preservatives level (%)	Average density ±Standard error (kg/m3)		
	Surface region #1	Core region	Surface region #2
0	665.31±23.95 (CD)	561.51±27.55 (A)	651.95±29.86 (C)
5	684.92±44.16 (D)	543.97±22.06 (A)	686.91±36.33 (D)
10	737.28±28.61 (E)	593.82±27.6 (B)	747.97±19 (E)

Note: Nine replicates. Means followed by the same letter are not significantly different (LSD, $p < 0.05$).

5.2.6   Internal bond strength of the panel

The IB strength of the panels treated with different concentrations of the βCD-AITC complex were significantly lower than the control group (Figure 5.9). The βCD-AITC complex did not affect resin curing under ideal conditions, as shown in the DSC analysis. However, the curing process might be changed because the OSB hot pressing process is more complicated. Factors include the moisture, the increased density near the surfaces and the relatively reduced compact ratio of the cores of the panel might contribute to the reduced cohesion of the panels (Hand et al., 2018). As previously stated, free hydroxyl groups in water and preservatives were more accessible by the pMDI resin, which might also result in reduced adhesion between pMDI resin and wood strands. Compatibility between preservatives and resin systems has long been identified as a major issue in composites. In this study, although the control panels had significantly higher IB than the treated one, our treated OSB panels prepared with both preservative formulations showed IB values well above the required standards for Type OSB/3 application (EN 300, 2006), indicating the feasibility of βCD-AITC complex application during OSB manufacturing.
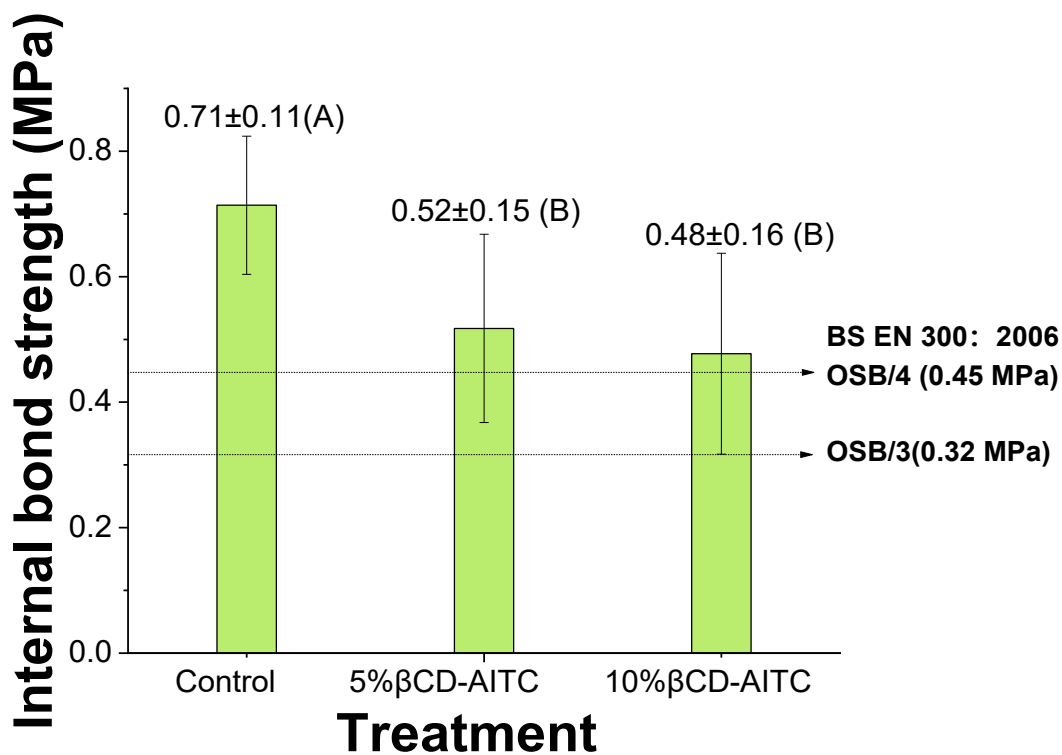
Figure 5.9   Internal bond strength of OSB panels with 0, 5 or 10% βCD-AITC. Error bars represent standard error of the mean. Means followed by the same letter are not significantly different (LSD, $p < 0.05$). For each treatment, four OSB panels were prepared ($n = 3$), and 8 replicates were used for each IB measurement

5.2.7   Decay resistance of βCD-AITC treated OSB against brown rot fungi

OSB blocks after exposure to fungi and the corresponding mass loss are shown in Figures 5.10a and b. Untreated OSB blocks with and without weathering show extensive decay by both fungi with a mass loss of over 35% (Figure 5.10b). Although the mass losses of untreated OSB decayed by *P.placenta* were slightly below 40%, as required in AWPA Standard E10-16, the results still indicate a high activity of the test fungus. βCD-AITC

treated specimens appeared unchanged after exposure to both fungi. Mass losses of treated OSB blocks were significantly lower than those for the controls even after weathering. No significant differences ($p < 0.05$) in mass losses were found in OSB treated with 5% or 10% βCD-AITC. βCD-AITC complex may be locked by pMDI resin in the strands-based panel, which protect the OSB cubes from fungi (Kalnins, 1982). The improved fungi resistance of βCD-AITC complex-treated specimens indicates the potential of the βCD-AITC complex for OSB protection.
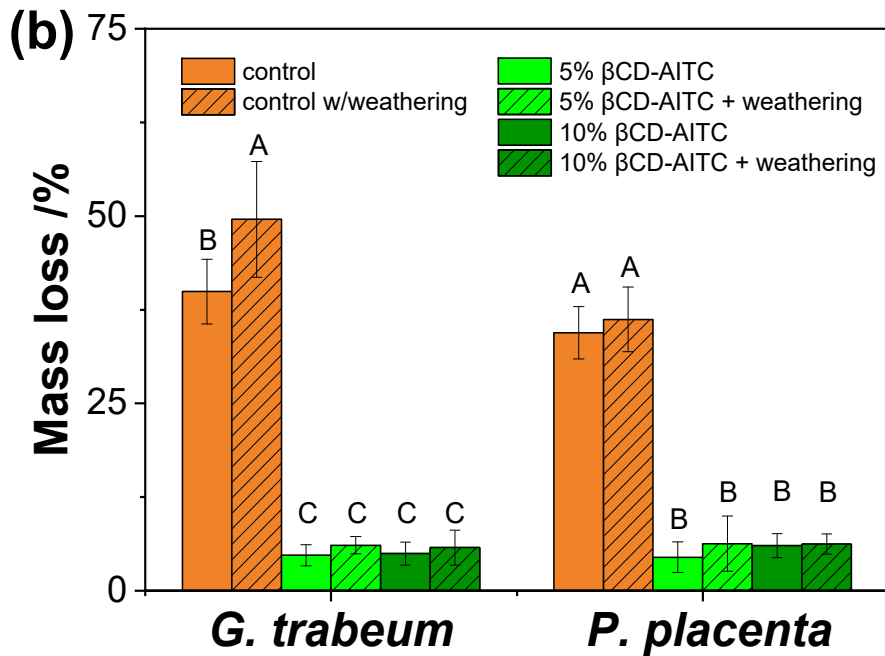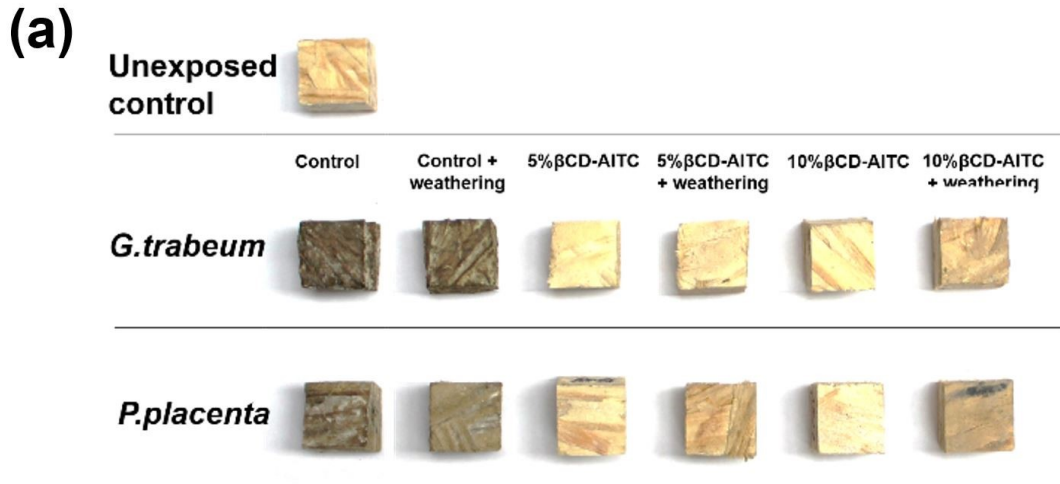
Figure 5.10 (a) Photographs of OSB blocks with different level of βCD-AITC treatments after an 8-week exposure to *G.t*rabeum or *P.placenta.* and (b) the corresponding mass losses.

5.3 Summary

Incorporation of βCD-AITC into OSB panel resulted in slight reductions in IB and altered the density of the resulting panels but also markedly improved decay resistance. The results suggest that incorporation of βCD-AITC can help improve the decay resistance of OSB panels.

CHAPTER VI

RANDOMLY ORIENTED STRAND BOARD PROTECTION BY β-

CYCLODEXTRIN-BORIC ACID COMPLEX

The objective of this study was to partially immobilize boric acid with βCD and apply β-cyclodextrin-boric acid complex in a powder form during the OSB manufacturing process. The leaching, fungicidal and mechanical properties of the boards were evaluated.

For Materials and methods, please refer to the Methods sections in Chapter 2 and Chapter 5 (5.1).

6.1 Results and Discussion

6.1.1 ATR-FTIR analysis of βCD-B complex

Formation of the βCD-B complex was evident by changes in IR spectra of the complex, as compared to the spectra of individual components and physical mixtures. Figure 6.1 shows the IR spectra of boric acid, βCD, inclusion complex (βCD-B) and the physical mixture (βCD & B, at a molar ratio of 1:7) in a solid state. The assignment of boric acid and βCD were listed in Table 6.1 and Table 6.2, respectively. In Figure 6.1, the O-H stretching vibration of the physical mixtures and complex is reflected: (1) the primary and secondary OH groups of βCD, (2) interstitial and intra-cavity crystallized water molecules and (3) the hydroxyl groups of the boric acid centered at 3193 cm^{-1}. These overlapping peaks gave rise to very broad bands that made the spectra interpretation difficult.
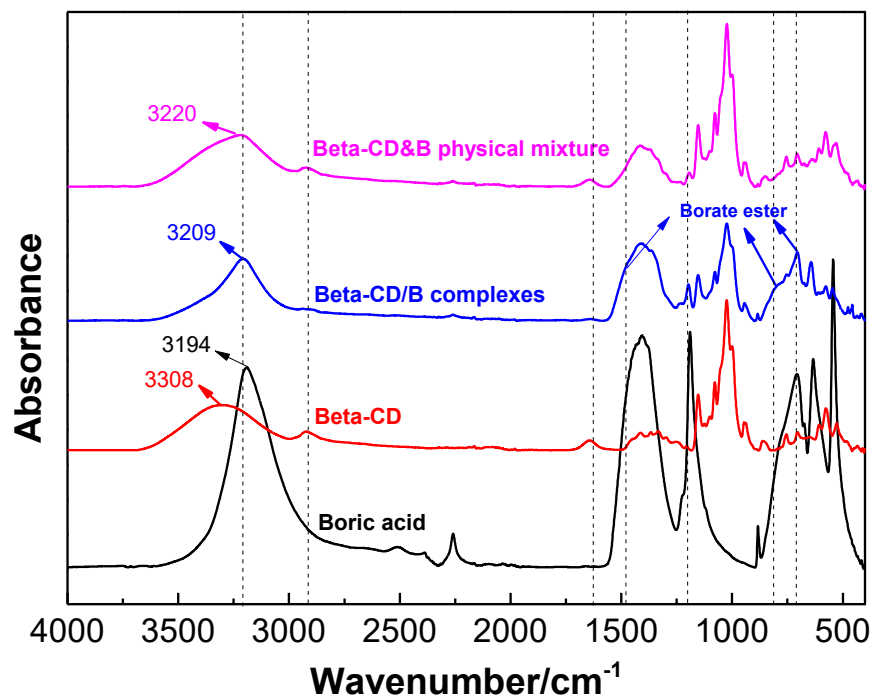
Figure 6.1   Infrared spectra of boric acid, βCD, βCD-B complex and their physical mixture

O-H stretching spectra of the βCD-B complex exhibited a different profile when compared with the physical mixture and pure βCD (Figure 6.1). The OH group in the spectrum of the βCD-B complex had a narrower band at a lower frequency (around 3209 cm^{-1}) than those of the physical mixture and pure βCD. This observation suggests the formation of a new bond between boric acid and βCD, and redistribution of the water molecules among the different hydrogen bonds sites. Moreover, the C-H stretching (~2924 cm^{-1}) in the βCD-B complex exhibited lower intensity and shifted to a lower frequency, suggesting a weakening of the C-H bonds as a result of an altered environment around these bonds upon complexation. The intensity of O-H stretching at 1645 cm^{-1} was greatly

decreased in βCD-B, as compared to βCD and the βCD & B mixture, indicating a reduced

number of H_2O molecules included in the cyclodextrin cavities or the OH groups of βCD

involved in complexation with boric acid. These results were also supported by the

appearance of new borate ester $B(OR)_3$ peaks at 1473, 805, 728 cm^{-1}. Therefore, the

formation of the βCD-B complex was indicated by the changes of OH groups and the

formation of new peaks attributed to borate ester.

Table 6.1   Infrared Spectroscopy assignment of boric acid

Boric acid	
IR (cm^{-1})	Assignment*
3193	v(O-H)
2521	v(O-H)
2373	
2353	
2260	
1409	$v_{asym.}$(B$_3$-O)
1191	$v_{asym.}$(B$_3$-O)
883	$v_{sym.}$(B$_3$-O)
706	γ(B$_3$-O)
634	γ(B$_3$-O)
544	δ(B$_3$-O)
* v: stretching; γ:out-of-plane bending;	
δ: scissoring; asym.: asymmetric;	
sym.: symmetric.	
B$_3$-O: three coordinate boron	

Adopted with modification from
Jun et al., 1995

Table 6.2   Infrared Spectroscopy peak assignments for β-cyclodextrin (βCD)

βCD	
IR (cm^{-1})	Assignment*
3308	v(O-H)
2924	v(CH)
1415	δ(O-H)
1367	δ(CH)
1333	δ(CH)
1330	δ(CH)
1246	δ(CH)
1153	$v_{asym.}$(C-O-C)pyranose ring vibration
1078	v(C-O)
1024	v(C-O)
1000	$v_{sym.}$(C-O-C)
946	$v_{sym.}$(C-O-C)
938	$v_{sym.}$(C-O-C)
862	Breath vibration of glucose ring
754	In-plane deformation vibration of glucose
705	In-plane deformation vibration of glucose
650	γ(O-H)
607	γ(O-H)
577	γ(O-H) Skeletal vibration
528	γ(O-H)
478	Skeletal vibration
440	γ(O-H)
* v: stretching; γ:out-of-plane bending; δ: scissoring; asym.: asymmetric; sym.: Symmetric.	

Adopted with modification from Li et al., 2010

Multivariate analysis

Principal component analysis

Most of the characteristic peaks of βCD overlap with βCD-B, making it difficult to differentiate each component in the βCD-B complex. Thus, changes in the ATR-FTIR

spectra were further statistically examined by principal component analysis (PCA) and Multivariate Curve Resolution (MCR) methods.

PCA is a variable-reduction technique that reduces redundant information in a data set and identifies interrelationships among a few principal components (PCs). Figure 6.2a shows PCA score plots of PC1 (variability of 92%) against PC2 (variability of 7%) obtained from ATR-FTIR full spectra data. PC1 showed overall spectral differences between boric acid and βCD. The βCD-B complex was differentiated from the physical mixtures and the pure components by PC2 with loadings characteristic of βCD-B complex absorption bands: borate ester functional groups at 1472, 808 and 728 cm^{-1}. These bands were, thus, a confirmation of βCD-B complexation, and supported the IR analysis
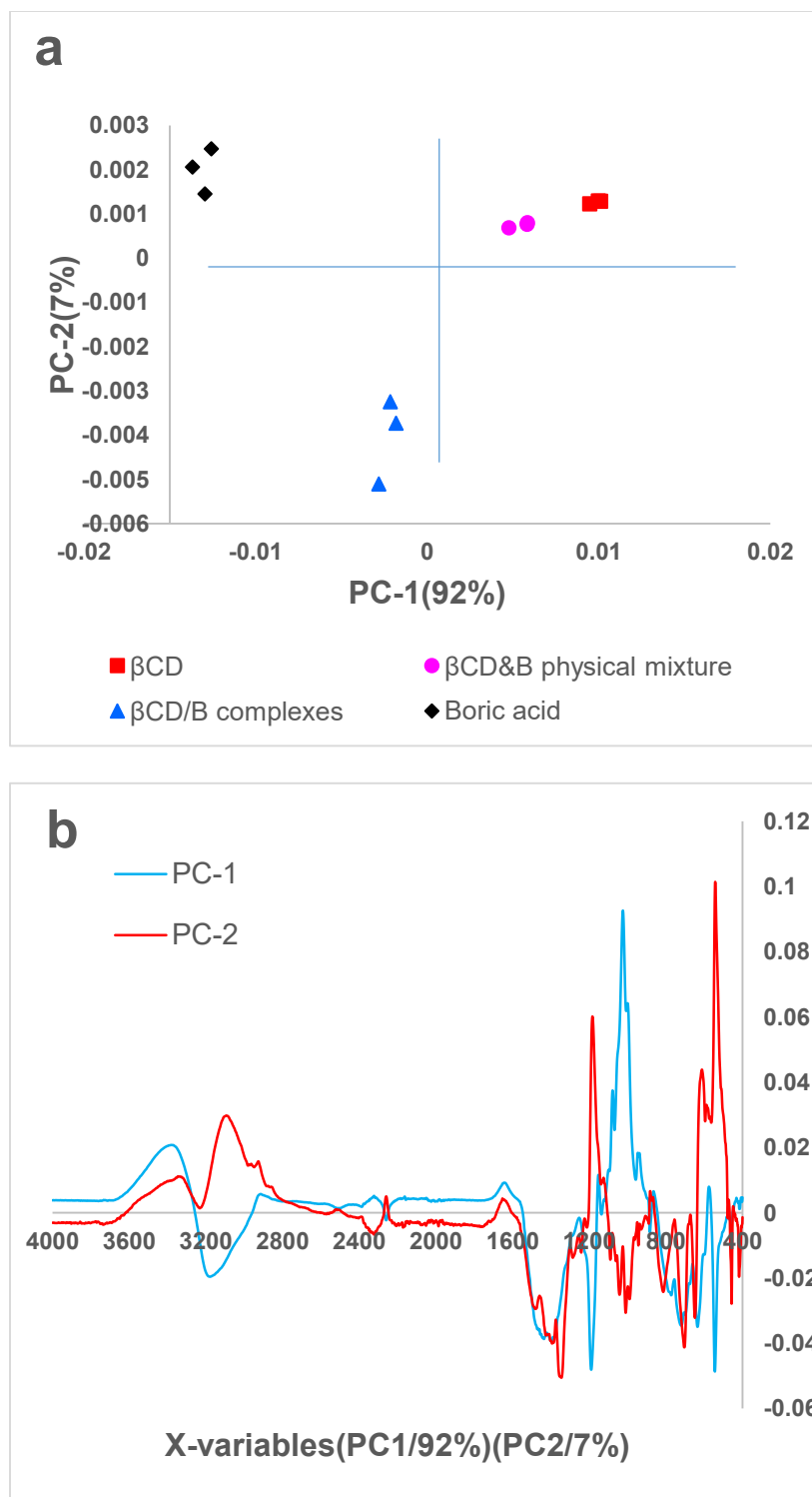
Figure 6.2   (a) PCA score plots (PC1× PC2) of normalized ATR-FTIR spectra of boric acid, βCD, βCD&B physical mixture, and βCD-B complex; (b) loading plots of the PC1 and PC2

Multivariate curve resolution (MCR) analysis

MCR is an effective method that resolves mixtures by determining the ingredient numbers, response profiles and estimating their concentrations (De Juan and Tauler, 2006). In Figure 6.3a, MCR components 1 and 2, resemble the spectra of boric acid and βCD, respectively. Figure 6.3b shows the relative concentration distribution of these two components in our four samples. As shown in Figure 6.3b, βCD contains most of component 2 and a little of component 1, while boric acid has mostly component 1 but a little of component 2. The concentration distribution of these two components in the βCD-B complex and the physical mixtures were totally different. The percentage of component 2, resembling βCD spectra, decreased from 80% in physical mixtures to 45% in the βCD-B complex, yielding higher boric acid absorption when compared to the mixture. The differences in the component concentrations indicate that there were some interactions between boric acid and βCD in the βCD-B complex, as the mole ratio of boric acid to βCD in both βCD-B complex and the physical mixture is the same (7:1).
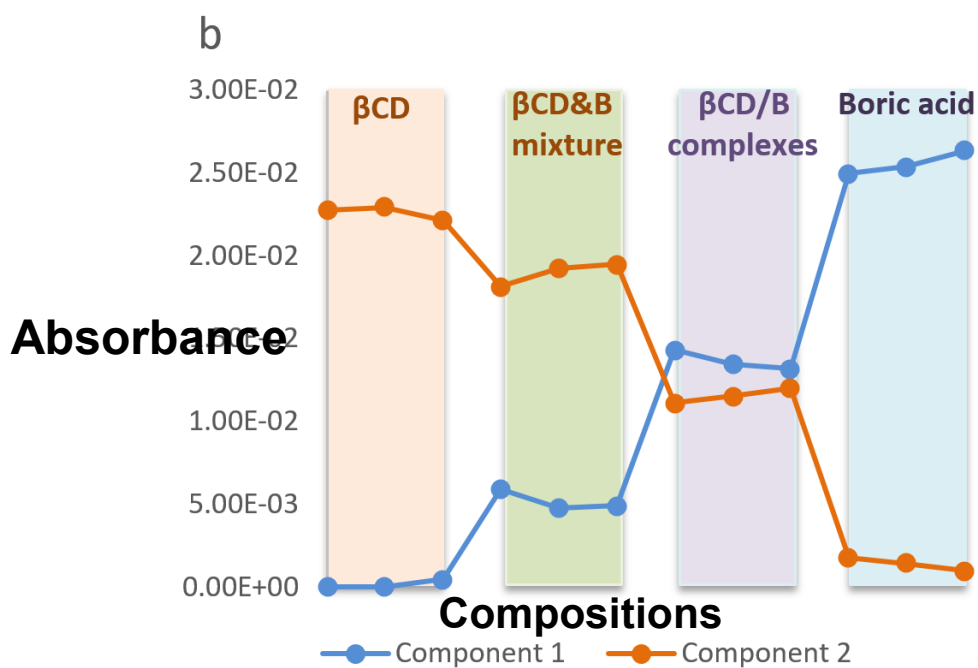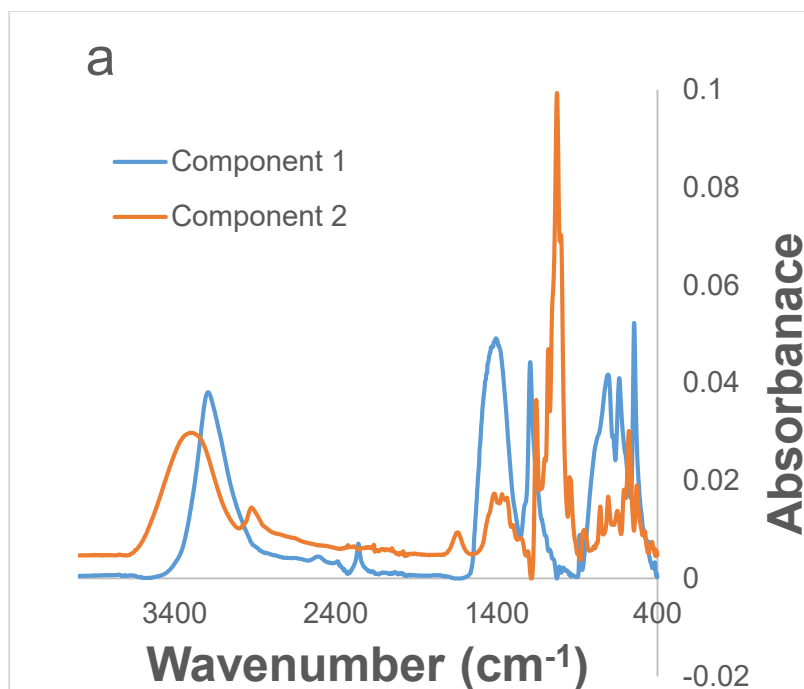
Figure 6.3   (a) Spectra obtained by MCR analysis and (b) component concentration distribution

6.1.2 ^{11}B NMR of βCD-B

The normalized ^{11}B NMR spectra of boric acid, βCD-B complex and the physical mixtures are shown in Figure 6.4. Only one peak (at around 20 ppm) was observed in ^{11}B NMR spectra of boric acid. However, there was a new peak at 1.41 ppm in the ^{11}B NMR spectrum of the βCD-B complex, which was assigned to the B-O-C bond containing residual -OH groups from boric acid (Ahmadi et al., 2018). A small peak at 1.38 pm was also observed at 1.38 ppm in the βCD&B physical mixture due to the tendency for poly-condensation between boric acid and polyols.
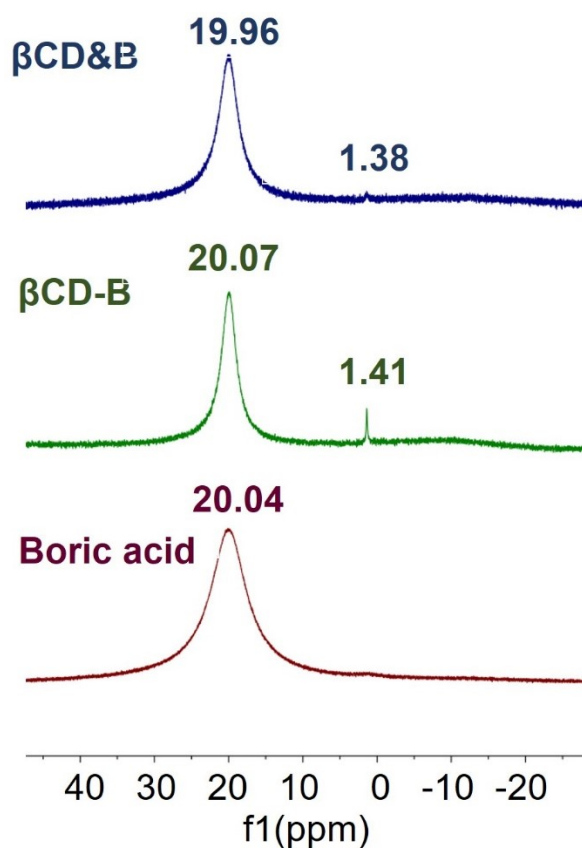
Figure 6.4 ^{11}B NMR of boric acid, βCD-B complex and βCD&B physical mixture in DMSO-D6 (normalized)

6.1.3   ¹HNMR of βCD-B

The ¹H NMR results of boric acid, βCD, and βCD-B complex were shown in Figure 6.5. A new peak at 6.25 ppm was observed in the ¹H NMR spectrum of βCD-B, as compared to that of the neat βCD. Also, the decreased intensities of the peaks of OH3 and OH6 relative to the peak of OH2 in βCD-B indicate that part of boric acid has bonded to the OH groups in βCD. According to the NMR results, the OH groups in boric acid may either attach to the OH2, OH3 or OH6 groups in cyclodextrins.
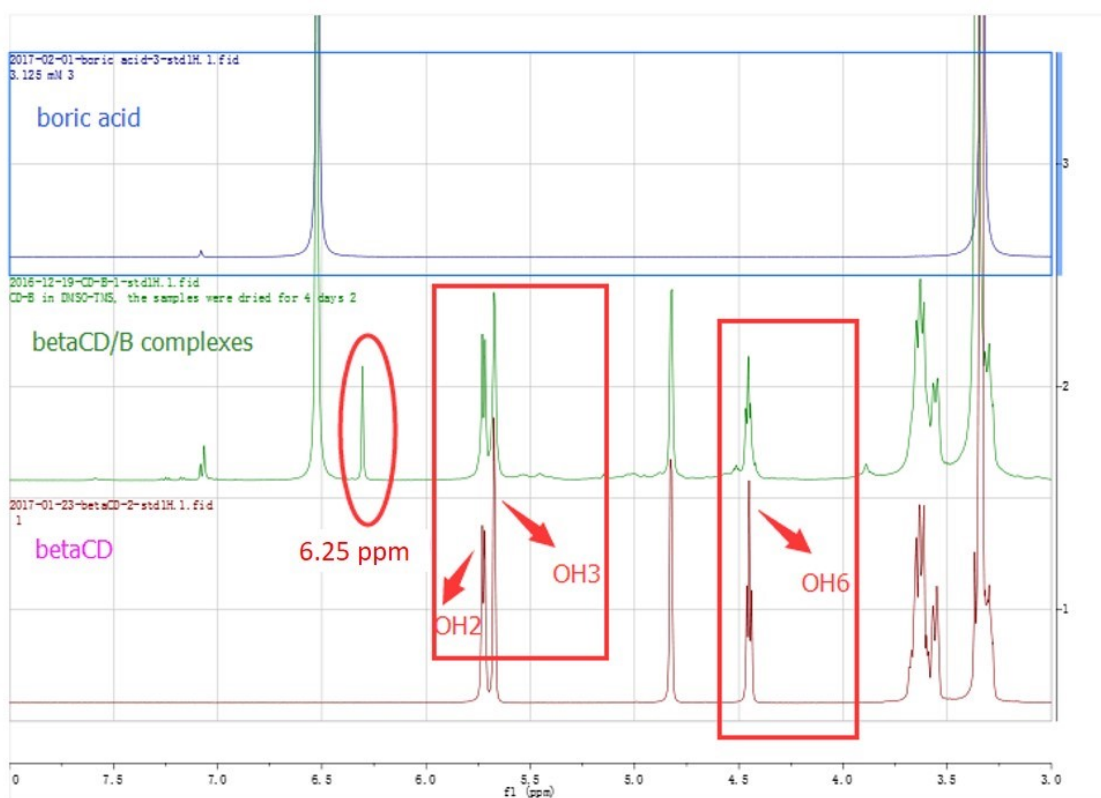
Figure 6.5   ¹H NMR of boric acid, βCD-B complex and βCD in DMSO-D6 (TMS as internal references)

6.1.4   Curing behavior of pMDI/βCD-B complex

Figure 6.6 presents the DSC curves of the third heating of the pMDI resin, βCD-B complex, wood and their physical mixture. An exothermic peak corresponding to the crystallization and crosslinking reaction of βCD-B complex was observed in all the samples containing βCD-B complex (Staroszczyk, 2009). This peak centered at 183 °C in βCD-B complex shifted to lower temperature of 158 °C in presence of the pMDI resin, and further shifted slightly to 156 °C when blended with wood (Figure 6.6b). The decreased exothermic temperature in the mixture of resin, wood and preservatives indicates that the addition of βCD-B complex possibly accelerated the curing of resin, as an elevated temperature is required to initiate the curing reaction of resin.
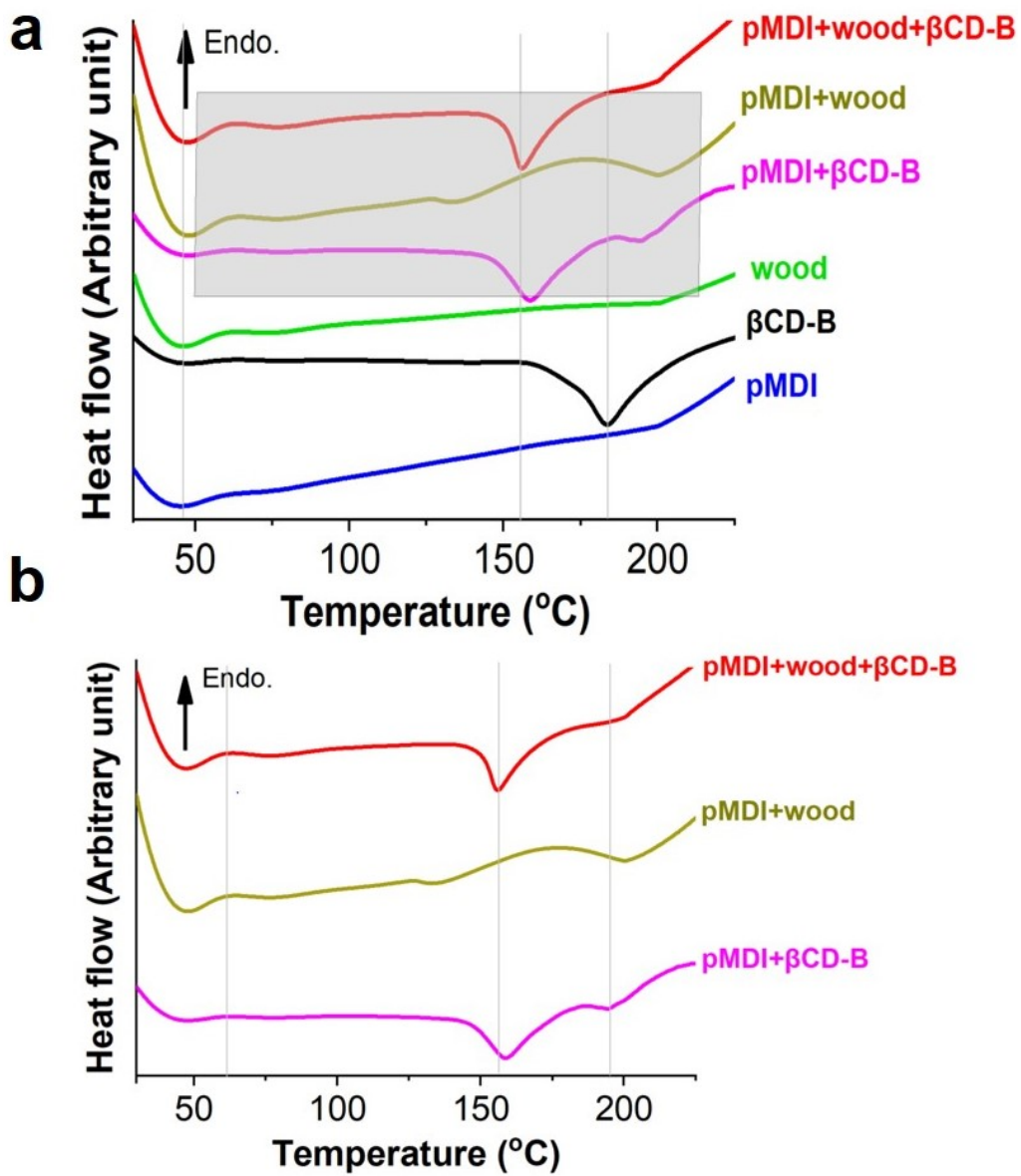
Figure 6.6   (a) DSC curves of pMDI resin, βCD-B complex, wood and their physical mixture; (b) enlarged DSC curves of the physical mixtures

6.1.5   Vertical Density profile and internal bonding of the panel

The vertical density profile (VDP) of the panels is presented in Figure 6.7a, which showed a conventional VDP with denser surface than the middle layer of the panels. Such density profiles are closely related to various processing parameters, such as the moisture distribution in the mat, press closing speed, and hot pressing methods, etc. (Wang and Winistorferl, 1999). The density differences between the surface and middle layer is larger in the preservative-treated samples than those in the control samples (Table 6.3), which might be an effect of the heat, moisture, and pressure transfer in the mat during hot pressing (Wong, et al, 2000).

Figure 6.7b shows the internal bond (IB) strength of the panel as a function of preservative level. The IB was found to be the highest in the control group and the lowest at the level of 5% βCD-B complex treatment. Addition of βCD-B complex to 10% significantly improved the internal bond of the panel ($p<0.05$). When the preservative level was low (5%), the strands of the treated OSB were less in the cores and the compaction ratio of the panel was lower compared to the control OSB, given the assumption that the preservatives and resin were evenly distributed. Also, the complex might react more easily with the resin, thus significantly reduce the IB. When the preservative level was high (10%), the compact ratio of this panel was relatively high and together with the fact that βCD-B complex might act as a crosslinking agent that accelerated the curing of pMDI resin, thus improve the bonding performance (as seen from our DSC results). (Aries, 1960; Leventis et al., 2015). Although the addition of βCD-B complex overall significantly reduced the internal bonding of the panel, their IB is well

above the BS EN 300 standard for load-bearing boards for use in humid conditions (Type OSB/3) (EN 300, 2006).
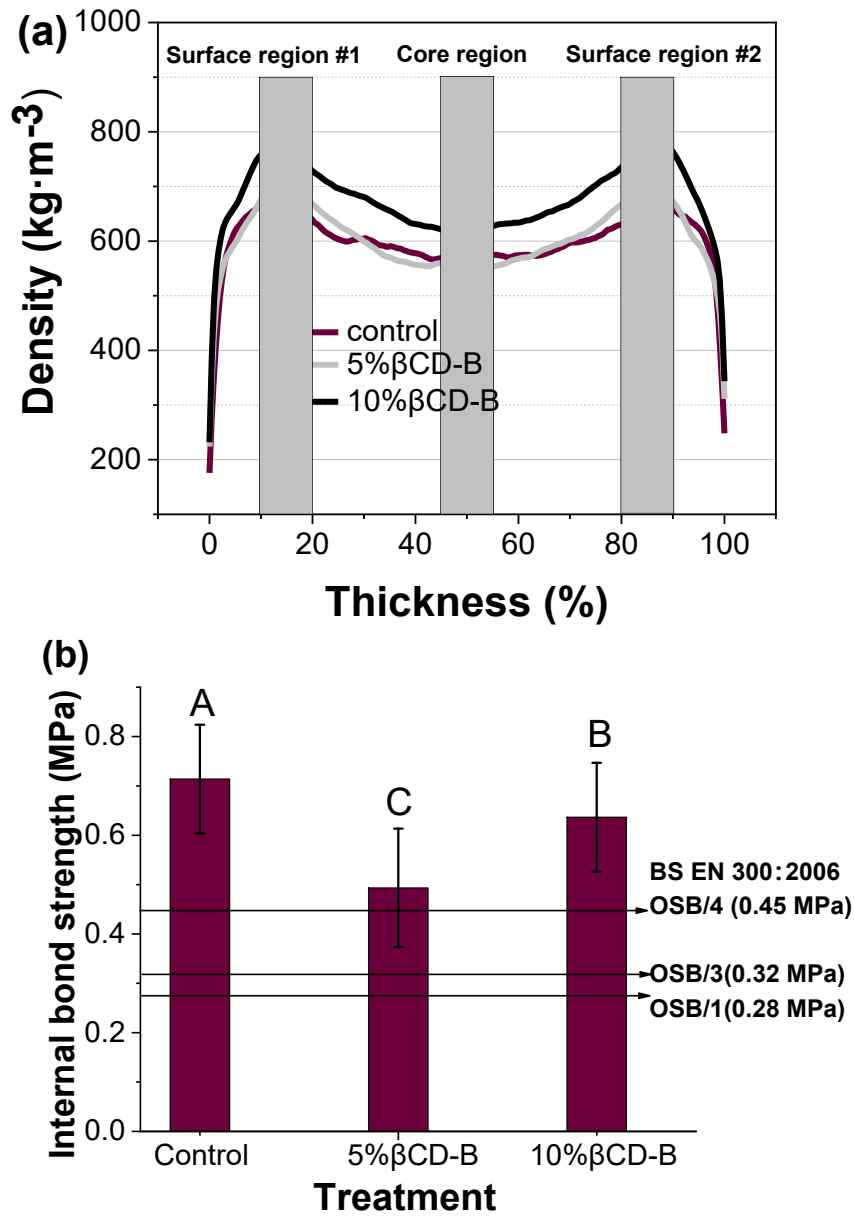
Figure 6.7   (a) Average vertical density profiles normalized based on the thickness of each panel, and (b) internal bond strength of OSB at 0%, 5% and 10%) βCD-B treatment

Table 6.3   Average density (±Standard error) at different regions in OSB panels

Preservatives level (%)	Average density ±Standard error (kg/m3)		
	Surface region #1	Core region	Surface region #2
0	665.31±23.95 (C)	561.51±27.55 (A)	651.95±29.86 (C)
5	712.45±32.87 (D)	567.81±24.08 (A)	711.37±30.13 (D)
10	770.28±36.33 (E)	605.55±26.17 (B)	774.43±39.92 (E)

Note: Means followed by the same letter are not significantly different (LSD, $p < 0.05$).

6.1.6   Decay resistance of βCD complex against brown rot fungi

The fungal resistance of southern pine based OSB treated with βCD-B at a level of 0%, 5% and 10% was tested against *G. trabeum* and *P. placenta* for an incubation time of 8 weeks. Figure 6.8a shows the decayed OSB samples after removing from the culture bottles. The unleached treated OSB cubes presented limited decay as compared to the extensively colonized control samples.

The mass loss of OSB after each treatment was shown in Figure 6.8b. The average percent mass loss caused by *G. trabeum* in control group (both unleached and leached) was greater than 45%, indicating a high activity of the tested fungus. In comparison, the mass loss of unleached OSB at 5% βCD-B complex treatment was decreased to approximately 3% ($p<0.05$), which is not significantly different from 10% βCD-B complex treatment. In the case of leached samples, the mass losses of 5% and 10% βCD-B complex treatment were not significantly different (~15%, $p<0.05$), but still significantly lower than the control groups (50-60%, $p<0.05$). These results indicate that βCD-B complex or part of boric acid might be leached from the samples, resulting in reduced durability against the fungus.
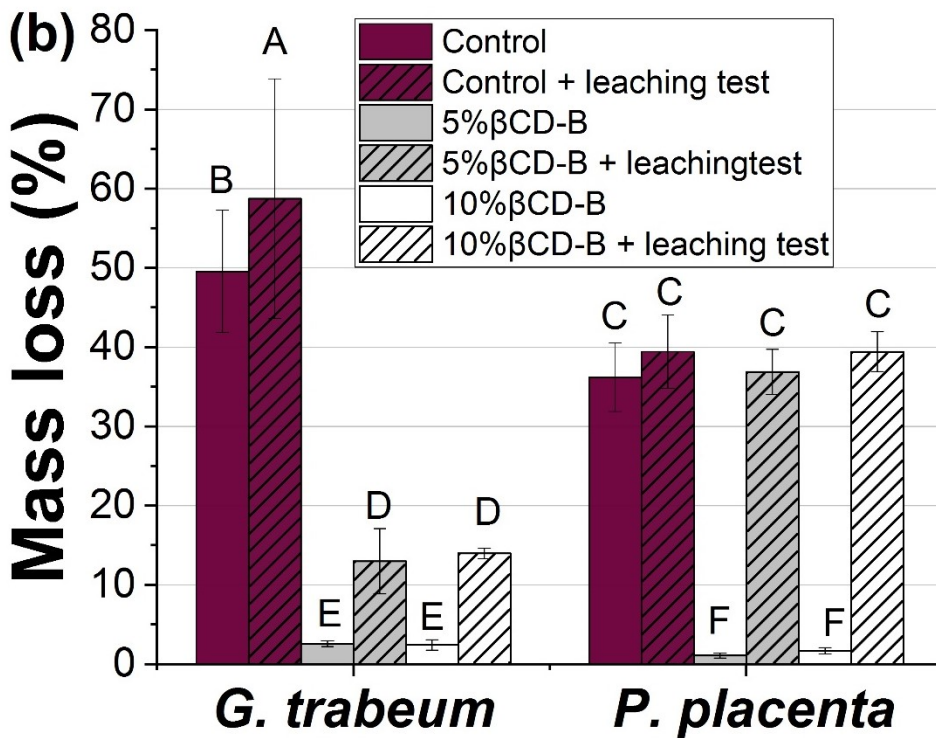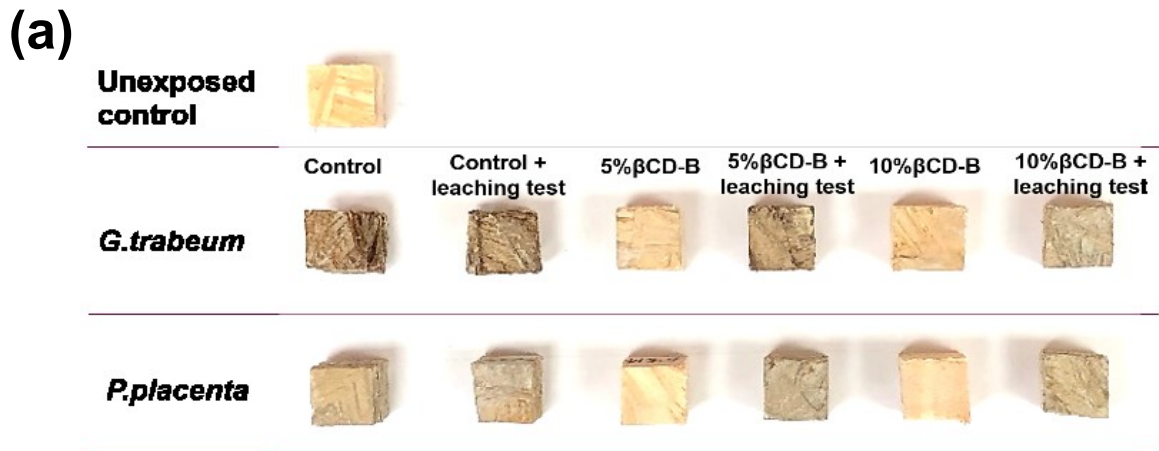
Figure 6.8   (a) Photograph and (b) mass loss of OSB at 0%, 5% and 10% βCD-B
treatment after 8-week exposure to *G. trabeum* and *P. placenta.*

Similar results were observed in *P. placenta* exposed samples, but the leached

samples treated with both preservative levels (at 5% and 10% βCD-B) showed significantly

higher mass loss than *G. trabeum* exposed sample with the same treatments ($p < 0.05$). Overall, the difference between the mass loss of control group and βCD-B complex treated OSB indicates the suitability of βCD-B as a potential wood preservative for wood composites protection where there is a minimum leaching hazard.

The leaching of boric acid in this study might be related to the hydrolysis of boric acid from βCD-B complex. As previously stated, βCD-B complex were obtained by the esterification reaction between boric acid and cyclodextrin. It has been reported that the greater the bulk of R group in the borate esters (Figure 6.9), the slower the hydrolysis rate (Hall, 2006; Steinberg and Hunter, 1957). However, the intrinsic low hydrolysis stability of boric acid esters remains (Steinberg and Hunter, 1957) because of the empty *p*-orbital in boron (Matsumi et al., 1998) (Figure 6.10). In other words, the boron atom in the boric acid ester was *sp2* hybridized. Three of the hybridized *sp2* orbital form covalent bond with other atoms, while one un-hybridized *p*-orbital left. The vacant *p*-orbital imparts the compounds with Lewis acid character and tend to accept unshared electrons from donor species, *e.g.* water molecular (Hall, 2006; Li et al., 2010). The nucleophilic attack of water on the central boron atom was shown in Figure 6.9 (Xiong et al., 2014).

Paradoxically, permanently immobilized borates will affect their biological efficacy (Efhamisisi et al., 2017; Tondi et al., 2012). Therefore, it might be beneficial to design borate esters with a controlled hydrolysis rate and evaluate their biological performance over time.
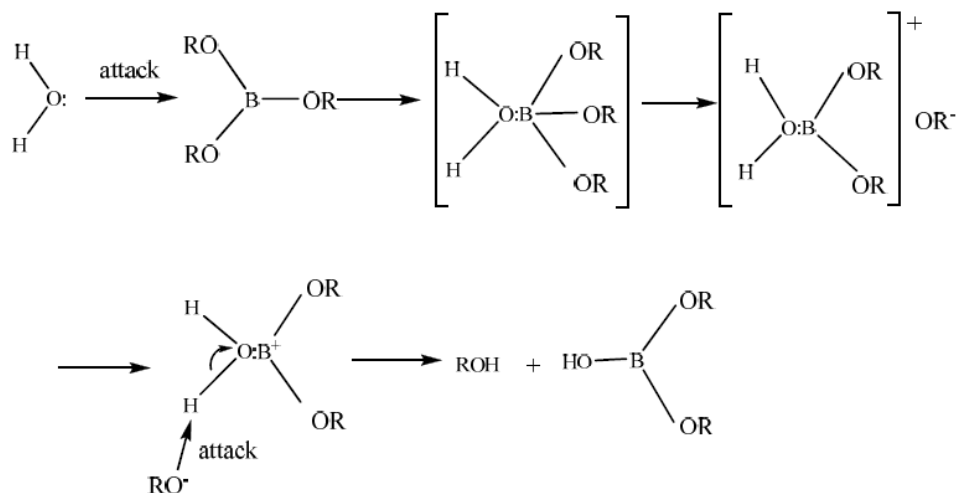
Figure 6.9   The hydrolysis mechanism of borate esters. Adapted from Xiong et al. (2014)
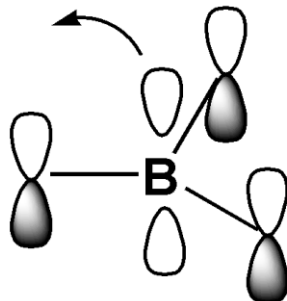
Figure 6.10   Empty p-orbital of boron

6.2   Summary

The present study investigated the feasibility of using βCD-B complex, one of the boron esters, for the protection of oriented strand board wood composites. Boric acid can be partially fixed by βCD. The preservative treated panel showed comparable vertical density profile and remarkable internal bond strength. However, the βCD-B complex is

107

prone to hydrolysis, thus the constructed OSB could be only used for heavy-duty load-bearing boards where there is a minimum leaching hazard.

CHAPTER VII

CONCLUSIONS AND FUTURE WORK

7.1   Conclusions

Seeking environmentally-friendly protection methods for wood and wood composites from fungal degradation has been a hot topic in the field of wood preservation. This proof-of-principle study examined the feasibility of using βCDs for stabilization of volatile and leachable biocides for solid wood and strand-based composites protection. The main findings from the study are:

1. βCD derivatives, such as MβCD and HPβCD, can effectively suppresses the volatility of AITC, a model non-aromatic natural preservative compound, and the βCD-AITC inclusion complexes demonstrate the potential for wood preservation.

2. βCD derivatives are effective sustained-release carriers for essential oils, such as EG, CN, TM and CV, for wood preservation regardless of the weathering test and the tested fungi.

3. The feasibility of βCD-AITC complex for OSB protection was also demonstrated. The βCD-AITC complex treated panels showed internal bonding well above the minimum requirement for OSB/3 panels for load-bearing boards for use in humid conditions and good biological performance with a mass loss lower than 10%.

4. βCD can be used to partially fix boric acid and form the βCD-B complex. This compound showed promising results for OSB protection without sacrificing the internal bond strength of the panels. However, the βCD-B complex is prone to hydrolyze and is not suitable for protection against *G. trabeum* and *P. placenta* in outdoor conditions.

Overall, this study provided a novel approach which stabilizes volatile and leachable biocides using βCDs, and offers an alternative environmentally-friendly protection method of wood and wood composites from fungal degradation.

7.2 Recommendations for future work

The following considerations with respect to the results obtained from this research are recommended:

Since this research provided promising results for using βCDs as carriers for volatile and leachable biocides for wood and strand-based wood composites protection, it would be beneficial to include known preservatives as a comparison for further lab fungal resistance tests and field tests. Future research can also be done by combining the proposed wood preservatives systems with other commercial available preservatives to provide synergistic effects and desirable protection performance against fungi, termites and mold.

This study has demonstrated the feasibility of applying βCD complexes for OSB manufacturing, so it would be very interesting to construct large-size panels and test the other properties, such as water absorption, thickness swelling, modulus of elasticity, modulus of rupture and rolling shear strength, etc. to provide comprehensive results of the βCDs complexes treated OSB. Future studies can also be extended to apply βCD

complexes in other wood composites, such as particle board, fiberboard and plywood, etc. and examine their physical and mechanical properties and durability.

From the boron fixation aspect, given the fact that permanently immobilized boron might lose their biocidal effects, while borate esters, which can be obtained by formation of covalent bond between polyols and boric acid, are subjected to hydrolysis, future work is recommended on designing control released boric acid systems that show the fungal efficacy over the time.

REFERENCES

Ahmadi, Y., Siddiqui, M.T., Haq, Q.M.R., Ahmad, S., 2018. Synthesis and characterization of surface-active antimicrobial hyperbranched polyurethane coatings based on oleo-ethers of boric acid. Arab. J. Chem. https://doi.org/10.1016/j.arabjc.2018.07.001

Al-Nasiri, G., Cran, M.J., Smallridge, A.J., Bigger, S.W., 2018. Optimisation of β-cyclodextrin inclusion complexes with natural antimicrobial agents: thymol, carvacrol and linalool. J. Microencapsul. 35, 26–35. https://doi.org/10.1080/02652048.2017.1413147

Anderson, K.B., Franich, R.A., Hedley, M.E., Kroese, H.W., Meder, R., Waals, J., 1997. Synthesis, characterisation and effectiveness of biguanide derivatives of boric acid as potential fixed-boron wood preservatives. Mater. und Org.

Arantes, V., Goodell, B., 2014. Current understanding of brown-rot fungal biodegradation mechanisms: A review. ACS Symp. Ser. https://doi.org/10.1021/bk-2014-1158.ch001

Aries, R.S., 1960. Process and product of reacting boric acid with isocyanates. U.S. Patent 2,931,831.

ASTM International, 2012. ASTM D1037-12 Standard Test Methods for Evaluating Properties of Wood-Base Fiber and Particle Panel Materials, in: ASTM. West Conshohocken, PA. https://doi.org/10.1520/D1037-12.1

AWPA, 2016a. E10-16: Laboratory method for evaluating the decay resistance of wood-based materials against pure basidiomycete cultures: soil/block test, in: AWPA Book of Standard. American Wood Protection Association Standard, Birmingham, AL, pp. 448–458.

AWPA, 2016b. E22-16: Laboratory method for rapidly evaluating the decay resistance of wood-based materials against pure basidiomycete cultures using compression strength: soil/wafer test, in: AWPA Book of Standard. American Wood Protection Association, Birmingham, AL, pp. 455–462.

AWPA, 2016c. E11-16: Standard Method for Accelerated Evaluation of Preservative Leaching, in: AWPA Book of Standard. American Wood Protection Association, Birmingham, AL, pp. 418–420.

Aytac, Z., Dogan, S.Y., Tekinay, T., Uyar, T., 2014. Release and antibacterial activity of

allyl isothiocyanate/β-cyclodextrin complex encapsulated in electrospun nanofibers. Colloids Surfaces B Biointerfaces 120, 125–131.

Baur, R., Macholdt, H.-T., 2000. Cyclooligosaccharide-boron complex. US patent 6,083,653.

Baysal, E., Ozaki, Æ.S.K., 2004. Dimensional stabilization of wood treated with furfuryl alcohol catalysed by borates 405–415. https://doi.org/10.1007/s00226-004-0248-2

Benny Green, P. David Jones, Laurence R. Schimleck, Darrel D. Nicholas, R.S., 2010. Rapid assessment of southern pine decayed by G. Trabeum by near infrared spectra collected from the radial surface. Wood Fiber Sci. 42, 450–459.

Bhat, S., Chandrasekaran, S., 1996. Oxygenation of alkenes with t-BuOOH catalysed by β-cyclodextrin borate. Tetrahedron Lett. 37, 3581–3584.

Buchanan, C.M., Buchanan, N.L., Edgar, K.J., Ramsey, M.G., 2007. Solubilty and dissolution studies of antifungal drug:hydroxybutenyl-$β$-cyclodextrin complexes. Cellulose 14, 35–47. https://doi.org/10.1007/s10570-006-9076-x

Cabrera, Y., Morrell, J.J., 2009. Effect of wood moisture content and rod dosage on boron or fluoride movement through Douglas-fir heartwood. For. Prod. J. 59, 93–97.

Cai, L., Jeremic, D., Lim, H., Kim, Y., 2019. β-Cyclodextrins as sustained-release carriers for natural wood preservatives. Ind. Crops Prod. 130, 42–48. https://doi.org/10.1016/j.indcrop.2018.12.061

Caldeira, F., 2010. Boron in Wood Preservation A Review in its Physico-Chemical Aspects. Silva Lusit. 18, 179–196.

Celebioglu, A., Yildiz, Z.I., Uyar, T., 2018. Fabrication of Electrospun Eugenol/Cyclodextrin Inclusion Complex Nanofibrous Webs for Enhanced Antioxidant Property, Water Solubility, and High Temperature Stability. J. Agric. Food Chem. 66, 457–466. https://doi.org/10.1021/acs.jafc.7b04312

Chang, Y.-N., Zhang, M., Xia, L., Zhang, J., Xing, G., 2012. The toxic effects and mechanisms of CuO and ZnO nanoparticles. Materials (Basel). 5, 2850–2871.

Chen, Z., Meng, H., Xing, G., Chen, C., Zhao, Y., Jia, G., Wang, T., Yuan, H., Ye, C., Zhao, F., 2006. Acute toxicological effects of copper nanoparticles in vivo. Toxicol. Lett. 163, 109–120.

Chittenden, C., Singh, T., 2011. Antifungal activity of essential oils against wood degrading fungi and their applications as wood preservatives. Int. Wood Prod. J. 2, 44–48. https://doi.org/10.1179/2042645311Y.0000000004

Chun, J.-Y., Jo, Y.-J., Bjrapha, P., Choi, M.-J., Min, S.-G., 2015. Antimicrobial Effect of

α- or β-Cyclodextrin Complexes with *Trans* -Cinnamaldehyde Against *Staphylococcus aureus* and *Escherichia coli*. Dry. Technol. 33, 377–383. https://doi.org/10.1080/07373937.2014.957388

Clausen, C.A., Green, F., 2003. Oxalic acid overproduction by copper-tolerant brown-rot basidiomycetes on southern yellow pine treated with copper-based preservatives. Int. Biodeterior. Biodegradation 51, 139–144.

Crupi, V., Ficarra, R., Guardo, M., Majolino, D., Stancanelli, R., Venuti, V., 2007. UV–vis and FTIR–ATR spectroscopic techniques to study the inclusion complexes of genistein with β-cyclodextrins. J. Pharm. Biomed. Anal. 44, 110–117.

Cui, W., Kamdem, P., 1999. Bioefficiency of boric acid grafted on to wood. Int. Res. Gr. Wood Preserv. IRG/WP 99–30202.

Das, S., 2005. Wood/Polymeric Isocyanate Resin Interactions: Species dependence.

De Juan, A., Tauler, R., 2006. Multivariate curve resolution (MCR) from 2000: progress in concepts and applications. Crit. Rev. Anal. Chem. 36, 163–176.

Del Valle, E.M.M., 2004. Cyclodextrins and their uses: A review. Process Biochem. 39, 1033–1046. https://doi.org/10.1016/S0032-9592(03)00258-9

Del Valle, E.M.M., 2004. Cyclodextrins and their uses: A review. Process Biochem. 39, 1033–1046. https://doi.org/10.1016/S0032-9592(03)00258-9

Divakar, S., Maheswaran, M.M., 1997. Structural studies on inclusion compounds of beta-cyclodextrin with some substituted phenols. J. Incl. Phenom. Mol. Recognit. Chem. 27, 113–126. https://doi.org/10.1023/a:1007949215051

Efhamisisi, D., Thevenon, M., Hamzeh, Y., Pizzi, A., Karimi, A., 2017. Tannin-boron complex as a preservative for 3-ply beech plywoods designed for humid conditions 71, 249–258. https://doi.org/10.1515/hf-2016-0130

EN 300, 2006. Oriented Strand Boards (OSB) -Definitions, classification and specifications.

Engelman, D.M., Steitz, T.A., Goldman, A., 1986. Identifying nonpolar transbilayer helices in amino acid sequences of membrane proteins. Annu. Rev. Biophys. Biophys. Chem. 15, 321–353.

Freeman, M.H., McIntyre, C.R., 2008. A comprehensive review of copper-based wood preservatives: with a focus on new micronized or dispersed copper systems. For. Prod. J. 58, 6–28.

Freeman, M.H., Mcintyre, C.R., Associates, M., 2009. A Critical and Comprehensive Review of Boron in Wood Preservation, in: Proceedings of the American Wood

Protection Assoc. pp. 297–294.

Gezer, E.D., Michael, J.H., Morrell, J.J., 2007. Effects of glycol on leachability and efficacy of boron wood preservatives. Wood fiber Sci. 31, 136–142.

Green III, F., Highley, T.L., 1997. Mechanism of brown-rot decay: paradigm or paradox. Int. Biodeterior. Biodegradation 39, 113–124.

Groenier, James Scott, and S.L., 2006. Preservative-treated Wood and alternative products in the forest service. US Dept. of Agriculture, Forest Service, Technology & Development Program, Missoula, MT.

Hall, D.G., 2006. Structure, properties, and preparation of boronic acid derivatives. Overview of their reactions and applications. Boronic acids Prep. Appl. Org. Synth. Med. 1, 1–99.

Hand, W.G., Ashurst, W.R., Via, B., Banerjee, S., 2018. Curing behavior of soy flour with phenol-formaldehyde and isocyanate resins. Int. J. Adhes. Adhes. 87, 105–108.

Hansmann, C.H., Wimmer, W.G.R., Teischinger, A., 2002. Permeability of wood-A review. Drev. Vysk. 47, 1–16.

Harper, D.P., Wolcott, M.P., Rials, T.G., 2001. Evaluation of the cure kinetics of the wood/pMDI bondline. Int. J. Adhes. Adhes. 21, 137–144.

He, G., Yan, N., 2005. Effect of moisture content on curing kinetics of pMDI resin and wood mixtures. Int. J. Adhes. Adhes. 25, 450–455.

Heinlaan, M., Ivask, A., Blinova, I., Dubourguier, H.-C., Kahru, A., 2008. Toxicity of nanosized and bulk ZnO, CuO and TiO2 to bacteria Vibrio fischeri and crustaceans Daphnia magna and Thamnocephalus platyurus. Chemosphere 71, 1308–1316.

Hill, L.E., Gomes, C., Taylor, T.M., 2013. Characterization of beta-cyclodextrin inclusion complexes containing essential oils (trans-cinnamaldehyde, eugenol, cinnamon bark, and clove bud extracts) for antimicrobial delivery applications. LWT - Food Sci. Technol. 51, 86–93. https://doi.org/10.1016/j.lwt.2012.11.011

Honeychurch, K., 2016. Review: The Application of Liquid Chromatography Electrochemical Detection for the Determination of Drugs of Abuse. Separations 3, 28. https://doi.org/10.3390/separations3040028

Jansook, P., Ogawa, N., Loftsson, T., 2018. Cyclodextrins: structure, physicochemical properties and pharmaceutical applications. Int. J. Pharm. 535, 272–284.

Janzen, S., Nicholas, D.D., 2016. Relation of transverse compression properties and the degree of brown rot biodeterioration of Pinus glabra in the soil block test. Holzforschung 70, 1067–1071.

Jebrane, M., Heinmaa, I., 2016. Covalent fixation of boron in wood through transesterification with vinyl ester of carboxyphenylboronic acid 70, 577–583. https://doi.org/10.1515/hf-2015-0118

Jeremic, D., Cooper, P., 2009. PEG quantification and examination of molecular weight distribution in wood cell walls. Wood Sci. Technol. 43, 317.

Jun, L., Shuping, X., Shiyang, G., 1995. FT-IR and Raman spectroscopic study of hydrated borates. Spectrochim. Acta Part A Mol. Biomol. Spectrosc. 51, 519–532.

Kalnins, M.A., 1982. Chemical modification of wood for improved decay resistance. Wood Sci. 15, 81–89.

Kartal, S.N., Green Iii, F., Clausen, C.A., 2009. Do the unique properties of nanometals affect leachability or efficacy against fungi and termites? Int. Biodeterior. Biodegradation 63, 490–495.

Kayaci, F., Ertas, Y., Uyar, T., 2013. Enhanced thermal stability of eugenol by cyclodextrin inclusion complex encapsulated in electrospun polymeric nanofibers. J. Agric. Food Chem. 61, 8156–8165. https://doi.org/10.1021/jf402923c

Kfoury, M., Landy, D., Fourmentin, S., 2018. Characterization of cyclodextrin/volatile inclusion complexes: a review. Molecules 23, 1204.

Kirkpatrick, J.W., Barnes, H.M., 2006. Biocide Treatments for Wood Composites - A Review. Int. Res. Gr. Wood Prot. Doc. No. IRG/WP, 6, 40323. 1–21.

Koch, P., 1972. Utilization of the Southern Pines-Volume 1, Agricultural Handbook SFES-AH-420. Asheville, NC: USDA-Forest Service, Southern Forest Experiment Station. 1-734.

Kubicek, C.P., Druzhinina, I.S., 2007. Environmental and microbial relationships. Springer Science & Business Media. https://doi.org/https://doi.org/10.1007/978-3-540-71840-6

Landy, D., Fourmentin, S., Salome, M., Surpateanu, G., 2000. Analytical improvement in measuring formation constants of inclusion complexes between β-cyclodextrin and phenolic compounds. J. Incl. Phenom. Macrocycl. Chem. 38, 187–198. https://doi.org/10.1023/a:1008156110999

Lebow, S., 2004. Alternatives to chromated copper arsenate (CCA) for residential construction. Madison.

Leventis, N., Sotiriou-Leventis, C., Saeed, A.M., Donthula, S., Majedi Far, H., Rewatkar, P.M., Kaiser, H., Robertson, J.D., Lu, H., Churu, G., 2015. Nanoporous polyurea from a triisocyanate and boric acid: a paradigm of a general reaction pathway for isocyanates and mineral acids. Chem. Mater. 28, 67–78.

Li, W., Lu, B., Sheng, A., Yang, F., Wang, Z., 2010. Spectroscopic and theoretical study on inclusion complexation of beta-cyclodextrin with permethrin. J. Mol. Struct. 981, 194–203.

Li, X., Jin, Z., Wang, J., 2007. Complexation of allyl isothiocyanate by α- and β-cyclodextrin and its controlled release characteristics. Food Chem. 103, 461–466. https://doi.org/10.1016/J.FOODCHEM.2006.08.017

Li, X.N., Zheng, G., Yang, H.X., 2010. Study on synthesis and properties of a novel borate ester surfactant, in: Advanced Materials Research. Trans Tech Publ, pp. 857–861.

Liang, S.-S., Shiue, Y.-L., Kuo, C.-J., Guo, S.-E., Liao, W.-T., Tsai, E.-M., 2013. Online monitoring oxidative products and metabolites of nicotine by free radicals generation with Fenton reaction in tandem mass spectrometry. Sci. World J. 2013.

Lim, L., Tung, M.A., 1997. Vapor pressure of allyl isothiocyanate and its transport in PVDC/PVC copolymer packaging film. J. Food Sci. 62, 1061–1062.

Lin, C.-M., PRESTON III, J.F., Wei, C.-I., 2000. Antibacterial mechanism of allyl isothiocyanate. J. Food Prot. 63, 727–734.

Liping Xiong, Zhongyi He, Liang Qian, Lin Mu, Aixi Chen, Sheng Han, Jianwei Qiu, X.F., 2014. Synthesis, tribological and hydrolysis stability study of novel benzotriazole borate derivative. PLoS One 9, e83501.

Lloyd, J.D., Dickinson, D.J., Murphy, R.J., 1990. The Probable Mechanisms of action of boric acid and borates as wood preservatives, in: International Research Group on Wood Preservation. IRG/WP/1450. IRG Secretariat, Stockholm Sweden. pp. 1–21.

Locci, E., Lai, S., Piras, A., Marongiu, B., Lai, A., 2004. 13C-CPMAS and1H-NMR study of the inclusion complexes of β-cyclodextrin with carvacrol, thymol, and eugenol prepared in supercritical carbon dioxide. Chem. Biodivers. 1, 1354–1366. https://doi.org/10.1002/cbdv.200490098

Marques, H.M.C., 2010. A review on cyclodextrin encapsulation of essential oils and volatiles. Flavour Fragr. J. 25, 313–326.

Matsumi, N., Naka, K., Chujo, Y., 1998. Extension of π-conjugation length via the vacant p-orbital of the boron atom. Synthesis of novel electron deficient π-conjugated systems by hydroboration polymerization and their blue light emission. J. Am. Chem. Soc. 120, 5112–5113.

Mattos, B.D., Tardy, B.L., Magalhães, W.L.E., Rojas, O.J., 2017. Controlled release for crop and wood protection: Recent progress toward sustainable and safe nanostructured biocidal systems. J. Control. Release 262, 139–150. https://doi.org/10.1016/j.jconrel.2017.07.025

Messner, K., 2003. Overview of white-rot research: where we are today, in: Wood Deterioration and Preservation. American Chemical Society, p. 77.

Mohajerani, A., Vajna, J., Ellcock, R., 2018. Chromated copper arsenate timber: A review of products, leachate studies and recycling. J. Clean. Prod. 179, 292–307.

Morrell, J., 2018. Protection of wood-based materials, in: Handbook of Environmental Degradation of Materials. pp. 343–368. https://doi.org/10.1016/B978-081551500-5.50017-3

Murphy, M., 1999. Plant products as antimicrobial agents. Clin. Microbiol. Rev. 12, 564–82. https://doi.org/0893-8512/99/$04.00□0

Muthumani, T., Sudhahar, V., Mukhopadhyay, T., 2015. Liposomes and Cyclodextrins as Delivery System for Cosmetic Ingredients: An Updated Review. Res. J. Top. Cosmet. Sci. 6, 21.

Neoh, T.L., Yamamoto, C., Ikefuji, S., Furuta, T., Yoshii, H., 2012. Heat stability of allyl isothiocyanate and phenyl isothiocyanate complexed with randomly methylated β-cyclodextrin. Food Chem. 131, 1123–1131. https://doi.org/10.1016/j.foodchem.2011.09.077

Nicholas, D.D., 1982. Wood deterioration and its prevention by preservative treatments: Degradation and Protection of Wood. Syracuse University Press.

Obanda, D.N., Shupe, T.F., Barnes, H.M., 2008. Reducing leaching of boron-based wood preservatives - A review of research. Bioresour. Technol. 99, 7312–7322. https://doi.org/10.1016/j.biortech.2007.12.077

Oberdürster, G., 2000. Toxicology of ultrafine particles: in vivo studies. Philos. Trans. R. Soc. London. Ser. A Math. Phys. Eng. Sci. 358, 2719–2740.

Ozaki, S.K., Yalınkılıc, M.K., Imamura, Y., Souza, M.F., 2001. Effect of Boron Compounds-Furfuryl Alcohol Treatment of Wood on Dimensional Stability, Termite Resistance and Boron Leachability, in: 32. IRG Annual Meeting.

Ozkan, G., Franco, P., De Marco, I., Xiao, J., Capanoglu, E., 2019. A review of microencapsulation methods for food antioxidants: Principles, advantages, drawbacks and applications. Food Chem. 272, 494–506.

Panek, M., Reinprecht, L., Hulla, M., 2014. Ten Essential Oils for Beech Wood Protection - Efficacy Against Wood-destroying Fungi and Moulds, and Effect on Wood Discoloration. BioResources 9, 5588–5603.

Pařil, P., Baar, J., Čermák, P., Rademacher, P., Prucek, R., Sivera, M., & Panáček, A., 2017. Antifungal effects of copper and silver nanoparticles against white and brown-rot fungi. J. Mater. Sci. 52, 2720–2729.

Park, S.-Y., Barton, M., Pendleton, P., 2012. Controlled release of allyl isothiocyanate for bacteria growth management. Food Control 23, 478–484. https://doi.org/10.1016/J.FOODCONT.2011.08.017

Peylo, A., Willeitner, H., 1995. The problem of reducing the leachability of boron by water repellents. Holzforschung-International J. Biol. Chem. Phys. Technol. Wood 49, 211–216.

Piercey, M.J., Mazzanti, G., Budge, S.M., Delaquis, P.J., Paulson, A.T., Hansen, L.T., 2012. Antimicrobial activity of cyclodextrin entrapped allyl isothiocyanate in a model system and packaged fresh-cut onions. Food Microbiol. 30, 213–218.

Pizzi, A., Baecker, A., 1996. A new boron fixation mechanism for environment friendly wood preservatives. Holzforschung-International J. Biol. Chem. Phys. Technol. Wood 50, 507–510.

Plackett, D., Ghanbari-Siahkali, A., Szente, L., 2007. Behavior of α-and β-cyclodextrin-encapsulated allyl isothiocyanate as slow-release additives in polylactide-co-polycaprolactone films. J. Appl. Polym. Sci. 105, 2850–2857.

Ratajczak, I., Mazela, B., 2007. The boron fixation to the cellulose, lignin and wood matrix through its reaction with protein. Holz als Roh - und Werkst. 65, 231–237. https://doi.org/10.1007/s00107-006-0154-4

Ringman, R., Pilgard, A., Brischke, C., Richter, K., 2014. Mode of action of brown rot decay resistance in modified wood: A review. Holzforschung 68, 239–246. https://doi.org/10.1515/hf-2013-0057

Romero, J., Vinden, P., Drysdale, J., 1995. Treatment of wood with boron esters, in: Document-the International Research Group on Wood Preservation. Sweden.

Rowell, R.M., 1995. Chemical modification of wood for improved adhesion in composites. Proceedings, wood Adhes. 15, 56–60.

Saliba, A.M., De Assis, M.-C., Nishi, R., Raymond, B., Marques, E. de A., Lopes, U.G., Touqui, L., Plotkowski, M.-C., 2006. Implications of oxidative stress in the cytotoxicity of Pseudomonas aeruginosa ExoU. Microbes Infect. 8, 450–459.

Sankhla, M.S., Kumari, M., Nandan, M., Kumar, R., Agrawal, P., 2016. Heavy metals contamination in water and their hazardous effect on human health—a review. Int. J. Curr. Microbiol. Appl. Sci. 5, 759–766.

Santos, E.H., Kamimura, J.A., Hill, L.E., Gomes, C.L., 2015. Characterization of carvacrol beta-cyclodextrin inclusion complexes as delivery systems for antibacterial and antioxidant applications. LWT - Food Sci. Technol. 60, 583–592. https://doi.org/10.1016/j.lwt.2014.08.046

Schultz, T.P., Nicholas, D.D., Preston, A.F., 2007. A brief review of the past, present and future of wood preservation. Pest Manag. Sci. 63, 784–788.

Shah, V., Dobiášová, P., Baldrian, P., Nerud, F., Kumar, A., Seal, S., 2010. Influence of iron and copper nanoparticle powder on the production of lignocellulose degrading enzymes in the fungus Trametes versicolor. J. Hazard. Mater. 178, 1141–1145.

Singh, T., Singh, A.P., 2012. A review on natural products as wood protectant. Wood Sci Technol 851–870. https://doi.org/10.1007/s00226-011-0448-5

Staroszczyk, H., 2009. Microwave-assisted boration of potato starch. Polimery 54, 31–41.

Steinberg, H., Hunter, D.L., 1957. Preparation and rate of hydrolysis of boric acid esters. Ind. Eng. Chem. 49, 174–181.

Szejtli, J., 2013. Cyclodextrin Technology. Springer-science+bus. Media, B.V. 53, 1689–1699. https://doi.org/10.1017/CBO9781107415324.004

Szejtli, J., 1988. Cyclodextrin inclusion complexes, in: Cyclodextrin Technology. Springer, pp. 79–185.

Tascioglu, C., Yalcin, M., Sen, S., Akcay, C., 2013. Antifungal properties of some plant extracts used as wood preservatives. Int. Biodeterior. Biodegrad. 85, 23–28. https://doi.org/10.1016/j.ibiod.2013.06.004

Thevenon, M.F., Pizzi, A., Haluk, J.P., 1997. Non-toxic albumin and soja protein borates as ground-contact wood preservatives. Holz als Roh - und Werkst. 55, 293–296. https://doi.org/10.1007/s001070050231

Tondi, G., Wieland, S., Lemenager, N., Petutschnigg, A., Pizzi, A., Thevenon, M.-F., 2012. Efficacy of tannin in fixing boron in wood: fungal and termite resistance. BioResources 7, 1238–1252.

Toussaint-Dauvergne, E., Soulounganga, P., Gérardin, P., Loubinoux, B., 2000. Glycerol/glyoxal: A new boron fixation system for wood preservation and dimensional stabilization. Holzforschung 54, 123–126. https://doi.org/10.1515/HF.2000.021

Trinh, T., Cappel, J.P., Geis, P.A., McCarty, M.L., Pilosof, D., Zwerdling, S.S., 1997. Uncomplexed cyclodextrin solutions for odor control on inanimate surfaces.

Tsunoda, K., 2000. Gaseous treatment with allyl isothiocyanate to control established microbial infestation on wood. J. Wood Sci. 46, 154–158. https://doi.org/10.1007/BF00777363

Turek, C., Stintzing, F.C., 2013. Stability of essential oils: a review. Compr. Rev. Food Sci. Food Saf. 12, 40–53.

Voncina, B., Vivod, V., 2013. Cyclodextrins in textile finishing, in: Eco-Friendly Textile Dyeing and Finishing. InTech.

Wadhwa, G., Kumar, S., Chhabra, L., Mahant, S., Rao, R., 2017. Essential oil–cyclodextrin complexes: an updated review. J. Incl. Phenom. Macrocycl. Chem. 89, 39–58. https://doi.org/10.1007/s10847-017-0744-2

Wang, S., Winistorferl, P.M., 1999. Density Formation Under Dynamic Conditions 12, 220–238.

Weaver, F.W., Owen, N.L., 1995. Isocyanate-wood adhesive bond. Appl. Spectrosc. 49, 171–176.

Weinbach, E.C., 1954. The effect of pentachlorophenol on oxidative phosphorylation. J. Biol. Chem. 210, 545–550.

Wilcox, W.W., 1978. Review of literature on the effects of early stages of decay on wood strength. Wood Fiber Sci. 9, 252–257.

Williams, L.H., 2016. Borate Wood-Protection Compounds: A Review of Research and Commercial Use. APT Bull. 27, 46–51.

Wong, Ee Ding; Zhang, Min; Wang, Qian; Han, Guangping; Shuichi, K., 2000. Formation of the density profile and its effects on the properties of fiberboard. J. Wood Sci. 9486101, 202–209.

Wong, E.D., 1998. Effects of mat moisture content and press closing speed on the formation of density profile and properties of particleboard. J. Wood Sci. 44, 287–295. https://doi.org/10.1007/BF00581309

Wong, E.D., Zhang, M., Wang, Q., Kawai, S., 1999. Formation of the density profile and its effects on the properties of particleboard. Wood Sci. Technol. 33, 327–340. https://doi.org/10.1007/s002260050119

Yang, D.-Q., 2009. Potential utilization of plant and fungal extracts for wood protection. For. Prod. J. 59, 97–103.

Zhang, Q.F., Jiang, Z.T., Li, R., 2007. Complexation of allyl isothiocyanate with β-cyclodextrin and its derivatives and molecular microcapsule of allyl isothiocyanate in β-cyclodextrin. Eur. Food Res. Technol. 225, 407–413. https://doi.org/10.1007/s00217-006-0431-9